Response to RC2

We wish to thank this reviewer for his thorough review of our manuscript and his helpful comments. We believe that we addressed all of the major comments as indicated in the discussion below and the updated document.

The updated manuscript and figures can be found at the end after this response.

RC2: Depth habitats of the foraminifers are used to link the habitat to oceanographic conditions at the core locations. The supplement has a fairly thorough explanation of how the various depths were determined (using d18Oc, MgCa-derived T, and published depth habitats; detailed in Table 6), but I couldn't determine which depth the authors chose to use for each species (or at least is wasn't consistently clear in the text) without seeking the information in Table 7. In the intro of the MS, the authors point the reader to table 3 for the depth habitats but table 3 doesn't include this information. Also, I don't understand why sometimes the authors used published references for depth habitats and in other instances is d18O or Mg/Ca derived temperatures. For example: For core FC-01a, the Sime reference is cited for the depths used for G. ruber, T. sacc, O. universa, but oxygen isotopes are used for P. obliquiloculata and Mg/Ca derived Ts are used for tumida and menardii. Clarification here is needed.

Response: *A table was given in a previous version of this manuscript, but reviewers thought that was redundant with the table in the supplement (it was table 3), I have added the selected CDs in Table S7. You are right, it has been difficult to carefully select the CDs, I have tried to do it rigorously but sometimes it still remains arbitrary. To explain:*
I derived both calcification depth (CD) using δ18O (CD1) and Mg/Ca (CD2). Because each of methods have their limits (species-specific calibrations for most of it, and analytical uncertainties for δ18O) I compared the calcification depths to previously published in literature (CD3). I can't say what method is the best, but in my case I would tend toward Mg/Ca because we have species-specific calibrations for most of the species and the measurements were done on the same sample analyzed for δ11B. For δ18O I had to pick again.
To select the CD, the first thing I did was to look at the water column structure at each site in order to have an idea of what depth I should expect the species to be depending on their habitats (mixed-dweller, within thermocline, below thermocline). Then I compared CD1, CD2 and CD3. If the CDs were in line with the water structure and two CDs were similar I chose that one. If CD1 and CD2 were different I chose CD3. I chose CD₃ when possible because even if I have confidence in my data, there are papers that have more robust CD reconstructions (main goal of their papers).
*Now, for G. tumida and G. menardii, there were not a lot of data in the literature to compare with and there is no species-specific δ18O calibrations but there are if using Mg/Ca. When I compared with the few data in the literature, my CD2 were in line than CD3 that is why I stick to CD2 for both species.*
For P. obliquiloculata, it was the same not a lot of data in the literature (only Sime et al.,), so we use Mg/Ca data (CD2), not δ18O even if they are similar except (FCO2a).

RC2: I don't understand why O. universa is considered a deeper dweller in this MS. There are some major assumptions made about why the d11B of this species falls below the 1:1 line – this is also discussed in Henehan et al., 2013. Why O. universa d11B is more like the deeper dweller non-spinose forams is indeed puzzling (esp. since it has same symbionts as G. ruber and T. sacculifer), but I don't think it can be attributed to a deep depth, especially given the size fraction used (>500). The larger size fraction of the samples used would suggest that these are living at a shallower depth (See Spero and Parker, 2003) and likely in the mixed layer. The correct depth habitat will impact the calibration.

Response: *Yes, it will change quite a lot the position of the data, especially for site FC0-1 that probably would be an outlier, but the calibration won't change significantly when compiling all data (see Figure below).*

Only based on the CD calculations, O. universa is found in average ~60-70m which is in line with other depth habitats reconstructions, the fact that δ11B is lowered than ambient pH can be explained by a depth habitat >50m. The data converge towards this low δ11B due to a decrease in light insolation at deeper depth. Its high symbiont density and photosynthetic activity might make it, as T. sacculifer, more sensitive to water depth changes as well, or we could assume a change in symbiont assemblage to ones that are more similar to what are found in deeper dweller species, changing host/symbiont interactions, photosynthesis and related microenvironment pH.
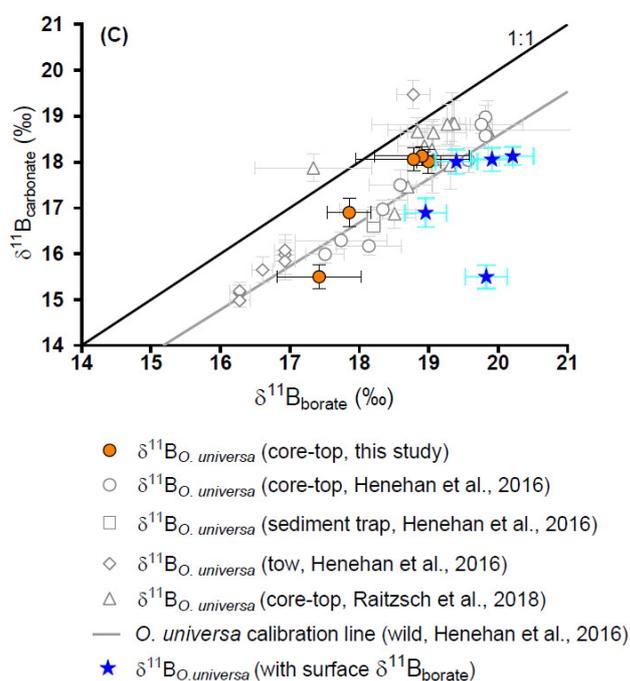
RC2: Samples were cleaned using the full cleaning method including the reductive step (cite Boyle and Kiegwin 1985/1986 as well, since they developed the method). Why was the reductive step included here? Yu et al., 2007 suggests the reductive step isn't detrimental to B/Ca ratios, but the effect of this cleaning step on for d11B analysis is unknown and according to Rae et al., 2018, the reductive step is typically not used during sample cleaning. There are documented dissolution effects that the authors discuss in the supplement (preferential dissolution of ontogenetic calcite occurs relative to the light d11B of gam calcite) and if cleaning preferentially removes ontogenetic calcite, then the primary d11B signal has been altered by the reductive cleaning. Additionally, the reductive cleaning step IS detrimental to other elements, like Mg/Ca ratios (decreases ratios by up to 15%), which were used to estimate depth habitat for some of the species investigated here. Including the reductive step should be justified with an explanation of how this additional cleaning step could have affected results.

Response: *Misra et al., (2014b) tested the different cleaning on the B/Ca and δ11B and observed no effect. However, in nodules (Mn-Fe) the concentration of B can be up to 120 ppm (Axelsson et al., 2002), Fe-Mn oxide and hydroxides can then result in non-negligible content of Mg and B contamination. We utilized the reductive step because some of the sites where not previously studied, overall the sites did not present high Mn, except for E035 which was removed due to that contamination.*

Also, results of Mg/Ca would lead to a deeper CDs which is not the case when comparing with CD1 and CD3.

Axelsson, M. D., Rodushkin, I., Ingri, J. and Öhlander, B.: Multielemental analysis of Mn–Fe nodules by ICP-MS: optimisation of analytical method, Analyst, 127, 76–82, 2002.

Misra, S., Owen, R., Kerr, J., Greaves, M. and Elderfield, H.: Determination of δ11B by HR-ICP-MS from mass limited samples: Application to natural carbonates and water samples, Geochim. Cosmochim. Acta, 140, 531–552, 2014b.

RC2: Li/Ca ratios are included in table 2, but never discussed?? Are they relevant for this MS? If not, perhaps remove?

Response: *Li/Ca are not discussed in this paper, however there is a growing interest for Li in foraminifera, we decided to publish those results in order to contribute to the existing data.*

RC2: Table 3: In the text on line 329 it is stated that chemo stratigraphic data is used to constrain depths, but this information is not summarized in the table, probably just a typo?

Response: *It was a typo, changed. The CD chosen are in Table S7.*

RC2: Other suggestions: Line 56-57: Not sure I agree with the statement in the abstract that the other species follow O. universa because of light limitation by symbiont bearing foraminifera. All of the deep dwellers have symbionts, all live in the photic zone.

Response: *I have tried to improve the discussion, focusing on the symbionts/photosynthesis, because the story is of course more complex.*
Yes, all of the species have algal symbionts but they can differ. From what I see in the literature is that T. sacculifer, G. ruber, O. universa have mostly dinoflagellates symbionts (can have chrysophyte as well) where G. tumida, G. menardii, P. obliquiloculata and N. dutertrei will have chrysophyte algal symbionts. The photosynthesis is dependent of the nature of the host/symbionts interactions, symbionts type (pigment associated for light absorption efficiency), symbionts density. The recent study from Tagaki et al., (2019) is really helpful as he constrained the photosynthesis activity, light absorption efficiency and the symbiont density of those species.

Fv/Fm (photosynthethic activity) T. sacculifer>G. menardii > O. universa> G. ruber (white) > N. dutertrei > P. obliquiloculata

σpsi (light absorption efficiency) N. dutertrei > P. obliquiloculata > G. menardii > G. ruber > T. sacculifer > O. universa

Chla/biomass   T. sacculifer>O.universa>G. ruber> N. dutertrei>G. menardii>P. obliquiloculata

What I assume is that T. sacculifer, O. universa and G. ruber photosynthesis are likely to be more affected by changes in insolation than other species due to their symbiont density, high photosynthetic capacity and their light absorption efficiency. Which is still in line with the argumentation we are giving. Also, the fact that the deeper dwellers have this low boron isotopic signature is likely due to a lower symbiont density, lower photosynthetic activity and a reduced insolated environment. P. obliquiloculata has the lowest density and photosynthetic activity, which would translate in a respiration driven environment the fact that most of the species are following this trend would go in the sense of a respiration driven environment.

Also the fact that O. universa is following this trend would, I think, whether be due light limitation and/or a different symbiont due to its deeper depth.

Lines 485-543.

I also changed Figure 7 to give more informations on the microenvironment pH.

I changed for "likely caused by light limitation and/or symbiont/host interactions"

RC2: Line 128: This sentence is poorly structured.

Response: *Changed for: "Furthermore, δ11B differences between foraminifera species from the same pH makes the acquisition of more core-top and culture data essential for testing and applying the proxy."*

RC2: Secition 2.4: Origin of biological fractionation Paragraph beginning on line 172: very speculative and based upon benthic foraminifer experiments.

We have added a statement (line 176) to this effect, that "We acknowledge this is speculative as it is based upon benthic foraminifer experiments."

RC2: Section 2.5: The annual vs seasonal preferences for forams is largely dependent on temperatures. For example, in some regions G. ruber and G. sacculifer can be present throughout the year if T > 25C, but will have a summer/fall preference when T drops below 15. Their choice on seasonal vs. annual presence of these species will affect the hydrographic data used and perhaps impact results.

Response: *Noted.*

RC2: Section 3.2: Size fractions listed in this paragraph don't agree with size fractions in the Table.

Response: *Changed for: "Around 50-100 foraminifera shells were picked from the 400-500 μm fraction size for Globorotalia menardii and Globorotalia tumida, >500 μm for Orbulina universa, from the 250-400 μm fraction size for Trilobatus sacculifer (w/o sacc, without sacc-like final chamber), Trilobatus sacculifer (sacc, sacc-like final chamber), Globigerinoides ruber (white, sensu stricto), Neogloboquadrina dutertrei, Pulleniatina obliquiloculata. The samples picked for analyses were visually well preserved."*

RC2: Section 3.8: This section could/should include some of the information in the supplement regarding the depth used to obtain hydrographic information.

Response: *We acknowledge it was not clear in the manuscript. The information can be found in Table S7. Line 341: "The depth habitats utilized to derive in situ parameters are summarized in Table S7."*

RC2: Line 339: Forams don't migrate in the water column (See Meiland et al., 2019), but deep dwellers may crust at depth during the END of their lifecycle, this should be clarified. This is later explained correctly (lines 452-453).

Response: *Changed: line 338 "As foraminifera can migrate in the water column along their ontogeny". It is still vague but I don't know how constrained is this depth change at the end of their life cycle.*

RC2: Lines 509-514: The concept of facultative symbiosis is outdated – all forams with symbionts are likely obligate and not facultative. See https://www.biogeosciences.net/16/3377/2019/. G. tumida doesn't have symbionts at all, so why does it align with the other species? Please discuss.

Response: *But Tagaki et al., (2019) didn't constrain G. tumida in his study.*
From what I have read the family Globorotaliidae have algal chrysphyte symbionts, which should include G. tumida. If there are no symbionts or a low symbiont density/low photosynthetic activity (like P. obliquiloculata) the respiration driven microenvironment resulting from the parameters aforementioned or again light limitation would be a plausible explanation.

I have made changes in this section in order to improve the discussion. Lines 485-543.

1   Seawater pH reconstruction using boron isotopes in multiple planktonic foraminifera species with
2   different depth habitats and their potential to constrain pH and pCO$_2$ gradients
3
4
5   Maxence Guillermic[1,2], Sambuddha Misra[3,4], Robert Eagle[1,2], Alexandra Villa[2,5], Fengming Chang[6],
6   Aradhna Tripati [1,2]
7
8
9
10
11   [1] Department of Earth, Planetary, and Space Sciences, Department of Atmospheric and Oceanic
12   Sciences, Institute of the Environment and Sustainability, UCLA, University of California – Los
13   Angeles, Los Angeles, CA 90095 USA
14   [2] Laboratoire Géosciences Océan UMR6538, UBO, Institut Universitaire Européen de la Mer, Rue
15   Dumont d'Urville, 29280, Plouzané, France
16   [3] Indian Institute of Science, Centre for Earth Sciences, Bengaluru, Karnataka 560012, India
17   [4] The Godwin Laboratory for Palaeoclimate Research, Department of Earth Sciences, University of
18   Cambridge, UK
19   [5] Department of Geology, University of Wisconsin-Madison, Madison, WI 53706 USA
20   [6] Key Laboratory of Marine Geology and Environment, Institute of Oceanology, Chinese Academy of
21   Sciences, Qingdao 266071, China
22
23
24
25
26
27
28
29
30
31
32
33
34
35
36
38
39
40
41   *Corresponding author:
42   E-mail address: maxence.guillermic@gmail.com
43

44 **ABSTRACT**

45

46   Boron isotope systematics of planktonic foraminifera from core-top sediments and culture experiments have

47   been studied to investigate the sensitivity of δ^{11}B of their calcite tests to seawater pH. However, our knowledge

48   of the relationship between δ^{11}B and pH remains incomplete for many taxa. Thus, to expand the potential scope

49   of application of this proxy, we report δ^{11}B data for 7 different species of planktonic foraminifera from sediment

50   core-tops. We utilize a method for the measurement of small samples of foraminifera and calculate the δ^{11}B-

51   calcite sensitivity to pH for *Globigerinoides ruber*, *Trilobus sacculifer* (sacc or w/o sacc), *Orbulina universa*,

52   *Pulleniatina obliquiloculata*, *Neogloboquadrina dutertrei*, *Globorotalia menardii* and *Globorotalia tumida*,

53   including for unstudied core-tops and species. The sensitivity of δ^{11}B$_{carbonate}$ to δ^{11}B$_{borate}$ (eg.

54   $\Delta\delta^{11}$B$_{carbonate}$/$\Delta\delta^{11}$B$_{borate}$) in core-tops is consistent with previous studies for *T. sacculifer* and *G. ruber* and close

55   to unity for *N. dutertrei*, *O. universa* and combined deep-dwelling species. Deep-dwelling species closely follow

56   the core-top calibration for *O. universa,* which is attributed to respiration-driven microenvironments, likely

57   caused by light limitation and/or symbiont/host interactions. These taxa have diverse ecological preferences and

58   are from sites that span a range of oceanographic regimes, including some that are in regions of air-sea

59   equilibrium and others that are out of equilibrium with the atmosphere. Our data support the premise that

60   utilizing boron isotope measurements of multiple species within a sediment core can be utilized to constrain

61   vertical profiles of pH and pCO$_2$ at sites spanning different oceanic regimes, thereby constraining changes in

62   vertical pH gradients and yielding insights into the past behavior of the oceanic carbon pumps.

1. Introduction

The oceans are absorbing a substantial fraction of anthropogenic carbon emissions resulting in declining surface ocean pH (Fig. 1; IPCC, 2014). Yet there is a considerable uncertainty over the magnitude of future pH change in different parts of the ocean and the response of marine biogeochemical cycles to physio-chemical parameters (T, pH) caused by climate change (Bijma et al., 2002; Ries et al., 2009). Therefore, there is an increased interest in reconstructing past seawater pH (Hönisch and Hemming, 2005; Liu et al., 2009; Wei et al., 2009; Douville et al., 2010), in understanding spatial variability in aqueous pH and carbon dioxide (pCO$_2$) (Foster et al., 2008; Martinez-Boti et al., 2015b; Raitzsch et al., 2018), and in studying the response of the biological carbon pump utilizing geochemical proxies (Yu et al., 2007, 2010, 2016).

Although proxies for carbon cycle reconstruction are complex in nature (Pagani et al., 2005; Tripati et al., 2009, 2011; Allen and Hönisch, 2012), the boron isotope composition of foraminiferal tests is emerging as one of the more robust candidates (Hönisch et al., 2005, 2009; Ni et al., 2007; Foster et al., 2008, 2012; Bartoli et al., 2011; Henehan et al., 2013; Martinez-Boti et al., 2015b; Chalk et al., 2017). The study of laboratory cultured foraminifera has demonstrated a systematic dependence of the boron isotope composition of tests on ambient pH (Sanyal et al., 1996, 2001; Henehan et al., 2013, 2016). Core-top measurements on globally distributed samples also show a δ^{11}B sensitivity to pH with taxa-specific offsets from the theoretical fractionation line of borate ion (Rae et al., 2011; Henehan et al., 2016; Raitzsch et al., 2018).

Knowledge of seawater pH, in conjunction with constraints on one other carbonate system parameter (Total Alkalinity (TA), DIC (dissolved inorganic carbon), [HCO$_3^-$], [CO$_3^{2-}$]), can be utilized to constrain aqueous pCO$_2$. Application of empirical calibrations for boron isotopes, determined for select species of foraminifera from core-tops and laboratory cultures, has resulted in accurate reconstructions of pCO$_2$ utilizing downcore samples from sites that are in quasi-equilibrium with the atmosphere at present. δ^{11}B$_{carbonate}$ based reconstructed values of pCO$_2$ are analytically indistinguishable from ice core CO$_2$ records (Hönisch et al., 2005, 2009; Foster et al., 2008; Henehan et al., 2013; Chalk et al., 2017).

Therefore, the last decade has produced several studies aiming at reconstructing past seawater pH using boron isotopes to constrain atmospheric pCO$_2$ in order understand the changes in the global carbon cycle (Hönisch et al., 2005, 2009; Foster et al., 2008, 2012, 2014; Seki et al., 2010; Bartoli et al., 2011; Henehan et al., 2013; Martinez-Boti et al., 2015a, 2015b; Chalk et al., 2017). In addition to reconstructing atmospheric pCO$_2$, in a few studies, the δ^{11}B proxy has been applied to mixed-layer planktonic foraminifera at sites out of equilibrium with the atmosphere to constrain past air-sea fluxes (Foster et al., 2014; Martinez-Boti et al., 2015b). A small body of work has examined whether data for multiple species in core-top (Foster et al., 2008) and down-core samples could be used to constrain vertical profiles of pH through time (Palmer et al., 1998; Pearson and Palmer, 1999).

In this study, we make critical additions to the emerging pool of boron isotope data of core-top planktonic foraminifera from different oceanographic regimes, including data for species that have not previously been examined. We utilize a low-blank (15 pg B to 65 pg B), high precision (2sd on the international standard JCP-1 is 0.20 ‰, n=6) δ^{11}B$_{carbonate}$ analysis method (down to ~250 µg CaCO$_3$), modified after Misra et al. (2014), to study multiple species of planktonic foraminifera from sediment core-tops that span a range of oceanographic regimes, including open-ocean oligotrophic settings and marginal seas. We constrain calibrations for different species, and compare results to published work (Foster et al., 2008; Henehan et al., 2013; Henehan

3

et al., 2016; Martinez-Boti et al., 2015b; Raitzsch et al., 2018). We also test whether these data support the application of boron isotope measurements of multiple species within a sediment core as a proxy for constraining vertical profiles of pH and pCO_2.

2. Background

2.1 Planktonic foraminifera as archives of seawater pH

Planktonic foraminifera are used as archives of past environmental conditions within the mixed layer and thermocline, as their chemical composition is correlated with the physio-chemical parameters of their calcification environment (Ravelo and Fairbanks, 1992; Elderfield and Ganssen, 2000; Dekens et al., 2002; Anand et al., 2003; Sanyal et al., 2001; Ni et al., 2007; Henehan et al., 2013, 2015, 2016; Howes et al., 2017; Raitzch et al., 2018). The utilization of geochemical data for multiple planktonic foraminifera species with different ecological preferences to constrain vertical gradients has been explored in several studies. The framework for such an approach was first developed using modern samples of planktonic foraminifera for oxygen isotopes, where it was proposed as a tool to constrain vertical temperature gradients and study physical oceanographic conditions during periods of calcification (Ravelo and Fairbanks, 1992).

Because planktonic foraminifera species complete their lifecycle in a particular depth habitat due to their ecological preference (Ravelo and Fairbanks, 1992; Farmer et al., 2007), it is theoretically possible to reconstruct water column profiles of pH using data from multiple taxa (Palmer and Pearson, 1998; Anagnostou et al., 2016). The potential use of an analogous approach to reconstruct past profiles of seawater pH was first highlighted by Palmer and Pearson (1998) on Eocene samples to constrain pH-depth gradients. However, in these boron isotope-based studies, it was assumed that boron isotope offset from seawater and foraminiferal carbonate were constant, which is an assumption not supported by subsequent studies (e.g., Hönisch et al., 2003; Foster et al., 2008; Henehan et al., 2013, 2016; Raitszch et al., 2018; Rae, 2018). Furthermore, $\delta^{11}B$ differences between foraminifera species that inhabit waters that are the same pH makes the acquisition of more core-top and culture data essential for applications of the proxy.

2.2 Boron systematics in seawater

Boron is a conservative element in seawater with a long residence time ($\tau_B \sim 14$ Myr) (Lemarchand et al., 2002a). In seawater, boron exists as trigonal boric acid $B(OH)_3$ and tetrahedral borate ion $B(OH)_4^-$ (borate). The relative abundance of boric acid and borate ion is a function of the ambient seawater pH. At standard open ocean conditions (T = 25 °C and S = 35), the dissociation constant of boric acid is 8.60 (Dickson, 1990), implying that boron mainly exists in the form of boric acid in seawater. Since the pK_B and seawater pH (e.g., ~8.1, NBS) values are similar, it implies that small changes in seawater pH will induce strong variations in the abundance of the two boron species (Fig. 2).

Boron has two stable isotopes, ^{10}B and ^{11}B, with average relative abundances of 19.9 and 80.1 %, respectively. Variations in B isotope ratio are expressed in conventional delta (δ) notation:

$$\delta^{11}B\ (‰) = 1000\ \text{x}\ \left(\frac{^{11}B/^{10}B_{Sample}}{^{11}B/^{10}B_{NIST\ 951-a}} - 1 \right) \tag{1}$$

142 where positive values represent enrichment in the heavy isotope [11]B, and negative values enrichment in the light

143 isotope [10]B, relative to the standard reference material. Boron isotope values are reported versus the NIST SRM

144 951 (Cantazaro et al., 1970).

145      $B(OH)_3$ is enriched in [11]B compared to $B(OH)_4^-$ with a constant offset between   the   two   chemical

146 species, within the range of physio-chemical variation observed in seawater, given by the fraction factor (α). The

147 fractionation (ε) between $B(OH)_3$ and $B(OH)_4^-$ of 27.2 ± 0.6 ‰ has been empirically determined by Klochko et

148 al., (2006) in seawater. Note, Nir et al., (2015) calculate this fractionation, using an independent method, to be

149 26 ± 1 ‰, which is within the analytical uncertainty of the Klochko et al., (2006) value.

150

151 **2.3 Boron isotopes in planktonic foraminifera calcite**

152   Many biogenic carbonate-based geochemical proxies are affected by "vital effects" or biological

153 fractionations (Urey et al., 1951). The $\delta^{11}B_{carbonate}$ in foraminifera exhibits species-specific offsets (see Rae et al.,

154 2018 for review) compared to theoretical predictions for the boron isotopic composition of $B(OH)_4^-$ (α=1.0272,

155 Klochko et al., 2006). As the analytical and technical aspects of boron isotope measurements have improved

156 (Foster et al., 2008; Rae et al., 2011; Misra et al., 2014; Lloyd et al., 2018), evidence for taxonomic differences

157 have not been eliminated, but have become increasingly apparent (Foster et al., 2008, 2018; Henehan et al 2013,

158 2016; Noireaux et al., 2015; Foster et al., 2016; Rae et al., 2018; Raitzsch et al., 2018).

159   At present, culture and core-top calibrations have been published for several planktonic species

160 including *Trilobatus sacculifer*, *Globigerinoides ruber*, *Globigerina bulloides*, *Neogloboquadrina pachyderma,*

161 *Orbulina universa* (Foster et al., 2008; Henehan et al., 2013; Henehan et al., 2015; Sanyal et al., 1996; Sanyal et

162 al., 2001). Although the boron isotopic composition of several species of foraminifera are now commonly used

163 tools for reconstructing surface seawater pH, for other species, there is a lack of data constraining boron isotope

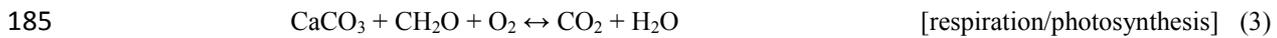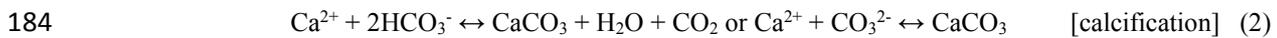164 sensitivity between foraminiferal carbonate and borate ion in seawater.

165

166 **2.4 Origin of biological fractionations in foraminifera**

167   Perforate foraminifera are calcifying organisms that maintain a large degree of biological control over

168 their calcification space, and thus, mechanisms of biomineralization may be of significant importance in

169 controlling the $\delta^{11}B$ of the biogenic calcite. The biomineralization of foraminifera is based on seawater

170 vacuolization (Erez, 2003; de Nooijer et al., 2014) with parcels of seawater being isolated by an organic matrix

171 thereby creating a vacuole filled with seawater. Recent work has also demonstrated that even if the chemical

172 composition of the reservoirs is modified by the organism, seawater is directly involved in the calcification

173 process with vacuoles formed at the periphery of the shell (de Nooijer et al., 2014). Culture experiments by

174 Rollion-Bard and Erez., (2010) have proposed that the pH at the site of biomineralization is elevated to an upper

175 pH limit of ~9 for the shallow-water, symbiont-bearing benthic foraminifera *Amphistegina lobifera*, which

176 would support a pH modulation of a calcifying fluid in foraminifera. We acknowledge this is speculative as it is

177 based upon benthic foraminifer experiments.

178   For taxa with symbionts, the microenvironment surrounding the foraminifera is chemically different

179 from seawater due to photosynthetic activity (Jorgensen et al., 1985; Rink et al., 1998; Köhler-Rink and Kühl,

180 2000). Photosynthesis by the symbionts elevates the pH of the microenvironment (Jorgensen et al., 1985; Rink et

181 al., 1998; Wolf-Gladrow et al., 1999; Köhler-Rink and Kühl, 2000), while calcification and respiration decrease

182 it (Equation 2 and 3).

183

184 $$Ca^{2+} + 2HCO_3^- \leftrightarrow CaCO_3 + H_2O + CO_2 \text{ or } Ca^{2+} + CO_3^{2-} \leftrightarrow CaCO_3 \quad \text{[calcification]} \quad (2)$$

185 $$CaCO_3 + CH_2O + O_2 \leftrightarrow CO_2 + H_2O \quad \text{[respiration/photosynthesis]} \quad (3)$$

186

187 $\delta^{11}B$ in foraminifera is primary controlled by seawater pH, but is also dependent of the pH alteration of

188 microenvironments due to calcification, respiration and symbiont photosynthesis. $\delta^{11}B$ should therefore reflect

189 the relative dominance of these processes and may account for species-specific $\delta^{11}B$ offsets. Theoretical

190 predictions from Zeebe et al. (2003) and foraminiferal data from Hönisch et al., (2003) highlighted the

191 dominance of microenvironment pH in $\delta^{11}B$ signature of foraminifera. Their work also suggested that for a given

192 species, there should be a constant offset observed between the boron isotope composition of foraminifera and

193 borate ion over a large range of pH, imparting confidence in utilizing species-specific boron isotope data as a

194 proxy for seawater pH.

195 Comparison of boron isotope data for multiple planktonic foraminiferal species indicate that taxa with

196 high levels of symbiont activity such as *T. sacculifer* and *G. ruber* show higher $\delta^{11}B$ values than the $\delta^{11}B$ of

197 ambient borate (Foster et al., 2008, Henehan et al., 2013, Raitzsch et al., 2018). The sensitivities

198 ($\Delta\delta^{11}B_{carbonate}/\Delta\delta^{11}B_{borate}$ referred to as the slope) of existing calibrations suggest a different species-specific

199 sensitivity for these species compared to other taxa (Sanyal et al., 2001; Henehan et al., 2013; Henehan et

200 al.,2015; Raitzsch et al., 2018). For example, *Orbulina universa* exhibits a lower $\delta^{11}B$ than *in situ* $\delta^{11}B$ values of

201 borate ion (Henehan et al., 2016), consistent with the species living deeper in the water column characterized by

202 reduced photosynthetic activity.

203 It is possible that photosynthetic activity by symbionts might not be able to compensate for changes in

204 calcification and/or respiration, leading to an acidification of the microenvironment. It is interesting to note that

205 for *O. universa* the slope determined for the field-collected samples is not statistically different from unity (0.95

206 $\pm$ 0.17) (Henehan et al. 2016), while culture experiments report slopes of ≤ 1 for multiple species including *G.*

207 *ruber* (Henehan et al., 2013), *T. sacculifer* (Sanyal et al., 2001), and *O. universa* (Sanyal et al., 1999). More

208 core-top and culture calibrations are needed to fully understand why different slopes are observed, which is part

209 of the motivation for this study.

210

211 **2.5 Planktic foraminifera depth and habitat preferences**

212 The preferred depth habitat of different species of planktonic foraminifera depends on their ecology,

213 which in turn relies on the hydrographic conditions. For example, *G. ruber is* commonly found in the mixed

214 layer (Fairbanks and Wiebe, 1980; Dekens et al., 2002; Farmer et al., 2007) during the summer (Deuser et al.,

215 1981) whereas *T. sacculifer* is present in the mixed layer until mid-thermocline depths (Farmer et al., 2007)

216 during spring and summer (Deuser et al., 1981, 1989). Specimens of *P. obliquiloculata* and *N. dutertrei* are

217 abundant during winter months (Deuser et al., 1989), with an acme in the mixed layer (~60m) for *P.*

218 *obliquiloculata*, and at mid-thermocline depths for *N. dutertrei* (Farmer et al., 2007). In contrast, *O. universa*

219 tends to record annual average conditions within the mixed layer. Specimens of *G. menardii* calcify within the

220 seasonal thermocline (Fairbanks et al., 1982, Farmer et al., 2007, Regenberg et al., 2009), and in some regions in

221   the upper thermocline (Farmer et al., 2007), and records annual temperatures. *G. tumida* is found at the lower

222   thermocline or below the thermocline and records annual average conditions (Fairbanks and Wiebe, 1980;

223   Farmer et al., 2007, Birch et al., 2013).

224

225   **3. Materials and Methods**

226

227   **3.1 Localities studied**

228   Core-top locations were selected to span a broad range of seawater pH, carbonate system parameters,

229   and oceanic regimes. Samples from Atlantic Ocean (CD107-A), Indian Ocean (FC-01a and FC-02a), Arabian

230   Sea (FC-13a and FC-12b) and Pacific Ocean (WP07-01, A14, and Ocean Drilling Program 806A and 807A)

231   were analyzed; characteristics of the sites are summarized in Table 1 and S7, Fig. 3, and Fig. 4.

232   Atlantic site CD107-a (CD107 site A) was drilled in 1997 by the Benthic Boundary Layer program

233   (BENBO) (K.S. Black et al., 1997 - cruise report RRS Charles Darwin Cruise 107). Arabian Sea sites FC-12b

234   (CD145 A150) and FC-13a (CD145 A3200) were retrieved by the *Charles Darwin* in the Pakistan Margin in

235   2004 (B.J. Bett et al., 2003 - cruise report n°50 RRS Charles Darwin Cruise 145). A14 was recovered by box

236   corer in the southern area of the South China Sea in 2012. Core WP07-01 was obtained from the Ontong Java

237   Plateau using a giant piston corer during the Warm Pool Subject Cruise in 1993. Holes 806A and 807A were

238   retrieved on Leg 130 by the Ocean Drilling Program (ODP). The top 10 cm of sediment from CD107-A have

239   been radiocarbon dated to be Holocene <3 ky (Thomson et al., 2000). Samples from multiple box cores from

240   Indian Ocean sites were radiocarbon dated as Holocene <7.3 ky (Wilson et al., 2012). Samples from western

241   equatorial Pacific Site 806B, close to site WP07-01, are dated to between 7.3-8.6 ky (Lea et al., 2000). Arabian

242   Sea and Pacific core-top samples were not radiocarbon dated but are assumed to be Holocene.

243

244   **3.2 Species**

245   Around 50-100 foraminifera shells were picked from the 400-500 μm fraction size for *Globorotalia*

246   *menardii* and *Globorotalia tumida*, >500 μm for *Orbulina universa*, from the 250-400 μm fraction size for

247   *Trilobatus sacculifer* (w/o sacc, without sacc-like final chamber), *Trilobatus sacculifer* (sacc, sacc-like final

248   chamber), *Globigerinoides ruber (*white, sensu stricto), *Neogloboquadrina dutertrei*, *Pulleniatina*

249   *obliquiloculata*. The samples picked for analyses were visually well preserved.

250

251   **3.3 Sample cleaning**

252   Briefly, picked foraminifera were gently cracked open, clay removed and checked for coarse-grained

253   silicates. The next stages of sample processing and chemical separation were performed in a class 1000 clean lab

254   equipped with boron-free HEPA filters. Samples were then cleaned using full reductive and oxidative cleaning

255   (Boyle and Keigwin, 1985; Barker et al., 2003). A final leaching step with 0.001N HCl was done before

256   dissolution in 1N HCl. Each sample was divided into two aliquots: an aliquot for boron purification and one

257   aliquot for trace element analysis.

258

259   **3.4 Reagents**

260   Double-distilled HNO_3 and HCl acids (from Merck® grade) and a commercial bottle of HF Ultrapure

261   grade were used at Brest. Double-distilled acids were used at Cambridge. All acids and further dilutions were

262 prepared using double-distilled 18.2 MΩ.cm-1 MQ water. Working standards for isotope ratio and trace element

263 measurements were freshly diluted on a daily basis with the same acids used for sample preparation to avoid any

264 matrix effect.

265

266 **32.5 Boron isotopes**

267 Boron purification for isotopic measurement was done utilizing microdistillation method developed by

268 Gaillardet et al., (2001), for Ca-rich matrices by Wang et al., (2010) and adapted at Cambridge by Misra et al.,

269 (2014a). 70 µL of dissolved carbonate sample was loaded on a cap of a clean fin legged 5 mL conical beaker

270 upside down. The tightly closed beaker was put on a hotplate at 95°C for 15 hours. The beakers were taken off

271 the hotplate and were allowed to cool for 15 min. The cap where the residue formed was replaced by a clean one.

272 Then, 100 µL of 0.5% HF were added to the distillate.

273 Boron isotopic measurements were carried out on a Thermo Scientific ®Neptune+ MC-ICP-MS at the

274 University of Cambridge. Neptune+ was equipped with Jet interface and two 10^{13} Ω resistors. The instrumental

275 setup included Savillex® 50µl/min C-flow self-aspirating nebulizer, single pass Teflon® Scott-type spray

276 chamber constructed utilizing Savillex® column components, 2.0 mm Pt injector from ESI®, Thermo® Ni 'H'

277 type sample cone and 'X' type skimmer cones. Both isotopes of boron were determined utilizing 10^{13} Ω resistors

278 (Misra et al., 2014a; Lloyd et al., 2018).

279 The sample size for boron isotope analyses typically ranged from 10 ppb B (~5 ng B) to 20 ppb B

280 samples (~10 ng B). Instrumental sensitivity for ^{11}B was 17 mV/ppb B (eg. 170 mV for 10ppb B) in wet plasma

281 at 50µl/min sample aspiration rate. Intensity of ^{11}B for a sample at 10ppb B was typically 165mV ± 5mV closely

282 matched the 170mV ± 5mV of the standard. Due to the low boron content of the samples extreme care was taken

283 to avoid boron contamination during sample preparation and reduce memory effect during analysis. Procedural

284 boron blanks ranged from 15pg B to 65 pg B (contributed to less than <1% of the sample signal). The acid blank

285 during analyses was measured at ≤ 1mV on the ^{11}B, meaning a contribution < 1% of the sample intensity, no

286 memory effect was observed within and across sessions.

287 Analyses of external standards were done to ensure data quality. For δ^{11}B measurements two carbonate

288 standards were utilized: the JCP-1 (Geological Survey of Japan, Tsukuba, Japan) international standard (Gutjahr

289 et al., 2014) and the NEP internal coral (Porites sp., δ^{11}B = 26.12 ± 0.92 ‰, 2SD, n=33 Holcomb et al., 2015 and

290 Sutton et al., 2018, Table S2) from University of Western Australia/Australian National University. Certified

291 boron isotopes liquid standard, the ERM© AE121 (δ^{11}B = 19.9 ± 0.6 ‰, SD, certified) was used to monitor

292 reproducibility and drift during each session (Vogl and Rosner, 2011; Foster et al., 2013; Misra et al., 2014).

293 Results for the isotopic composition of the NEP standard are shown in Table S2, average values are δ^{11}B $_{NEP}$ =

294 25.70 ± 0.93 ‰ (2SD, n=22) over different 7 analytical sessions with each number representing an ab-initio

295 processed sample - this study). Our results are within error of published values of 26.20 ± 0.88 ‰ (2SD, n = 27)

296 and 25.80 ± 0.89 ‰ (2SD, n = 6) by Holcomb et al. (2015) and Sutton et al. (2018) respectively. Chemically

297 cleaned JCP$_1$ samples were measured at 24.06 ± 0.20 (2SD, n=6) and is within error of published values of 24.37

298 ± 0.32 ‰ and 24.42 ± 0.28 ‰ by Holcomb et al. (2015) and Sutton et al. (2018) respectively.

299

300 **3.6 Trace elements**

301   The calcium concentration of each sample was measured on an ICP-AES ® Ultima 2 HORIBA at the

302   Pôle spectrometrie Océan (PSO), UMR6538 (Plouzané, France). Samples were then diluted to fixed calcium

303   concentrations (typically 10 ppm or 30 ppm Ca) using 0.1 M HNO3 & 0.3 M HF matching multi-element

304   standards Ca concentration to avoid any matrix effect (Misra et al., 2014b). Trace elements (e.g. X/Ca ratios)

305   were analyzed on a Thermo Scientific ® Element XR HR-ICP-MS at the PSO, Ifremer (Plouzané, France).

306   Trace element analyses were done at a Ca concentration of 10 or 30 ppm. The typical blanks for a 30

307   ppm Ca session were: ^{7}Li < 2%, ^{11}B < 7%, ^{25}Mg < 0.2% and ^{43}Ca < 0.02%. Additionally, blanks for a 10 ppm Ca

308   session were: ^{7}Li < 2.5%, ^{11}B < 10%, ^{25}Mg < 0.4% and ^{43}Ca < 0.05%. Due to strong memory effect for boron

309   and instrumental drift on the Element XR, long sessions of conditioning were done prior analyses. Boron blanks

310   were driven below 5% of signal intensity usually after 4 to 5 days of continuous analyses of carbonate samples.

311   External reproducibility was determined on the consistency standard Cam-Wuellestorfi (courtesy of the

312   University of Cambridge) (Misra et al., 2014b), Table S3. Our X/Ca ratio measurements on the external standard

313   Cam-Wuellestorfi were all the time within error of the published value (Table S3) validating the robustness of

314   our trace elements data. Analytical uncertainty of a single measurement was calculated from the reproducibility

315   of the Cam-Wuellestorfi, measured during a particular mass spectrometry session. The analytical uncertainties

316   on the X/Ca ratios are: 0.4 μmol/mol for Li/Ca, 7 μmol/mol for B/Ca and 0.01 mmol/mol for Mg/Ca (2SD,

317   n=31) respectively.

318

3.7 Oxygen isotopes

320   Carbonate δ^{13}C and δ^{18}O were measured on a Gas Bench II coupled to a Delta V mass spectrometer at

321   the stable isotope facility of Pôle spectrometrie Océan (PSO), Plouzané. Around 20 shells were weighed, crushed

322   and clay removed. The recovered foraminifera were weighed in tubes and flushed with He gas. Samples were

323   then digested in phosphoric acid and analyzed. Results were calibrated to the VPDB scale by international

324   standard NBS19 and analytical precision on the in-house standard Ca21 was better than 0.11‰ for δ^{18}O (1SD,

325   n=5) and 0.03‰ for δ^{13}C (1SD, n=5).

326

3.8 Calcification depth determination

328   We utilized two different chemo-stratigraphic methods to estimate the calcification depth in this study

329   (Table S6 and S7). The first method, commonly used in paleoceanography, utilizes δ^{18}O measurements of the

330   carbonate (δ^{18}O$_c$) to estimate calcification depths (referred to as δ^{18}O-based calcification depths) (Schmidt et al.,

331   2002; Mortyn et al., 2003; Sime et al., 2005; Farmer et al., 2007; Birsh et al., 2013). The second method utilizes

332   Mg/Ca-based temperature estimates ($T_{Mg/Ca}$) to constrain calcification depths (Quintana Krupinski et al., 2017).

333   In both cases, the postulate was that vertical profiles of seawater temperature are available for different seasons

334   in ocean atlases and cruise reports, and that hydrographic data and geochemical proxy signatures can be

335   compared to assess the depth in the water column that represents the species maximum abundance.

336   The two different methods to estimate calcification depth were then compared to published depth

337   estimates for the basin, and where available, for the same site (Table S6). We chose literature values for

338   calcification depths when available, or depths that were closest to what is known for the region or basin. As

339   foraminifera can migrate in the water column along their ontogeny, we applied (based on uncertainties of our

340 measurements) an uncertainty of ±10m for calcification depths > 70 m and an uncertainty of ±20 m when

341 calcification depths <70 m. The depth habitats utilized to derive *in situ* parameters are summarized in Table S7.

342

343 **3.9 $\delta^{11}B_{borate}$**

344   Two carbonate system parameters are needed to fully constrain the carbonate system. Following the

345 approach of Foster et al., (2008) we used the GLODAP database (Key et al., 2004) corrected for anthropogenic

346 inputs in order to estimate pre-industrial carbonate system parameters at each site. Temperature, salinity and

347 pressure for each site are from the World ocean database 2013 (Boyer et al., 2013). We utilized the R[©] code in

348 Henehan et al, (2016) (courtesy of Michael Henehan) to calculate the $\delta^{11}B_{borate}$ and derive our calibrations.

349 Uncertainty for $\delta^{11}B_{borate}$ utilizing the code was similar to the one calculated by applying 2 standard deviations of

350 the calculated $\delta^{11}B_{borate}$ within the limits imposed by the calcification depth.

351   The Matlab[©] template provided by Zeebe and Wolf-Gladow, (2001) was used to calculate pCO_2 from

352 TA; temperature, salinity and pressure were included into the calculations. Total boron was calculated from Lee

353 et al., (2010), K_1 and K_2 were calculated from Mehrbach et al. (1973) refitted by Dickson and Millero (1987).

354   Statistical tests were made utilizing GraphPad[©] software, linear regressions for calibration where

355 derived utilizing R[©] code in Henehan et al, (2016) (courtesy of Michael Henehan) with a k=500.

356

357 **4. Results**

358

359 **4.1 Depth habitat**

360   The calcification depths utilized in this paper are summarized in Tables S6 and S7, including a

361 comparison of calcification depth determination methods. The calculated calcification depths are consistent with

362 the ecology of each species and the hydrography of the sites. Specimens of *G. ruber* and *T. sacculifer* appear to

363 be living in the shallow mixed layer (0-100 m), with *T. sacculifer* living or migrating deeper than *G. ruber*

364 (down to 125 m). Specimens of *O. universa* and *P. obliquiloculata* are living in the upper thermocline; *G.*

365 *menardii* is found in the upper thermocline until the thermocline depth specific to the location; *N. dutertrei* is

366 living around the thermocline depth and specimens of *G. tumida* are found in the lower thermocline.

367   Data from both approaches implies that some species inhabit deeper environments in the Western

368 Equatorial Pacific (WEP) relative to the Arabian Sea, which in turn are deeper dwelling than in the Indian

369 Ocean. In some cases, we find evidence for differences in habitat depth of up to ~100m between the WEP and

370 the Arabian Sea. This trend is observed for *G. ruber* and *T. sacculifer*, but not for *O. universa*.

371   Some differences in calcification depth are observed between the two calcification depth determination

372 methods. These differences might be due to the choice of calibrations. Alternatively, our uncertainties for $\delta^{18}O$

373 implies larger uncertainties on the calcification depth determination using this approach, compared to Mg/Ca

374 measurements.

375

376 **4.2 Empirical calibrations of foraminiferal $\delta^{11}B_{carbonate}$ to $\delta^{11}B_{borate}$**

377   Results for the different species analyzed in this study are presented in Fig. 5, Fig. 6 and summarized in

378 Table 2; additionally, published calibrations for comparison are summarized in Table 3.

379

4.2.1 *G. ruber*

Our results for *G. ruber* (Fig. 5) are in good agreement with published data from other core-tops, sediment traps, tows, and culture experiments for $\delta^{11}B_{borate} > 19$ ‰ (Foster et al., 2008, Henehan et al., 2013, Raitzsch et al., 2018). However, for $\delta^{11}B_{borate} < 19$ ‰ our results show lighter $\delta^{11}B_{carbonate}$ compared to published values. Whilst this species has been widely studied previously, the sites selected in this study allow us to extend the calibration. The positive offset from the 1:1 curve has been explained by the high photosynthetic activity (Hönisch et al., 2003; Zeebe et al., 2003). Two calibrations have been derived. Utilizing only our data, the sensitivity of $\delta^{11}B_{carbonate}$ to $\delta^{11}B_{borate}$ of our linear regression is not statistically different from 1 and do not follow the low sensitivity trend of the culture experiments from Sanyal et al., (2001) or Henehan et al., (2013), ($p < 0.05$). The uncertainty on this regression is important due to our small dataset and not inconsistent with the second calibration made compiling all data from literature. The sensitivity of this regression is similar (e.g. 0.46 (± 0.34)) to the one recently published by Raitzsch et al., (2018) (e.g. 0.45 (± 0.16), Table 3).

4.2.2 *T. sacculifer*

$\delta^{11}B_{carbonate}$ results for *T. sacculifer* (sacc and w/o sacc) (Fig. 5) are compared to published data (Foster et al., 2008; Martinez-Boti et al., 2015b, Raitzsch et al., 2018). Results for *T. sacculifer* are in good agreement with the literature and fall above the 1:1 line. Linear regression on our data yields a slope of 1.3 ± 0.2 but is not statistically different to the results from Martinez-Boti et al., (2015b) (Table 3), ($p > 0.05$). However, when compiled with published data using the bootstrap method a slope of 0.83 ± 0.48 is calculated, with a large uncertainty given the variability in the data. It is also noticeable that *T. sacculifer* (w/o sacc) samples from the WEP have a $\delta^{11}B_{carbonate}$ close or below the 1:1 line and are significantly lower compared to the combined *T. sacculifer* of other sites ($p = 0.01$, unpaired t-test).

4.2.3 *O. universa* and deeper dwelling species: *N. dutertrei, P. obliquiloculata, G. menardii* and *G. tumida*

Our results for *O. universa* (Fig. 5), *N. dutertrei, P. obliquiloculata, G. menardii* and *G. tumida* (Fig. 6) fall below the 1:1 line. These data for *O. universa* are not statistically different from the Henehan et al. (2016) calibration ($p > 0.05$). Our results for *N. dutertrei* expand upon the initial measurements presented in Foster et al., (2008). The different environments experienced by *N. dutertrei* in our study permit us to extend the range and derive a calibration for this species; the slope is close to unity (0.93 ± 0.55), and is similar to the (0.95 ± 0.17) previously reported by Henehan et al., (2016) for *O. universa* and not statistically different ($p > 0.05$). The data for *P. obliquiloculata* exhibits the largest offset from the theoretical line. The range of $\delta^{11}B_{borate}$ from the samples we have of *G. menardii* and *G. tumida* is not sufficient to derive calibrations, but the points are in good agreement with the *N. dutertrei* calibration and Henehan et al. (2016) calibration for *O. universa*.

For all species, the slopes are not statistically different from Henehan et al. (2016) ($p > 0.05$) and are close to unity. If data for deep-dwelling foraminiferal species are pooled together with each other and with data from Henehan et al., (2016) and Raitzch et al., (2018), we calculate a slope of 0.95 (± 0.13) ($R^2 = 0.7987$, $p < 0.0001$); if only our data are used, we calculate a slope that is not significantly different (0.82 ± 0.27; $p < 0.05$). However, it may remain premature to assume that a unique calibration with a slope of ~0.9 can be used for all deeper-dwelling species; more data is needed for *P. obliquiloculata*, *G. menardii* and *G. tumida* to robustly test this assertion.

4.2.4 Comparison of core-top and culture data

The data for *G. ruber* and *T. sacculifer* from the core-tops we measured are broadly consistent with previous published results. The calibrations between these core-top derived estimates and culture experiments are not statistically different due to small datasets and uncertainties on the linear regressions (Henehan et al., 2013; Marinez-Boti et al., 2015; Raitzsch et al., 2018; Table 3). The sensitivities of the species analyzed are not statistically different and are close to unity.

4.3 B/Ca ratios

B/Ca ratios are presented in Table 2. Values are species specific consistent with previous work (e.g., compiled in Henehan et al., 2016) with ratios higher for *G. ruber* > *T. sacculifer* > *T. sacculifer* (w/o sacc) > *P. obliquicloculata* > *O. universa* > > *G. menardii* > *N. dutertrei* > *G. tumida* > *G. inflata* > *N. pachyderma* > *G. bulloides* (Fig. 7). This study supports interspecific B/Ca ratios (Yu et al., 2007; Tripati et al., 2009, 2011; Allen and Hönisch, 2012; Henehan et al., 2016). Differences between surface- and deep-dwelling foraminifera are observed, with lower values and a smaller range for the deeper dwelling taxa (58-126 µmol/mol vs 83-190 µmol/mol for shallow dwellers). The B/Ca data for deep-dwelling taxa exhibits a significant correlation with $[B(OH)_4^-]/[HCO_3^-]$ ($p<0.05$), but no correlation with $\delta^{11}B_{carbonate}$ and temperature (Fig. S3). Surface-dwelling species have B/Ca ratios that exhibit significant correlations with $[B(OH)_4^-]/[HCO_3^-]$, $\delta^{11}B_{carbonate}$ and temperature. The sensitivity of B/Ca to $[B(OH)_4^-]/[HCO_3^-]$ is lower for deep-dwelling species compared to surface dwelling species. When all the B/Ca data are compiled, significant trends are observed with $[B(OH)_4^-]/[HCO_3^-]$, $\delta^{11}B_{carbonate}$ and temperature (Fig. S3). We also observe that if we compare data from all sites together, correlations exist between B/Ca and the water depths of the cores (not significant, Fig. S4) but these correlations may also be related to the different the depth habitats of different taxa in each region, a significant trend is observed when all the data are plotted ($R^2=0.11$, $p<0.05$, Fig. S4).

5. Discussion

5.1 Sources of uncertainty relating to depth habitat and seasonality at studied sites

5.1.1 Depth habitats and $\delta^{11}B_{borate}$

Because foraminifera will record ambient environmental conditions during calcification, the accurate characterization of *in-situ* data is needed not only for calibrations, but also to understand the reconstructed record of pH or pCO$_2$. The species we examined are ordered here from shallower to deeper depth habitats: *G. ruber* > *T. sacculifer* (sacc) > *T. sacculifer* (w/o sac) > *O. universa* > *P. obliquiloculata* > *G. menardii* > *N. dutertrei* > *G. tumida* (this study; Birch et al., 2013; Farmer et al., 2007), although the specific water depth will vary depending on the hydrology of the site (Kemle-von and Oberhänhsli, 1999). We note that calculation of absolute calcification depths can be challenging in some cases as many species migrate during their ontogeny (Steinhardt et al., 2015).

We find that assumptions about the specific depth habitat a species of foraminifera is calcifying over, in a given region, can lead to differences of a few per mil in calculated isotopic compositions of borate (Fig. 4).

460 Hence this can cause a bias in calibrations if calcification depths are assumed instead of being calculated (i.e.,

461 with $\delta^{18}O$ and/or Mg/Ca). Factors including variations in thermocline depth can impact depth habitats for some

462 taxa. At the sites we examined, most of the sampled species live in deeper depth habitats in the WEP relative to

463 the Indian Ocean, which in turn is characterized by deeper depth habitats than in the Arabian Sea. In the tropical

464 Pacific, *T. sacculifer* is usually found deeper than *G. ruber* except at sites characterized by a shallow

465 thermocline, in which case they tend to overlap their habitat (e.g., ODP Site 806 in the WEP which has a deeper

466 thermocline than at ODP Site 847 in the Eastern Equatorial Pacific; EEP) (Rickaby et al., 2005). The difference

467 in depth habitats for *T. sacculifer* and *N. dutertrei* between the WEP and EEP can be as much as almost 100 m

468 (Rickaby et al., 2005).

469

470 **5.1.2 Seasonality and *in-situ* $\delta^{11}B_{borate}$**

471 As discussed by Raitzsch et al., (2018), depending of the study area, foraminiferal fluxes can change

472 throughout the year, so seasonality can have a major impact on hydrographic carbonate parameters calculations

473 for any given water depth. We therefore recalculated the theoretical $\delta^{11}B_{borate}$ using seasonal data for temperature

474 and salinity and annual values for TA and DIC for each depth at each site. The GLODAP (2013) database does

475 not provide seasonal TA or DIC values.

476 The low sensitivity of $\delta^{11}B_{borate}$ to temperature and salinity means that calculated $\delta^{11}B_{borate}$ for each

477 water depth at our sites were not strongly impacted (Fig. S1). Thus, these findings support Raitzsch et al. (2018),

478 who concluded that calculated $\delta^{11}B_{borate}$ values corrected for seasonality was within error of non-corrected values

479 for each water depth. As Raitzsch et al, (2018) highlight, seasonality might be more important at high latitude

480 sites where seasonality is more marked, however, the seasonality of primary production will also be more tightly

481 constrained due to the seasonal progression of winter light limitation and intense vertical mixing and summer

482 nutrient limitation.

483 Data for our sites suggests that most $\delta^{11}B_{borate}$ variability we observe does not come from seasonality but

484 from the assumed water depths for calcification. With the exception of a few specific areas such as the Red Sea

485 (Henehan et al., 2016, Raitzsch et al., 2018), at most sites examined, seasonal $\delta^{11}B_{borate}$ at a fixed depth does not

486 vary by more than ~0.2‰. We conclude that seasonality is not an important factor impacting carbonate system

487 parameters at the sites we examined.

488

489 **5.2 $\delta^{11}B$, microenvironment pH and depth habitats**

490 In planktonic foraminifera, algal symbiosis is the more common symbiotic relationship. For most of

491 planktonic foraminifera, the host presents only one species of symbionts (Gast and Caron, 2001). The family

492 Globigerinidae, including *G. ruber*, *T. sacculifer* and *O. universa*, commonly have dinoflagellates or chrysophyte

493 algal symbionts (Anderson and Be, 1976; Spero, 1987). The families Pulleniatinidae, Globorotaliidae, including

494 *N. dutertrei*, *P. obliquiloculata, G. menardii* and *G. tumida*, have chrysophyte algal symbionts (Gastrich, 1988).

495 The relationship between the symbionts and the host is complex by nature. Nevertheless, this symbiotic

496 relationship provides energy (Hallock, 1981b) and promotes calcification of the foraminifera (Duguay, 1983;

497 Erez et al., 1983) by providing the inorganic carbon to the host (Jorgensen et al., 1985). Also, for *T. sacculifer*

498 and *O. universa* photosynthesis increases with higher insolation (Jorgensen et al., 1985; Rink et al., 1998).

499   Dinoflagellate-bearing foraminifera (*G. ruber*, *T. sacculifer* and *O. universa*) tend to have a higher
500   symbiont density and photosynthesis activity while *P. obliquiloculata*, *G. menardii* and *N. dutertrei* have
501   lowered symbiont density and *P. obliquiloculata*, *N. dutertrei* lower photosynthetic activity (Takagi et al., 2019).
502   *P. obliquiloculata* showed the minimum symbiont density and photosynthetic activity (Takagi et al., 2019).

503   It is now accepted that the foraminifera $\delta^{11}B$ signature comes from the microenvironment pH
504   (Jorgensen et al., 1985; Rink et al., 1998; Köhler-Rink and Kühl, 2000, Hönisch et al., 2003; Zeebe et el., 2003).
505   Foraminifera with high photosynthetic activity and symbiont density like *G. ruber* and *T. sacculifer* present a pH
506   of microenvironment higher than ambient seawater, $\delta^{11}B$ higher than 1:1 line (Foster et al., 2008, Henehan et al.,
507   2013, Raitzsch et al., 2018). The opposite can also be true, from our study, species with lower photosynthetic
508   activity and lower symbiont density present microenvironments lower than ambient seawater, $\delta^{11}B$ lower than
509   1:1 line (Martinez-Boti et al., 2015b; Henehan et al., 2016), this is the case in our data for *N. dutertrei*, *G.*
510   *menardii* and *P. obliquiloculata* and likely *G. tumida*. Nevertheless, the low $\delta^{11}B$ of *O. universa* and *T.*
511   *sacculifer (w/o sacc)* from the WEP are difficult to reconcile with a high photosynthetic activity compared to *T.*
512   *sacculifer* et *G. ruber*.

513   The photosynthetic activity is also function of the light level they received which is, in the natural
514   system, dependent of their depth in the water column, for the purpose of this study we will not consider turbidity
515   which also influences the light penetration in the water column. In this case, the photosynthetically active
516   foraminifera living close to the surface should see their microenvironment pH (thus $\delta^{11}B$) more sensitive to water
517   depth changes. A deeper depth habitat will change the light intensity they received and as a consequence may
518   lower their photosynthetic activity reducing their microenvironment pH. This thought is supported by the
519   significant trend observed between our $\Delta^{11}B$ and the calcification depth for *G. ruber* and *T. sacculifer* of our sites
520   (Fig. S2). This trend basically supports the fact that the microenvironment pH decrease with calcification depth.
521   We observe a decrease of $\delta^{11}B$ in the WEP for *T. sacculifer (w/o sacc)*, significantly different from the other sites
522   (p<0.05). The $\Delta^{11}B$ of *G. ruber*, *T. sacculifer* (w/o sacc and sacc) is also significantly lower in the WEP
523   compared to the other sites (p<0.05). To test if the $\delta^{11}B$ signature was inferred to a light driven, we have been
524   able to independently calculate the depth of the foraminifera based on various light insolation culture
525   experiments (Jorgensen et al., 1985) and the Δmicroenvironment pH derived from our data (Fig. 8A and B). This
526   exercise verified that this low $\delta^{11}B$ can be explained by the reduced light environment due to a deeper depth
527   habitat in the WEP (Fig. 8B). Also, *T. sacculifer* has the potential to support more photosynthesis due to its
528   higher symbiont density. Higher photosynthetic activity is observed compared to other species potentially
529   supporting higher symbiont/host interactions. Those results could be in line with a greater sensitivity of *T.*
530   *sacculifer* photosynthetic activity with changes in insolation/water depth. It can also be noted that this species
531   presents the largest variations in symbiont density versus its test size. When applied to the other species *O.*
532   *universa* data suggest a microenvironment pH 0.10 to 0.20 lower than ambient seawater pH which would be in
533   line with species living deeper than 50m (light compensation point (Ec), Rink et al., 1998) also consistent with
534   our calcification depth reconstructions. Δmicroenvironment pH is higher in *T. sacculifer* > *G. ruber* > *T.*
535   *sacculifer* (w/o sacc - WEP) > *O. universa*, *N. dutertrei*, *G. menardii, G. tumida* > *P. obliquiloculata* in line with
536   photosymbiosis findings from Tagazaki et al., (2019). Also, the higher $\delta^{11}B$ data from the African upwelling
537   published by Raitzsch et al., (2018) for *G. ruber* and *O. universa* might reflect the higher microenvironment pH
538   due to a shallower depth habitat. This could highlight a potential issue with calibration when applied to sites with

539 different oceanic regimes as the $\delta^{11}B$ specie-specific calibrations could be also location-specific for the mixed

540 dweller species.

541   Microenvironment pH results for *N. dutertrei, G. menardii, G. tumida,* are similar to *O. universa* and

542 suggest a threshold for respiration driven $\delta^{11}B$ signature. This threshold can be driven by a change of

543 photosynthetic activity due to lower light intensity at deeper depth and/or a change in the symbiont assemblage

544 with non-dinoflagellate symbionts at deeper depth. We can explain this threshold because deep dweller species

545 do not experience important changes of insolation at those depths so their microenvironments should be

546 respiration driven and relatively stable. We can also note that *P. obliquiloculata* which has the lowest symbiont

547 density and photosynthetic activity has the lowest microenvironment pH compared to other deeper dweller

548 species supporting this respiration driven microenvironment.

549

550 **5.3 $\delta^{11}B$ sensitivity to $\delta^{11}B_{borate}$ and relationship with B/Ca signatures**

551       $\delta^{11}B_{carbonate}$ and B/Ca data have shown to be sensitive to precipitation rate with at higher precipitation

552 rate increasing $\delta^{11}B_{carbonate}$ (Farmer et al., 2019) and B/Ca (Farmer et al., 2019; Gabitov et al., 2014; Kaczmarek

553 et al., 2016; Mavromatis et al., 2015; Ushikawa et al., 2015). A recent study from Farmer et al, (2019) has

554 proposed that in foraminifera at higher precipitation rates, more borate ion is incorporated into the carbonate

555 mineral, while at lower precipitation rates, more boric acid is incorporated. They also suggest this may explain

556 low sensitivies of culture experiments.

557   When combining all literature data, *T. sacculifer* and *G. ruber* have sensitivities of $\delta^{11}B_{carbonate}$ to

558 $\delta^{11}B_{borate}$ of 0.83 ± 0.48 and 0.46 ± 0.34 respectively in line with previous literature and paleo-CO$_2$

559 reconstructions. Also, if we only take into account our data, the observation that the sensitivity of $\delta^{11}B_{carbonate}$ to

560 $\delta^{11}B_{borate}$ are not statistically different from unity for most of the species investigated we can speculate that for

561 these taxa, changes in precipitation rate and contributions of boric acid are not likely to be important. If

562 considering only the data from this study, *G. ruber* (1.12 ± 1.67) and *T. sacculifer* (1.38± 1.35) present higher

563 sensitivities of $\delta^{11}B_{carbonate}$ to $\delta^{11}B_{borate}$. We can then again speculate that the observed high values for $\delta^{11}B_{carbonate}$

564 at high seawater pH can be due to higher precipitation rates. We note this could also be consistent with the

565 higher sensitivity of B/Ca signatures in these two surface dwelling species to ambient $[B(OH)_4^-]/[HCO_3^-]$ relative

566 to deeper dwelling species. Those interspecific differences still remain to be explained, however, part of this

567 variability is likely due to changes in the carbonate chemistry of the microenvironment resulting in changing

568 competition between borate and bicarbonate. A caveat is that we can not exclude specific biological processes,

569 and that in taxa with a non respiration-driven microenvironment, changes in day/night calcification ratios also

570 impacting observed values. As indicated by Farmer et al., (2019), studies of calcite precipitation rates in

571 foraminifera may help to improve our understanding of the fundamental basis of boron-based proxies.

572

573 **5.4 Evaluation of species for pH reconstructions and water depth pH reconstructions**

574   This data set allows us to reassess the utility of boron-based proxies for the carbonate system. The main

575 interest with utilizing boron-based proxies relates to the reconstruction of past oceanic conditions - specifically

576 pH and pCO$_2$. Mixed-layer species (eg. *G. ruber* and *T. sacculifer)* are potential archives for atmospheric CO$_2$

577 reconstructions. Other species can shed light on other aspects of the carbon cycle including the physical and

578 biological carbon pumps.

579   There are a few main inferences we can make. When compiled with data from the literature,
580   sensitivities of $\delta^{11}B_{carbonate}$ to $\delta^{11}B_{borate}$ for *G. ruber* and *T. sacculifer* are similar to previous studies (Martinez-
581   Boti et al., 2015b; Raitzsch et al., 2018) which is also supporting of previous paleo-reconstructions. Our data
582   also support the observations of Henehan et al., (2016) for *O. universa*.
583   In order to derive accurate reconstructions of past ambient pH and pCO$_2$, accurate species-specific
584   calibrations need to be used that are constrained by core-tops or samples from similar types of settings (Fig. 9,
585   10, S6). Lighter $\delta^{11}B$ signatures in *T. sacculifer* (w/o sacc) are observed in the WEP, which may be explained by
586   the deeper depth habitat for these taxa, where lower light levels might reduce symbiont photosynthetic activity.
587   Also, correction will be needed for *T. sacculifer* (w/o sacc) in the WEP. When applying the calibrations n°2 and
588   4 to *T. sacculifer* and *G. ruber* (compilation of all data, Table 3) our data show more variability, especially for *G.*
589   *ruber* which lead to the larger mismatch compared to *in-situ* parameters. Henehan et al., (2013) reported a lighter
590    $\delta^{11}B$ with smaller test size, our sample add a weight/shell of 11 ± 4 µg (n=4, SD) which, despite a narrow range,
591   could still explain this variability. The higher divergence of reconstructed values from *in-situ* measurements are
592   observed at site WPO7-01 for both *T. sacculifer* (w/o sacc) and *G. ruber*. More data would be needed to
593   determine a proper correction for both species, coretop study will be determinant for future downcore
594   reconstructions, especially in the WEP.
595   We also find that for two species, the boron proxy is a relatively straightforward recorder of ambient
596   pH, with sensitivities close to unity for and *O. universa, and N. dutertrei*. There is also promise in using multiple
597   species in a sample from different hydrographic regimes to reconstruct vertical profiles of pH and pCO$_2$. We are
598   able to reproduce pH and pCO$_2$ profiles from multiple sites with different water column structures (Fig. 9) with
599   those reconstructions within error of the *in-situ* values, for most sites. In order to avoid circularity, to validate
600   these calibrations, we recalculated ambient pH and pCO$_2$ by first excluding site-specific data and then
601   recalculating species-specific calibrations, followed by application to each specific site. The comparison of the
602   two methods does not show significant differences and validates the robustness of the calibrations (Fig. S5). We
603   utilized the calibrations derived from our data for *G. ruber* (calibration n°1 and 2, Table 3), *T. sacculifer*
604   (calibration n°3 and 4, Table 3), *O. universa* (calibration n°8, Table 3), for *P. obliquiloculata* (calibration n°11,
605   Table 3), and for *N. dutertrei*, *G. tumida* and *G. menardii* the calibration made on the compilation of the deep-
606   dweller (calibration n°13, Table 3). Results are shown in Fig. 9 and evaluated in Fig. 10. For *G. menardii*, more
607   data would be helpful to provide additional constraints. Results for *G. ruber* are the sparsest, potentially due to
608   difference in test sizes (Henehan et al., 2013) or undocumented diagenetic effects. Results reaffirm the
609   importance of working with narrow size fractions (Henehan et al., 2013) and the importance of core-top study to
610   determine corrections.
611
612   **6. Conclusions and future implications**
613   Our study has extended the boron isotope proxy with data for new species and sites. The work supports
614   previous work showing that depth habitats of foraminifera vary depending on the oceanic regime, and this
615   impacts boron isotope signatures. Low $\delta^{11}B$ values in the WEP compared to other regions for *T. sacculifer* (w/o
616   sacc) may be explained by a reduction in microenvironment pH due to a deeper depth habitat associated with
617   reduced irradiance and thus photosynthetic activity. Those results might also highlight a potential need for

618 studying core-tops in order to establish what factors are important to accurately develop reconstructions in
619 different areas.

620   The sensitivity of $\delta^{11}B$ to pH is in line with previously published data for *T. sacculifer*, *G. ruber*. The
621 sensitivity of $\delta^{11}B$ to pH of *O. universa* (mixed dweller), *N. dutertrei*. *G. menardii* and *G. tumida* (deep-
622 dwellers) are similar but more data are needed to fully determine those sensitivities. The similarity of boron
623 isotope calibrations for deep-dwelling taxa might be related to respiration-driven microenvironments.

624   Reconstruction of seawater pH and carbonate system parameters is achievable using foraminiferal $\delta^{11}B$
625 but additional core-top and down-core studies reconstructing depth profiles will be needed in order to further
626 verify those calibrations. Past pH and pCO_2 water depth profiles can potentially be created by utilizing multiple
627 foraminiferal species in concert with taxa-specific calibrations for similar settings. This approach has much
628 potential for enhancing our understanding of the past workings of the oceanic carbon cycle, and the biological
629 pump.
630

References

Allen, K. A. and Hönisch, B.: The planktic foraminiferal B/Ca proxy for seawater carbonate chemistry: A critical evaluation, Earth Planet. Sci. Lett, 345–348, 203–211, 2012.

Anand, P., Elderfield, H. and Conte, M. H.: Calibration of Mg/Ca thermometry in planktonic foraminifera from a sediment trap time series. Paleoceanography 18, 2003.

Anderson, O. R. and Bé, A.W. H.: The ultrastructure of a planktonic foraminifer, Globigerinoides sacculifer (Brady), and its symbiotic dinoflagellates, J. Foramin. Res., 6, 1–21, 1976.

Arbuszewski, J., DeMenocal, P., Kaplan, A. and Farmer, E. C.: On the fidelity of shell-derived δ18Oseawater estimates, Earth Planet. Sci. Lett., 300, 185–196, 2010.

Axelsson, M. D., Rodushkin, I., Ingri, J. and Öhlander, B.: Multielemental analysis of Mn–Fe nodules by ICP-MS: optimisation of analytical method, Analyst, 127, 76–82, 2002.

Babila, T.L., Rosenthal, Y., Conte, M.H.: Evaluation of the biogeochemical controls on B/Ca of Globigerinoides ruber white from the Oceanic Flux Pro-gram, Bermuda. Earth Planet. Sci. Lett.404, 67–76, 2014.

Barker S., Greaves M. and Elderfield H.: A study of cleaning procedures used for foraminiferal Mg/Ca paleothermometry. Geochemistry, Geophys. Geosystems 4, 1–20, 2003.

Bartoli, G., Hönisch, B. and Zeebe, R. E.: Atmospheric CO2 decline during the Pliocene intensification of Northern Hemisphere glaciations. Paleoceanography 26, 1–14, 2011.

Bemis, B. E., Spero, H. J., Bijma, J. and Lea, D. W.: Reevaluation of the oxygen isotopic composition of planktonic foraminifera: Experimental results and revised paleotemperature equations. Paleoceanography 13, 150–160, 1998.

Bemis, B. E., Spero, H. J. and Thunell, R. C.: Using species-specific paleotemperature equations with foraminifera: a case study in the Southern California Bight, Mar. Micropaleontol, 46, 405–430, 2002.

Bijma, J., Faber Jr., W.W., Hemleben, C.: Temperature and salinity limits for growth and survival of some planktonic foraminifers in laboratory cultures, J. Foraminiferal Res. 20 (2), 95–116, 1990.

Bijma, J., Hönisch, B. and Zeebe, R. E.: Impact of the ocean carbonate chemistry on living foraminiferal shell weight: Comment on "Carbonate ion concentration in glacial-age deep waters of the Caribbean Sea" by W. S. Broecker and E. Clark, Geochemistry, Geophys. Geosystems, 3, 1–7, 2002.

Birch, H., Coxall, H. K., Pearson, P. N., Kroon, D. and O'Regan, M.: Planktonic foraminifera stable isotopes and water column structure: Disentangling ecological signals, Mar. Micropaleontol., 101, 127–145, 2013.

Boyer, T.P., Antonov, J. I., Baranova, O. K., Coleman, C., Garcia, H. E., Grodsky, A., Johnson, D. R., Locarnini, R. A., Mishonov, A. V., O'Brien, T.D., Paver, C.R., Reagan, J.R., Seidov, D., Smolyar, I. V., and Zweng, M. M.: World Ocean Database, NOAA Atlas NESDIS 72, S. Levitus, Ed., A. Mishonov, Technical Ed., Silver Spring, MD, 209, 2013.

Boyle, E. A.: Manganese carbonate overgrowths on foraminifera tests, Geochim. Cosmochim. Acta., 47, 1815–1819, 1983.

Branson, O., Kaczmarek, K., Redfern, S. A. T., Misra, S., Langer, G., Tyliszczak, T., Bijma, J. and Elderfield, H.: The coordination and distribution of B in foraminiferal calcite, Earth Planet. Sci. Lett., 416, 67–72, 2015.

690 Catanzaro, E.J., Champion, C.E., Garner, A.L., Marinenko, G., Sappenfield, K.M. and Shields, W.R.: Boric
691   Acid; Isotopic and Assay Standard Reference Materials. U.S. Natl. Bur. Stand. Spec., Publ. 260-17, 70p,
692   1970.

693 Chalk, T. B., Hain, M. P., Foster, G. L., Rohling, E. J., Sexton, P. F., Badger, M. P. S., Cherry, S. G., Hasenfratz,
694   A. P., Haug, G. H., Jaccard, S. L., Martínez-García, A., Pälike, H., Pancost, R. D. and Wilson, P. A.:
695   Causes of ice age intensification across the Mid-Pleistocene Transition, Proc. Natl. Acad. Sci., 114,
696   13114–13119, 2017.

697 Coadic, R., Bassinot, F., Dissard, D., Douville, E., Greaves, M. and Michel, E.: A core-top study of dissolution
698   effect on B/Ca in Globigerinoides sacculifer from the tropical Atlantic: Potential bias for paleo-
699   reconstruction of seawater carbonate chemistry, Geochemistry, Geophys. Geosystems 14, 1053–1068,
700   2013.

701 de Nooijer, L. J., Spero, H. J., Erez, J., Bijma, J. and Reichart, G. J.: Biomineralization in perforate foraminifera.
702   Earth-Science Rev., 135, 48–58, 2014.

703 Dekens, P. S., Lea, D. W., Pak, D. K. and Spero, H. J.: Core top calibration of Mg/Ca in tropical foraminifera:
704   Refining paleotemperature estimation, Geochemistry, Geophys. Geosystems 3, 1–29, 2002.

705 Deuser, W.G., Ross, E.H., Hemleben, Ch., Spindler, M.: Seasonal changes in species composition, numbers,
706   mass, size, and isotopic composition of planktonic foraminifera settling into the deep Sargasso Sea,
707   Palaeogeogr., Palaeoclimat., Palaeoecol., 33:103-127, 1981.

708 Deuser, W. G. and Ross, E. H.: Seasonally abundant planktonic foraminifera of the Sargasso Sea; succession,
709   deep-water fluxes, isotopic compositions, and paleoceanographic implications, J. Foraminifer. Res. 19,
710   268–293, 1989.

711 Dickson, A. G.: Thermodynamics of the dissociation of boric acid in synthetic seawater from 273.15 to 318.15
712   K., Deep Sea Res., Part A, Oceanogr. Res. Pap. 37, 755–766, 1990.

713 Dickson, A.G., Millero, F.J.: A comparison of the equilibrium constants for the dissociation of carbonic acid in
714   seawater media, Deep-Sea Res., 34, 1733–1743, 1987.

715 Douville, E., Paterne, M., Cabioch, G., Louvat, P., Gaillardet, J., Juillet-Leclerc, A. and Ayliffe, L.: Abrupt sea
716   surface pH change at the end of the Younger Dryas in the central sub-equatorial Pacific inferred from
717   boron isotope abundance in corals (Porites), Biogeosciences 7, 2445–2459, 2010.

718 Duguay, L.E.: Comparative laboratory and field studies on calcification and carbon fixation in foraminiferal-
719   algal associations, Journal of Foraminiferal Research 13, 252-261, 1983.

720 Duplessy, J., Labeyrie, L., Juilletleclerc, A., Maitre, F., Duprat, J. and Sarnthein, M.: Surface salinity
721   reconstruction of the north-atlantic ocean during the last glacial maximum, Oceanol. Acta, 14, 311–324,
722   1991.

723 Elderfield, H., Yu, J., Anand, P., Kiefer, T. and Nyland, B.: Calibrations for benthic foraminiferal Mg/Ca
724   paleothermometry and the carbonate ion hypothesis, Earth Planet. Sci. Lett., 250, 633–649., 2006.

725 Elderfield, H. and Granssen, G.: Past temperatures and O18 of surface ocean waters inferred from foraminiferal
726   Mg/Ca ratios, Nature 405, 442–445, 2000.

727 Erez J.: Calcification Rates, Photosynthesis and Light in Planktonic Foraminifera. In: Westbroek P., de Jong
728   E.W. (eds) Biomineralization and Biological Metal Accumulation. Springer, Dordrecht, 1983.

729 Erez, J.: The Source of Ions for Biomineralization in Foraminifera and Their Implications for Paleoceanographic
730   Proxies, Rev. Mineral. Geochemistry, 54, 115–149, 2003.

731 Fairbanks, R. G. and Wiebe, P. H.: Foraminifera and Chlorophyll Maximum: Vertical Distribution, Seasonal
732   Succession, and Paleoceanographic Significance, Science, 209, 1524–1526, 1980.

733 Fairbanks, R. G., Sverdlove, M., Free, R., Wiebe, P. H. and Bé, A. W. H.: Vertical distribution and isotopic
734   fractionation of living planktonic foraminifera from the Panama Basin, Nature, 298, 841–844, 1982.

735 Farmer, E. C., Kaplan, A., de Menocal, P. B. and Lynch-Stieglitz, J.: Corroborating ecological depth preferences
736   of planktonic foraminifera in the tropical Atlantic with the stable oxygen isotope ratios of core top
737   specimens, Paleoceanography, 22, 1–14, 2007.

738 Feely, R.: Impact of Anthropogenic CO_2 on the $CaCO_3$ System in the Oceans, Science, 305, 362–366, 2004.

739 Ferguson, J. E., Henderson, G. M., Kucera, M. and Rickaby, R. E. M.: Systematic change of foraminiferal
740   Mg/Ca ratios across a strong salinity gradient, Earth Planet. Sci. Lett., 265, 153–166, 2008.

741 Foster, G. L.: Seawater pH, pCO2 and [CO_3^{2-}] variations in the Caribbean Sea over the last 130 kyr: A boron
742   isotope and B/Ca study of planktic foraminifera, Earth Planet. Sci. Lett., 271, 254–266, 2008.

743 Foster, G. L. and Sexton, P. F.: Enhanced carbon dioxide outgassing from the eastern equatorial Atlantic during
744   the last glacial, Geology, 42, 1003–1006, 2014.

745 Foster, G. L., Lear, C. H. and Rae, J. W. B.: The evolution of pCO2, ice volume and climate during the middle
746   Miocene, Earth Planet. Sci. Lett., 341–344, 243–254, 2012.

747 Foster, G. L. and Rae, J. W. B.: Reconstructing Ocean pH with Boron Isotopes in Foraminifera, Annu. Rev.
748   Earth Planet. Sci., 44, 207–237, 2016.

749 Gabitov, R. I., Rollion-bard, C., Tripati, A. and Sadekov, A.: In situ study of boron partitioning between calcite
750   and fluid at different crystal growth rates, Geochim. Cosmochim. Acta, 137, 81–92, 2014.

751 Gaillardet, J., Lemarchand, D., Göpel, C. and Manhès, G.: Evaporation and Sublimation of Boric Acid :
752   Application for Boron Purification from Organic Rich Solutions, Geostand. Newsl., 25, 67–75, 2001.

753 Gast R. J. and Caron D. A.: Photosymbiotic associations in planktonic foraminifera and radiolaria, 1–7, 2001.

754 Gastrich, M.D.: Ultrastructure of a new intracellular symbiotic alga found within planktonic foraminifera,
755   Journal of Phycology 23, 623-632, 1988.

756 Gattuso, J.P. and Hansson, L.: Ocean acidification, Oxford University Press, 2011.

757 Hallock P.: Algal Symbiosis : A Mathematical Analysis Marine Biology 62, 249-255, 1981b.

758 Hemming, N. G. and Hanson, G. N. Boron isotopic composition and concentration in modern marine carbonates,
759   Geochim. Cosmochim. Acta, 56, 537–543, 1992.

760 Hendry, K.R., Rickaby, R.E.M., Meredith, M.P., Elderfield, H.: Controls on sta-ble isotope and trace metal
761   uptake in Neogloboquadrina pachyderma (sinis-tral) from an Antarctic sea-ice environment. Earth Planet.
762   Sci. Lett.278, 67–77, 2009.

763 Henehan, M. J., Foster, G. L., Bostock, H. C., Greenop, R., Marshall, B. J. and Wilson, P. A.: A new boron
764   isotope-pH calibration for Orbulina universa, with implications for understanding and accounting for 'vital
765   effects', Earth Planet. Sci. Lett., 454, 282–292, 2016.

766 Henehan, M. J., Foster, G. L., Rae, J. W. B., Prentice, K. C., Erez, J., Bostock, H. C., Marshall, B. J. and Wilson,
767   P. A.: Evaluating the utility of B/Ca ratios in planktic foraminifera as a proxy for the carbonate system: A
768   case study of Globigerinoides ruber, Geochemistry, Geophys. Geosystems 16, 1052–1069, 2015.

769 Henehan, M. J., Rae, J. W. B., Foster, G. L., Erez, J., Prentice, K. C., Kucera, M., Bostock, H. C., Martínez-Botí,
770   M. A., Milton, J. A., Wilson, P. A., Marshall, B. J. and Elliott, T.: Calibration of the boron isotope proxy in
771   the planktonic foraminifera Globigerinoides ruber for use in palaeo-CO2reconstruction, Earth Planet. Sci.
772   Lett. 364, 111–122, 2013.

773 Holcomb, M., Decarlo, T. M., Schoepf, V., Dissard, D., Tanaka, K. and McCulloch, M.: Cleaning and pre-
774   treatment procedures for biogenic and synthetic calcium carbonate powders for determination of elemental
775   and boron isotopic compositions, Chem. Geol., 398, 11–21, 2015.

776 Hönisch, B., Hemming, N. G., Archer, D., Siddall, M. and McManus, J. F.: Atmospheric Carbon Dioxide
777   Concentration Across the Mid-Pleistocene Transition, Science, 324, 1551–1554, 2009.

778 Hönisch, B., Bijma, J., Russell, A. D., Spero, H. J., Palmer, M. R., Zeebe, R. E. and Eisenhauer, A.: The
779   influence of symbiont photosynthesis on the boron isotopic composition of foraminifera shells, Mar.
780   Micropaleontol., 49, 87–96, 2003.

781 Hönisch, B. and Hemming, N. G.: Ground-truthing the boron isotope-paleo-pH proxy in planktonic foraminifera
782   shells: Partial dissolution and shell size effects, Paleoceanography 19, 1–13, 2004.

783 Hönisch, B., Bickert, T. and Hemming, N. G.: Modern and Pleistocene boron isotope composition of the benthic
784   foraminifer Cibicidoides wuellerstorfi, Earth Planet. Sci. Lett., 272, 309–318, 2008.

785 Howes, E. L., Kaczmarek, K., Raitzsch, M., Mewes, A., Bijma, N., Horn, I., Misra, S., Gattuso, J. P. and Bijma,
786   J.: Decoupled carbonate chemistry controls on the incorporation of boron into Orbulina universa,
787   Biogeosciences, 14, 415–430, 2017.

788 IPCC: Climate Change 2014 - The Physical Science Basis, edited by Intergovernmental Panel on Climate
789   Change, Cambridge University Press, Cambridge., 2014.

790 Jørgensen, B. B., Erez, J., Revsbech, P. and Cohen, Y.: Symbiotic photosynthesis in a planktonic foraminifera,
791   Globigerinoides sacculifer (Brady), studied with microelectrodes, Limnol. Oceanogr., 30, 1253–1267
792   1985.

793 Kaczmarek, K., Nehrke, G., Misra, S., Bijma, J. and Elderfield, H.: Investigating the effects of growth rate and
794   temperature on the B/Ca ratio and δ11B during inorganic calcite formation, Chem. Geol., 421, 81–92,
795   2016.

796 Kemle-von Mücke S. and Oberhänsli H.: The Distribution of Living Planktic Foraminifera in Relation to
797   Southeast Atlantic Oceanography, Use Proxies Paleoceanogr., 91–115, 1999.

798 Key, R.M.: A global ocean carbon climatology: Results from Global Data Analysis Project (GLODAP), Global
799   Biogeochem. Cycles, 18, GB4031, 2004.

800 Kim, S.-T. and O'Neil, J. R.: Equilibrium and nonequilibrium oxygen isotope effects in synthetic carbonates,
801   Geochim. Cosmochim. Acta, 61, 3461–3475, 1997.

802 Klochko, K., Cody, G. D., Tossell, J. A., Dera, P. and Kaufman, A. J.: Re-evaluating boron speciation in
803   biogenic calcite and aragonite using 11B MAS NMR, Geochim. Cosmochim. Acta, 73, 1890–1900, 2009.

804 Klochko, K., Kaufman, A. J., Yao, W., Byrne, R. H. and Tossell, J. A.: Experimental measurement of boron
805   isotope fractionation in seawater, Earth Planet. Sci. Lett., 248, 276–285, 2006.

806 Köhler-Rink, S. and Kühl, M.: Microsensor studies of photosynthesis and respiration in larger symbiotic
807   foraminifera. I. The physico-chemical microenvironment of Marginopora vertebralis, Amphistegina
808   lobifera and Amphisorus hemrichii, Mar. Biol., 137, 473–486, 2000.

809   Köhler-Rink, S. and Kühl, M., Microsensor studies of photosynthesis and respiration in the larger symbiont
810   bearing foraminifera Amphistegina lobifera, and Amphisorus hemprichii, Ophelia, 55, 111–122, 2001.

811   Lea, D. W., Pak, D. K. and Spero, H. J.: Climate impact of late quaternary equatorial Pacific sea surface
812   temperature variations, Science, 289, 1719–1724, 2000.

813   Lemarchand, D., Gaillardet, J., Lewin, A. and Allègre, C. J.: Boron isotope systematics in large rivers:
814   Implications for the marine boron budget and paleo-pH reconstruction over the Cenozoic, Chem. Geol.,
815   190, 123–14, 2002.

816   Liu, Y., Liu, W., Peng, Z., Xiao, Y., Wei, G., Sun, W., He, J., Liu, G. and Chou, C.-L.: Instability of seawater
817   pH in the South China Sea during the mid-late Holocene: Evidence from boron isotopic composition of
818   corals, Geochim. Cosmochim. Acta, 73, 1264–1272, 2009.

819   Lloyd, N. S., Sadekov, A. Y. and Misra, S.: Application of 1013ohm Faraday cup current amplifiers for boron
820   isotopic analyses by solution mode and laser ablation multicollector inductively coupled plasma mass
821   spectrometry, Rapid Commun. Mass Spectrom., 32, 9–18, 2018.

822   Martínez-Botí, M. A., Foster, G. L., Chalk, T. B., Rohling, E. J., Sexton, P. F., Lunt, D. J., Pancost, R. D.,
823   Badger, M. P. S. and Schmidt, D. N.: Plio-Pleistocene climate sensitivity evaluated using high-resolution
824   CO2 records, Nature, 518, 49–54, 2015a.

825   Martínez-Botí M. A., Marino G., Foster G. L., Ziveri P., Henehan M. J., Rae J. W. B., Mortyn P. G. and Vance
826   D.: Boron isotope evidence for oceanic carbon dioxide leakage during the last deglaciation. Nature, 518,
827   219–222, 2015b.

828   Martínez-Botí, M. A., Mortyn, P. G., Schmidt, D. N., Vance, D. and Field, D. B.: Mg/Ca in foraminifera from
829   plankton tows: Evaluation of proxy controls and comparison with core tops, Earth Planet. Sci. Lett., 307,
830   113–125, 2011.

831   Mavromatis, V., Montouillout, V., Noireaux, J., Gaillardet, J. and Schott, J.: Characterization of boron
832   incorporation and speciation in calcite and aragonite from co-precipitation experiments under controlled
833   pH, temperature and precipitation rate, Geochim. Cosmochim. Acta, 150, 299–313, 2015.

834   McCulloch, M. T., D'Olivo, J. P., Falter, J. L., Georgiou, L., Holcomb, M., Montagna, P. and Trotter, J. A.
835   Boron Isotopic Systematics in Scleractinian Corals and the Role of pH Up-regulation, Boron Isot. Adv.
836   Isot. Geochemistry, 2018.

837   Millero, F.: Speciation of metals in natural waters, Geochem. Trans., 2, 57, 2001.

838   Millero, F., Woosley, R., DiTrolio, B. and Waters, J.: Effect of Ocean Acidification on the Speciation of Metals
839   in Seawater, Oceanography 22, 72–85, 2009.

840   Misra, S., Greaves, M., Owen, R., Kerr, J., Elmore, A. C. and Elderfield, H.: Determination of B/Ca of natural
841   carbonates by HR-ICP-MS, Geochemistry, Geophys. Geosystems, 15, 1617–1628, 2014a.

842   Misra, S., Owen, R., Kerr, J., Greaves, M. and Elderfield, H.: Determination of δ11B by HR-ICP-MS from mass
843   limited samples: Application to natural carbonates and water samples, Geochim. Cosmochim. Acta, 140,
844   531–552, 2014b.

845   Mortyn, P. G. and Charles, C. D.: Planktonic foraminiferal depth habitat and δ 18 O calibrations: Plankton tow
846   results from the Atlantic sector of the Southern Ocean, Paleoceanography, 18, 2003.

847   Mulitza, S., Boltovskoy, D., Donner, B., Meggers, H., Paul, A. and Wefer, G.: Temperature:δ18O relationships
848   of planktonic foraminifera collected from surface waters, Palaeogeogr. Palaeoclimatol. Palaeoecol., 202,
849   143–152, 2003.

850 Ni, Y., Foster, G. L., Bailey, T., Elliott, T., Schmidt, D. N., Pearson, P., Haley, B. and Coath, C.: A core top
851   assessment of proxies for the ocean carbonate system in surface-dwelling foraminifers, Paleoceanography
852   22, 2007.

853 Nir, O., Vengosh, A., Harkness, J. S., Dwyer, G. S. and Lahav, O.: Direct measurement of the boron isotope
854   fractionation factor: Reducing the uncertainty in reconstructing ocean paleo-pH, Earth Planet. Sci. Lett.,
855   414, 1–5, 2015.

856 Noireaux, J., Mavromatis, V., Gaillardet, J., Schott, J., Montouillout, V., Louvat, P., Rollion-Bard, C. and
857   Neuville, D. R.: Crystallographic control on the boron isotope paleo-pH proxy, Earth Planet. Sci. Lett.,
858   430, 398–407, 2015.

859 Orr, J. C., Fabry, V. J., Aumont, O., Bopp, L., Doney, S. C., Feely, R. A., Gnanadesikan, A., Gruber, N., Ishida,
860   A., Joos, F., Key, R. M., Lindsay, K., Maier-Reimer, E., Matear, R., Monfray, P., Mouchet, A., Najjar, R.
861   G., Plattner, G. K., Rodgers, K. B., Sabine, C. L., Sarmiento, J. L., Schlitzer, R., Slater, R. D., Totterdell, I.
862   J., Weirig, M. F., Yamanaka, Y. and Yool, A.: Anthropogenic ocean acidification over the twenty-first
863   century and its impact on calcifying organisms, Nature, 437, 681–686, 2005.

864 Pagani. M.: Marked Decline in Atmospheric Carbon Dioxide Concentrations During the Paleogene, Science,
865   309, 600–603, 2005.

866 Palmer, M. R., Pearson, P. N. and Cobb, S. J., Reconstructing Past Ocean pH-Depth Profiles, Science, 282,
867   1468–1471, 1998.

868 Pearson, P. N. and Palmer, M. R.: Middle Eocene seawater pH and atmospheric carbon dioxide concentrations,
869   Science, 284, 1824–1826, 1999.

870 Peeters, F. J. C. and Brummer, G.-J. a.: The seasonal and vertical distribution of living planktic foraminifera in
871   the NW Arabian Sea, Geol. Soc. London, Spec. Publ., 195, 463–497, 2002.

872 Quintana Krupinski, N. B., Russell, A. D., Pak, D. K. and Paytan, A.: Core-top calibration of B/Ca in Pacific
873   Ocean Neogloboquadrina incompta and Globigerina bulloides as a surface water carbonate system proxy,
874   Earth Planet. Sci. Lett., 466, 139–151, 2017.

875 Rae, J.W.B.: Boron Isotopes in Foraminifera: Systematics, Biomineralisation, and CO_2 Reconstruction. In:
876   Marschall, H., Foster, G. (eds), Boron Isotopes. Advances in Isotope Geochemistry. Springer, Cham, 2018.

877 Rae, J. W. B., Foster, G. L., Schmidt, D. N. and Elliott, T.: Boron isotopes and B/Ca in benthic foraminifera:
878   Proxies for the deep ocean carbonate system, Earth Planet. Sci. Lett., 302, 403–413, 2011.

879 Raitzsch, M., Bijma, J., Benthien, A., Richter, K.-U., Steinhoefel, G. and Kučera, M.: Boron isotope-based
880   seasonal paleo-pH reconstruction for the Southeast Atlantic – A multispecies approach using habitat
881   preference of planktonic foraminifera, Earth Planet. Sci. Lett., 487, 138–150, 2018.

882 Ravelo, A. C. and Fairbanks, R. G.: Oxygen isotopic composition of multiple species of planktonic foraminifera:
883   recorder of the modern photic zone temperature gradient, Palaeogeogr. Palaeoclimatol. Palaeoecol., 7,
884   815–831, 1992.

885 Regenberg, M., Nürnberg, D., Steph, S., Groeneveld, J., Garbe-Schönberg, D., Tiedemann, R. and Dullo, W.-C.:
886   Assessing the effect of dissolution on planktonic foraminiferal Mg/Ca ratios: Evidence from Caribbean
887   core tops, Geochemistry, Geophys. Geosystems, 7, 2006.

888 Regenberg, M., Steph, S., Nürnberg, D., Tiedemann, R. and Garbe-Schönberg, D.: Calibrating Mg/Ca ratios of
889   multiple planktonic foraminiferal species with δ18O-calcification temperatures: Paleothermometry for the
890   upper water column, Earth Planet. Sci. Lett., 278, 324–336, 2009.

891 Rickaby, R. E. M. and Halloran, P.: Cool La Nina During the Warmth of the Pliocene?, Science, 307, 1948–
892   1952, 2005.

893 Ries, J. B., Cohen, A. L. and McCorkle, D. C.: Marine calcifiers exhibit mixed responses to CO2-induced ocean
894   acidification, Geology, 37, 1131–1134, 2009.

895 Rink, S., Kühl, M., Bijma, J. and Spero, H. J.: Microsensor studies of photosynthesis and respiration in the
896   symbiotic foraminifer Orbulina universa, Mar. Biol., 131, 583–595, 1998.

897 Rollion-Bard, C. and Erez, J.: Intra-shell boron isotope ratios in the symbiont-bearing benthic foraminiferan
898   Amphistegina lobifera: Implications for δ11B vital effects and paleo-pH reconstructions, Geochim.
899   Cosmochim. Acta, 74, 1530–1536, 2010.

900 Rostek, F., Ruhland, G., Bassinot, F. C., Muller, P. J., Labeyrie, L. D., Lancelot, Y. and Bard, E.: Reconstructing
901   Sea-Surface Temperature and Salinity Using δ18O and Alkenone Records, Nature, 364, 319–321, 1993.

902 Russell, A. D., Hönisch, B., Spero, H. J. and Lea, D. W.: Effects of seawater carbonate ion concentration and
903   temperature on shell U, Mg, and Sr in cultured planktonic foraminifera, Geochim. Cosmochim. Acta, 68,
904   4347–4361, 2004.

905 Sanyal, A., Bijma, J., Spero, H. J. and Lea, D. W.: Empirical relationship between pH and the boron isotopic
906   composition of Globigerinoides sacculifer: Implications for the boron isotopes paleo-pH proxy,
907   Paleoceanography, 16, 515–519, 2001.

908 Sanyal, A., Hemming, N. G., Broecker, W. S., Lea, D. W., Spero, H. J., & Hanson, G. N. Oceanic pH control on
909   the boron isotopic composition of foraminifera: evidence from culture experiments, Paleoceanography,
910   11(5), 513-517, 1996.

911 Schmidt, G. A. and Mulitza, S.: Global calibration of ecological models for planktic foraminifera from core-top
912   carbonate oxygen-18, Mar. Micropaleontol., 44, 125–140, 2002.

913 Seki, O., Foster, G. L., Schmidt, D. N., Mackensen, A., Kawamura, K. and Pancost, R. D.: Alkenone and boron-
914   based Pliocene pCO2records, Earth Planet. Sci. Lett., 292, 201–211, 2010.

915 Shirayama, Y.: Effect of increased atmospheric CO2 on shallow water marine benthos, J. Geophys. Res., 110,
916   C09S08, 2005.

917 Sime, N. G., De La Rocha, C. L. and Galy, A.: Negligible temperature dependence of calcium isotope
918   fractionation in 12 species of planktonic foraminifera, Earth Planet. Sci. Lett., 232, 51–66, 2005.

919 Spero H. J.: Symbiosis in the planktonic foraminifer, orbulina universa, and the isolation of its symbiotic
920   dinoflagellate, gymnodinium beii sp.nov, J. Phycol 23, 307-317, 1987.

921 Sutton, J. N., Liu, Y. W., Ries, J. B., Guillermic, M., Ponzevera, E. and Eagle, R. A.: δ11B as monitor of
922   calcification site pH in divergent marine calcifying organisms, Biogeosciences, 15, 1447–1467, 2018.

923 Takagi H., Kimoto K., Fujiki T., Saito H., Schmidt C. and Kucera M.: Characterizing photosymbiosis in modern
924   planktonic foraminifera, biogeosciences, 3377–3396, 2019.

925 Thomson, J., Brown, L., Nixon, S., Cook, G. T. and MacKenzie, A. B.: Bioturbation and Holocene sediment
926   accumulation fluxes in the north-east Atlantic Ocean (Benthic Boundary Layer experiment sites), Mar.
927   Geol., 169, 21–39, 2000.

928 Tripati, A.: Deep-Sea Temperature and Circulation Changes at the Paleocene-Eocene Thermal Maximum.
929   Science, 308, 1894–1898, 2005.

930   Tripati, A. K., Roberts, C. D. and Eagle, R. A.: Coupling of CO2 and Ice Sheet Stability Over Major Climate
931   Transitions of the Last 20 Million Years, Science, 326, 1394–1397, 2009.

932   Tripati, A. K., Roberts, C. D., Eagle, R. A. and Li, G.: A 20 million year record of planktic foraminiferal B/Ca
933   ratios: Systematics and uncertainties in pCO2reconstructions, Geochim. Cosmochim. Acta, 75, 2582–
934   2610, 2011.

935   Uchikawa, J., Penman, D. E., Zachos, J. C. and Zeebe, R. E.: Experimental evidence for kinetic effects on B/Ca
936   in synthetic calcite: Implications for potential B(OH)4− and B(OH)3 incorporation, Geochim. Cosmochim.
937   Acta, 150, 171–191, 2015.

938   Urey, H.C., Lowenstam, H.A., Epstein, S. & McKinney, C.R.: Measurement of paleo-temperature and
939   temperatures of the upper cretaceous of England, Denmark, and the southeastern United-States. Geol. Soc.
940   Am. Bull., 62, 399-416, 1951.

941   Wang, B.-S., You, C.-F., Huang, K.-F., Wu, S.-F., Aggarwal, S. K., Chung, C.-H. and Lin, P.-Y.: Direct
942   separation of boron from Na- and Ca-rich matrices by sublimation for stable isotope measurement by MC-
943   ICP-MS, Talanta, 82, 1378–1384, 2010.

944   Wang, G., Cao, W., Yang, D. and Xu, D.: Variation in downwelling diffuse attenuation coefficient in the
945   northern South China Sea, Chinese J. Oceanol. Limnol., 26, 323–333, 2008.

946   Weare, B. C., Strub, P. T. and Samuel, M. D. Annual Mean Surface Heat Fluxes in the Tropical Pacific Ocean, J.
947   Phys. Oceanogr., 11, 705–717, 1981.

948   Wei, G., McCulloch, M. T., Mortimer, G., Deng, W. and Xie, L.: Evidence for ocean acidification in the Great
949   Barrier Reef of Australia, Geochim. Cosmochim. Acta, 73, 2332–2346, 2009.

950   Wilson, D. J., Piotrowski, A. M., Galy, A. and McCave, I. N.: A boundary exchange influence on deglacial
951   neodymium isotope records from the deep western Indian Ocean, Earth Planet. Sci. Lett., 341–344, 35–47,
952   2012.

953   Wolf-Gladrow, D. A., Riebesell, U., Burkhardt, S. and Buma, J.: Direct effects of CO2 concentration on growth
954   and isotopic composition of marine plankton, Tellus B Chem. Phys. Meteorol., 51, 461–476, 1999.

955   Yu, J., Menviel, L., Jin, Z. D., Thornalley, D. J. R., Barker, S., Marino, G., Rohling, E. J., Cai, Y., Zhang, F.,
956   Wang, X., Dai, Y., Chen, P. and Broecker, W. S.: Sequestration of carbon in the deep Atlantic during the
957   last glaciation, Nat. Geosci., 9, 319–324, 2016.

958   Yu, J., Thornalley, D. J. R., Rae, J. W. B. and McCave, N. I.: Calibration and application of B/Ca, Cd/Ca, and δ
959   11 B in Neogloboquadrina pachyderma (sinistral) to constrain CO 2 uptake in the subpolar North Atlantic
960   during the last deglaciation, Paleoceanography, 28, 237–252, 2013.

961   Yu, J., Foster, G. L., Elderfield, H., Broecker, W. S. and Clark, E.: An evaluation of benthic foraminiferal B/Ca
962   and δ11B for deep ocean carbonate ion and pH reconstructions, Earth Planet. Sci. Lett., 293, 114–120, 20,
963   2010.

964   Yu, J., Elderfield, H., Hönisch, B.: B/Ca in planktonic foraminifera as a proxy for surface seawater pH.
965   Paleoceanography22, PA2202, 2007.

966   Yu, J., Day, J., Greaves, M. and Elderfield, H., Determination of multiple element/calcium ratios in foraminiferal
967   calcite by quadrupole ICP-MS, Geochemistry, Geophys. Geosystems 6, 2005.

968   Zeebe, R. E. and Wolf-Gladrow, D., CO2 in Seawater: Equilibrium, Kinetics, Isotopes Elsevier Oceanography
969   Series 65, Amsterdam, 2001.

970   Zeebe, R. E., Wolf-Gladrow, D. A., Bijma, J. and Hönisch, B.,Vital effects in foraminifera do not compromise
971   the use of δ 11 B as a paleo- pH indicator: Evidence from modeling, Paleoceanography, 18, 2003.

972   **Figure caption**

973

974   **Figure 1:** Reactions governing dissolved inorganic carbon equilibria.

975

976   **Figure 2:** (A) Speciation of H_3BO_3 and $H_4BO_4^-$ as function of seawater pH (total scale), (B) $\delta^{11}B$ of dissolved

977   inorganic boron species as a function of seawater pH, (C) sensitivity of $\delta^{11}B$ of $H_4BO_4^-$ for a pH ranging from

978   7.6 to 8.4. T=25°C, S=35, $\delta^{11}B$=39.61 ‰ (Foster et al., 2010), dissociation constant α = 1.0272 (Klochko et al.,

979   2006).

980

981   **Figure 3:** Map showing locations of the core-tops used in this study (white diamonds). Red open circles

982   represent the sites used for *in-situ* carbonate parameters from GLODAP database (Key et al., 2004).

983

984   **Figure 4:** Pre-industrial data versus depth of the sites used in this study. The figure shows seasonal temperatures

985   (extracted from World Ocean Database 2013), density anomaly (kg/m^3), pre-industrial pH and pre-industrial

986    $\delta^{11}B$ of $H_4BO_4^-$ (calculated from the GLODAP database and corrected for anthropogenic inputs).

987

988   **Figure 5:** Boron isotopic measurements of mixed-layer foraminifera plotted against the $\delta^{11}B_{borate}$. $\delta^{11}B_{borate}$ were

989   characterized by determination of the calcification depth of the foraminifera, A) *G. ruber*, B) *T. sacculifer*, C) *O.*

990   *universa*. Mono-specific calibrations are summarized in Table 3.

991

992   **Figure 6:** Boron isotopic measurements of deep-dwelling foraminifera ($\delta^{11}B_{carbonate}$) plot against $\delta^{11}B_{borate}$.

993    $\delta^{11}B_{borate}$ were characterized by determining the calcification depth of foraminifera, A) *P. obliquiloculata*, B) *G.*

994   *menardii*, C) *N. dutertrei*, D) *G. tumida* and E) Compilation of deep dweller species. Mono-specific calibrations

995   are summarized in Table 3.

996

997   **Figure 7:** Boxplots of B/Ca ratios for multiple species, *T. sacculifer* (this study; Foster et al., 2008; Ni et al;

998   2007; Seki et al., 2010), *G. ruber* (this study; Babila et al., 2014; Foster et al., 2008; Ni et al., 2007), *G. inflata*,

999   *G. bulloides* (Yu et al., 2007), *N. pachyderma* (Hendry et al., 2009; Yu et al., 2013), *N. dutertrei* (this study;

1000   Foster et al., 2008), *O. universa, P.obliquiloculata, G. menardii, G. tumida* (this study).

1001

1002   **Figure 8:** A) Boxplot showing the calculated microenvironment pH difference (Δmicroenvironment pH)

1003   between microenvironment and external pH based on the $\delta^{11}B$ data. B) This figure shows that a decrease in

1004   insolation can explain the low $\delta^{11}B$ from the WEP. Light penetration profile in the Western Pacific, with E_0 in

1005   the WEP of 220 J.s-1.m-2 (Weare et al., 1981) and a light attenuation coefficient of 0.028 (Wang et al., 2008).

1006   Theoretical depths were calculated for a decrease in microenvironment pH of ΔpH_1= -0.02 (e.g. WP07-a);

1007 ΔpH_1= -0.04 (e.g. A14), ΔpH_2= -0.06 (e.g. 806A). Light penetration corresponding to Ec is ~12%, ΔpH_0~7%,

1008 ΔpH_1 ~5%, ΔpH_2 ~1% respective depth are 75m, 90m, 110m and 150m. Grey band is the calcification depth of

1009   *T. sacculifer* (w/o sacc) utilized in this study.

1010

1011   **Figure 9:** Water depth pH profiles reconstructed at every site applying the mono-specific calibrations derived

1012   from our results (Table 3). Figure is showing measured $\delta^{11}B_{calcite}$, $\delta^{11}B_{borate}$ calculated according to different

1013   calibrations (see Table 3 and text), calculated pH based on $\delta^{11}B$ ($pH_{\delta11B}$) and pCO_2 calculated from $pH_{\delta11B}$ and

1014   alkalinity.

1015

1016   **Figure 10:** Evaluation of the reconstructed parameters, $\delta^{11}B_{borate}$, pH and pCO_2 versus *in-situ* parameter. The

1017   recalculated parameters are consistent with *in-situ* data, except for *G. ruber*. This variability might be explained

1018   by the different test sizes.

1019   **Table caption**
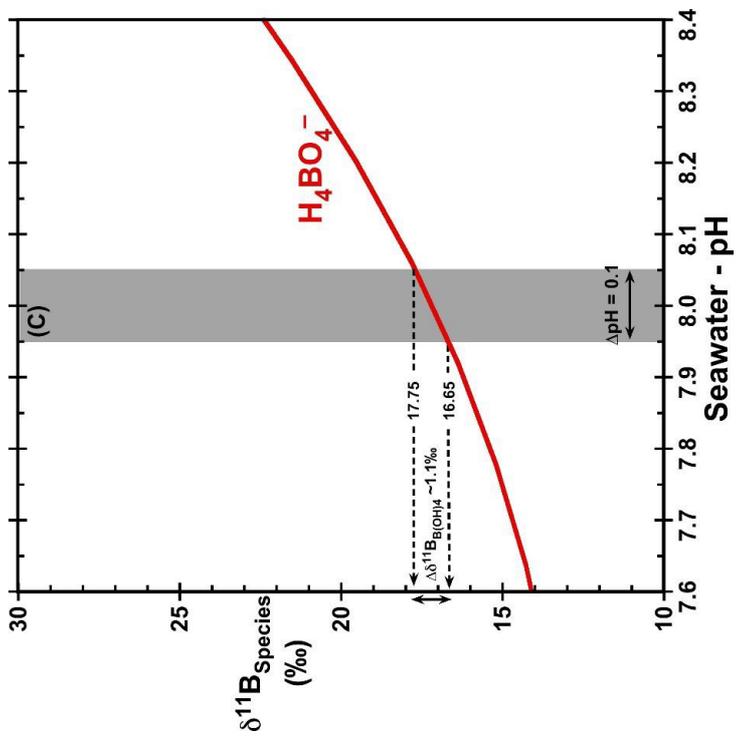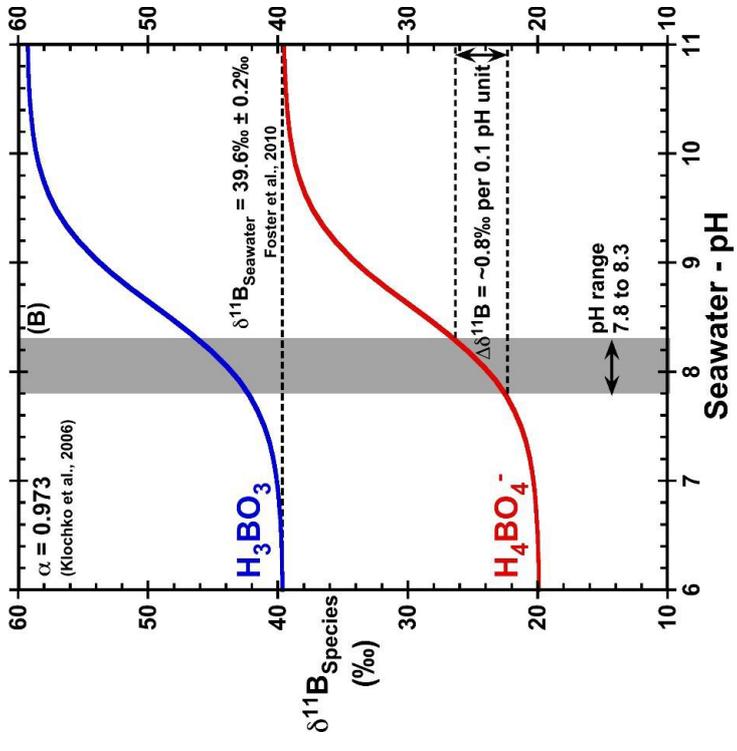
1020

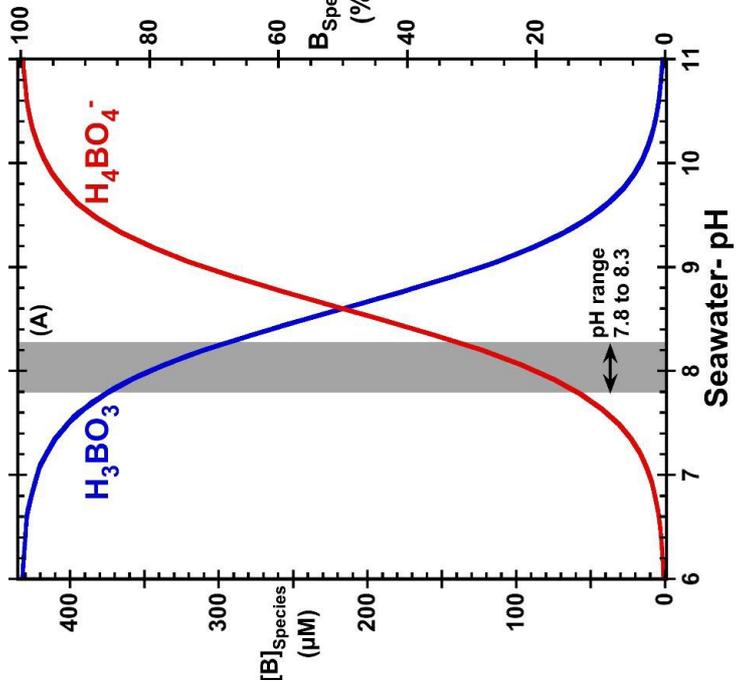1021   **Table 1:** Box-core information

1022

1023   **Table 2:** Analytical results of $\delta^{13}C$, $\delta^{18}O$, $\delta^{11}B$ and elemental ratios Li/Ca, B/Ca and Mg/Ca

1024

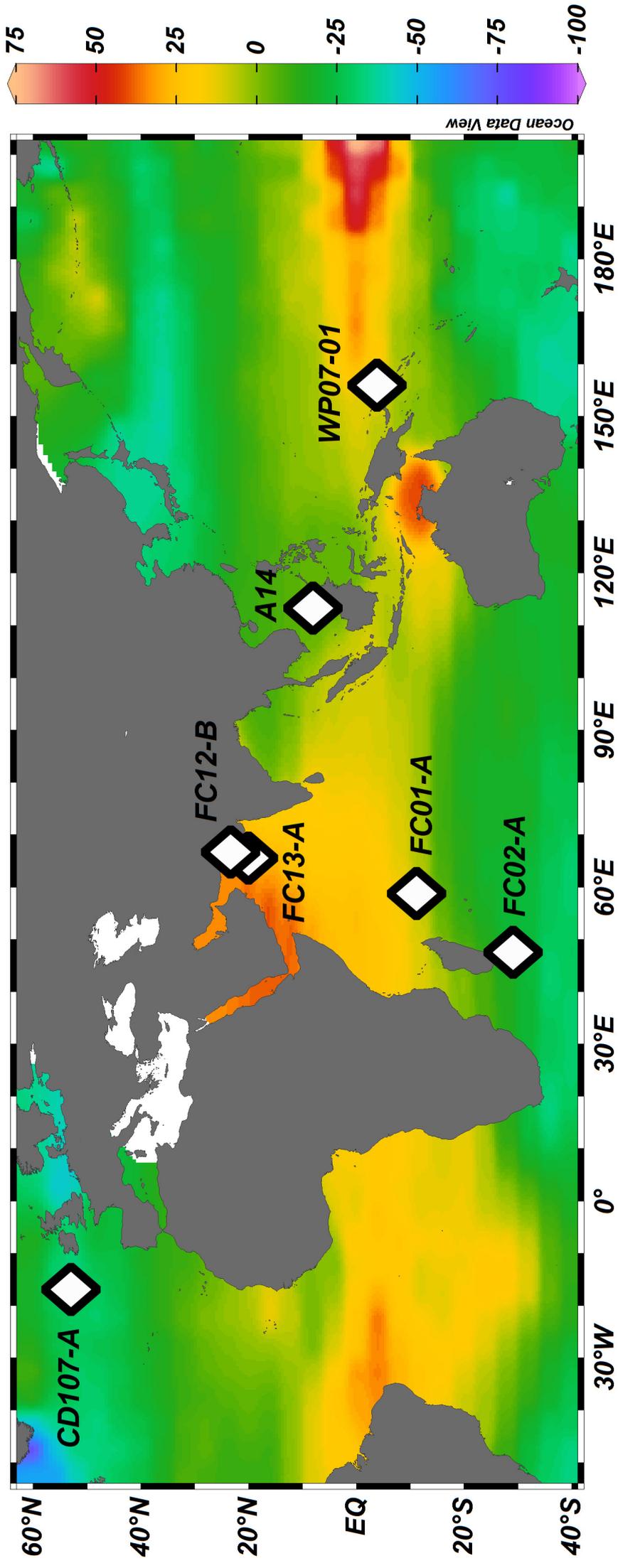1025   **Table 3:** Species-specific $\delta^{11}B_{carbonate}$ to $\delta^{11}B_{borate}$ calibrations from literature and from our data

atmosphere

seawater

CO_2

$CO_2\ (aq) + H_2O \rightleftharpoons HCO_3^- + H^+ \rightleftharpoons CO_3^{2-} + 2H^+$

(A)

$B_{Species}$
(%)

$H_4BO_4^-$

H_3BO_3

pH range
7.8 to 8.3

Seawater- pH

$[B]_{Species}$
(μM)

(B)

$\alpha = 0.973$
(Klochko et al., 2006)

H_3BO_3

$\delta^{11}B_{Seawater} = 39.6‰ \pm 0.2‰$
Foster et al., 2010

$\Delta\delta^{11}B = \sim0.8‰$ per 0.1 pH unit

$H_4BO_4^-$

pH range
7.8 to 8.3

Seawater - pH

$\delta^{11}B_{Species}$
(‰)

(C)

$H_4BO_4^-$

17.75

$\Delta\delta^{11}B_{B(OH)4} \sim1.1‰$

16.65

ΔpH = 0.1

Seawater - pH

$\delta^{11}B_{Species}$
(‰)
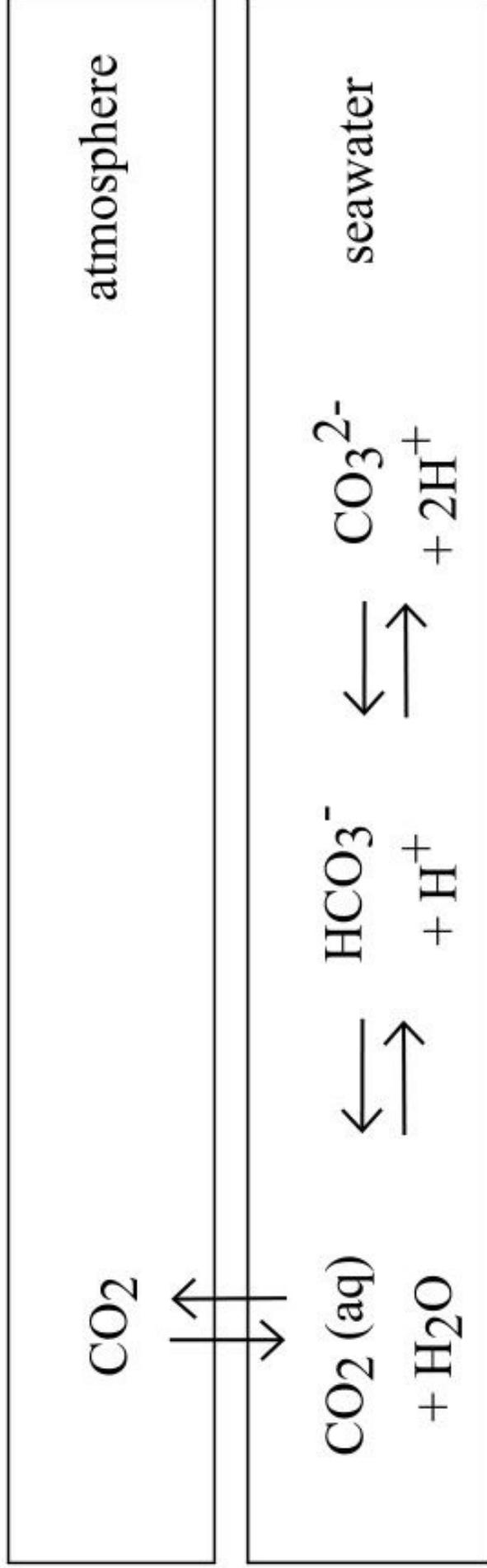
Delta pCO2 [μatm]
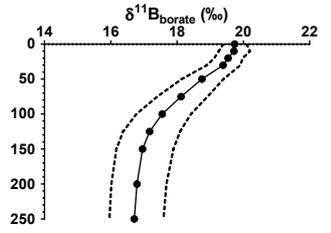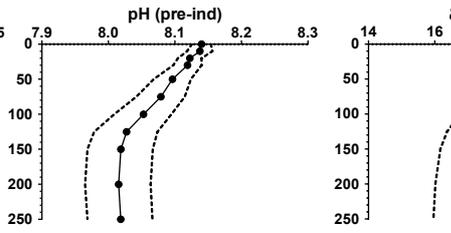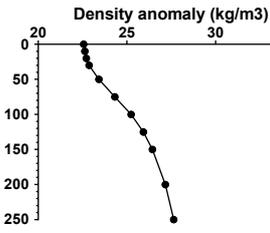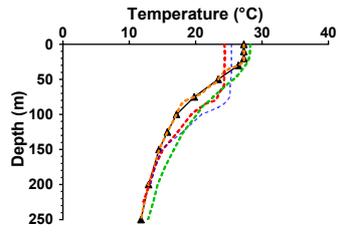
Temperature   **Density anomaly**   **pH (pre-ind)** $\delta^{11}B_{borate}$ (‰)

Atlantic Ocean

CD107-a
52.9°N, -16.9°E
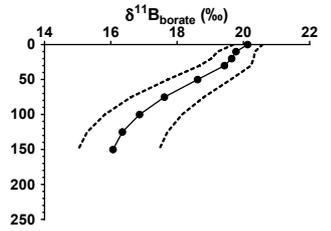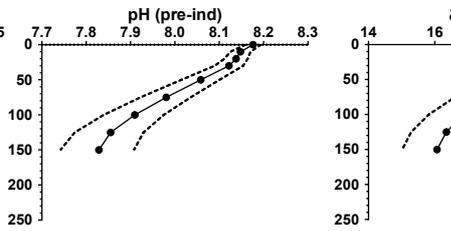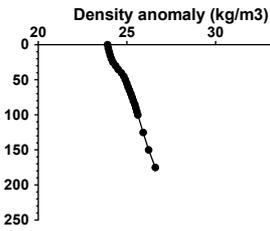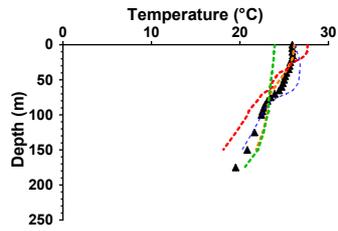3569 m

January-March
October-December
July-September
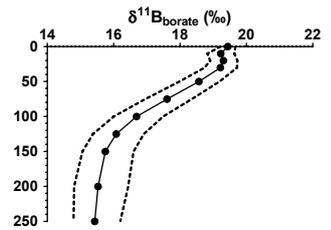April-June
Annual average
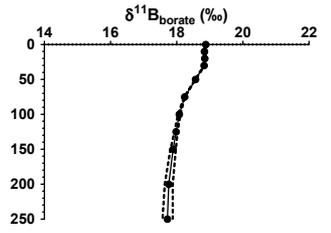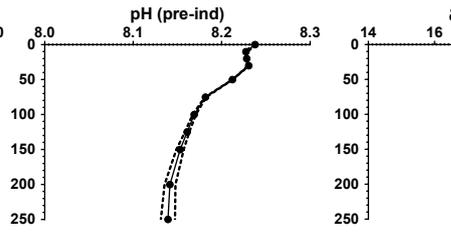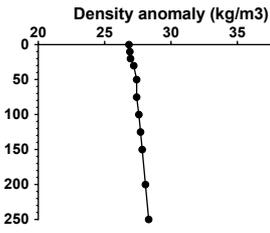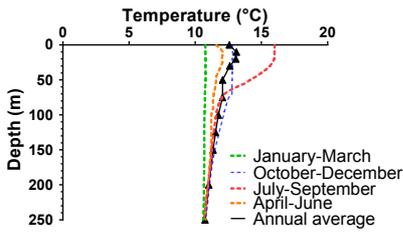
Indian Ocean

FC-01a
-11.2°N, 58.8°E
3520 m

FC-02a
-29.1°N, 47.5°E
2871 m
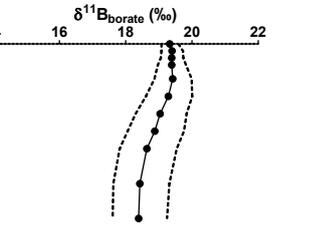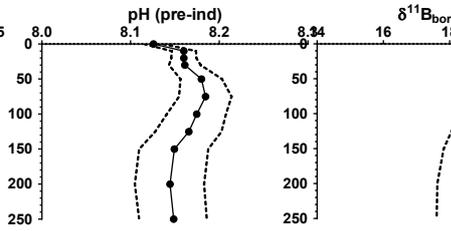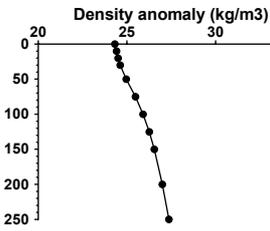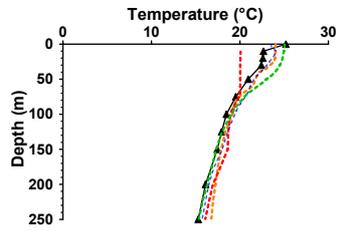
Arabian Sea

FC-12b
23.3°N, 66.7°E
151 m

FC-13a
20.0°N, 65.6°E
3190 m
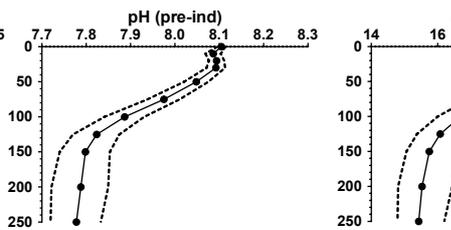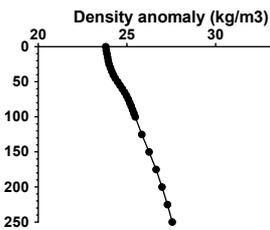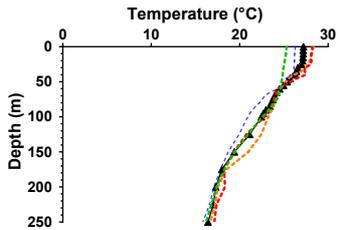
Pacific Ocean

WP07-01
-3.9°N,156.0°E
1800 m

A14
8.0°N,113.4°E
1911 m

(A)

δ¹¹B_carbonate (‰) vs δ¹¹B_borate (‰) — *G. ruber*
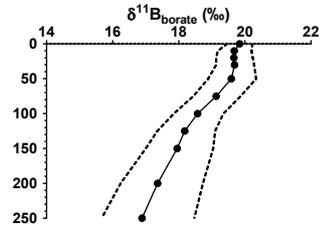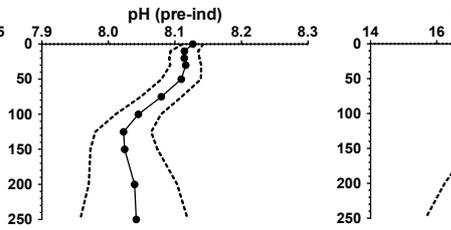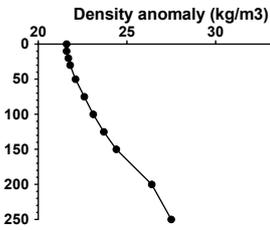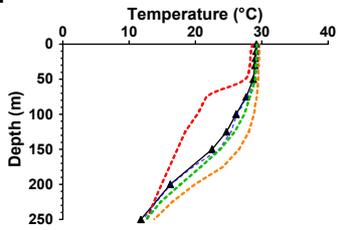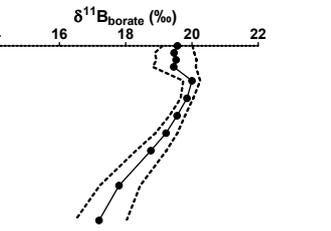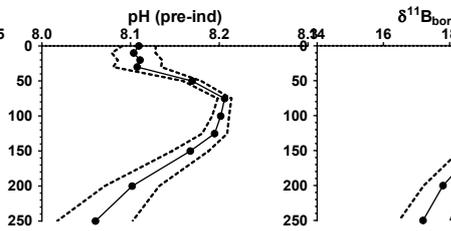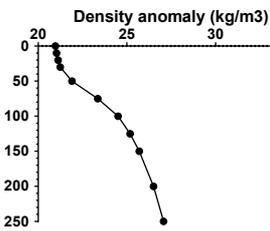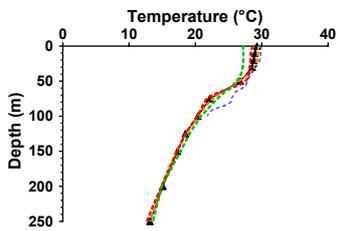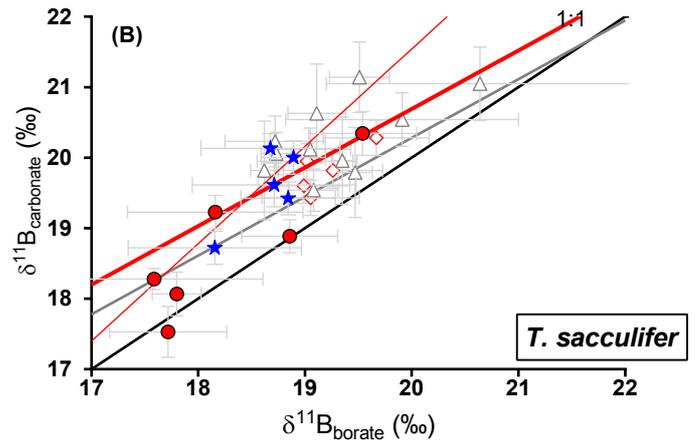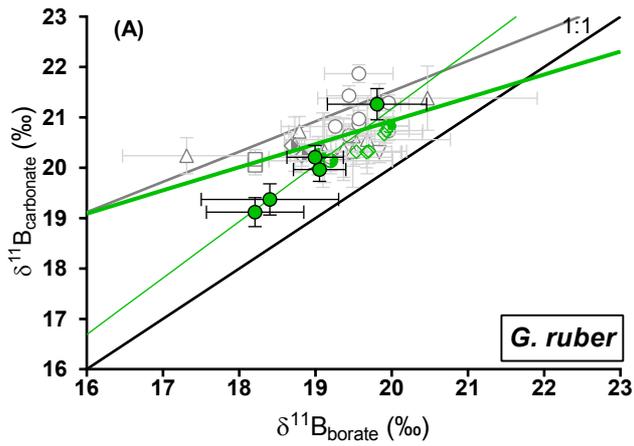
- ● δ¹¹B_{G. ruber} (core-top, this study)
- ◇ δ¹¹B_{G. ruber} (core-top, Foster et al., 2008)
- ◐ δ¹¹B_{G. ruber} (core-top, 250-300μm, Henehan et al., 2013)
- ○ δ¹¹B_{G. ruber} (core-top, Henehan et al., 2013)
- □ δ¹¹B_{G. ruber} (sediment trap, Henehan et al., 2013)
- ◈ δ¹¹B_{G. ruber} (tow, Henehan et al., 2013)
- ▽ δ¹¹B_{G. ruber} (grab sample, Henehan et al., 2013)
- △ δ¹¹B_{G. ruber} (Raizsch et al., 2018)
- —— *G. ruber* calibration line (All data, this study)
- — *G. ruber* calibration line (Core-top, this study)
- — *G. ruber* calibration line (Culture, Henehan et al., 2013)

(B)

δ¹¹B_carbonate (‰) vs δ¹¹B_borate (‰) — *T. sacculifer*

- ● δ¹¹B_{T.sacculifer (w/o sacc)} (core-top, this study)
- △ δ¹¹B_{T. sacculifer (w/o sacc)} (core-top, Raitzsch et al., 2018)
- ★ δ¹¹B_{T.sacculifer (sacc)} (core-top, this study)
- ◇ δ¹¹B_{T. sacculifer (sacc)} (core-top, Foster et al., 2008)
- —— *T. sacculifer (w/o sacc and sacc)* calibration line (All data, this study)
- — *T. sacculifer (w/o sacc and sacc)* calibration line (Core-top, this study)
- — *T. sacculifer (s)* calibration line (Martinez-Boti et al., 2015)

(C)

δ¹¹B_carbonate (‰) vs δ¹¹B_borate (‰) — *O. universa*
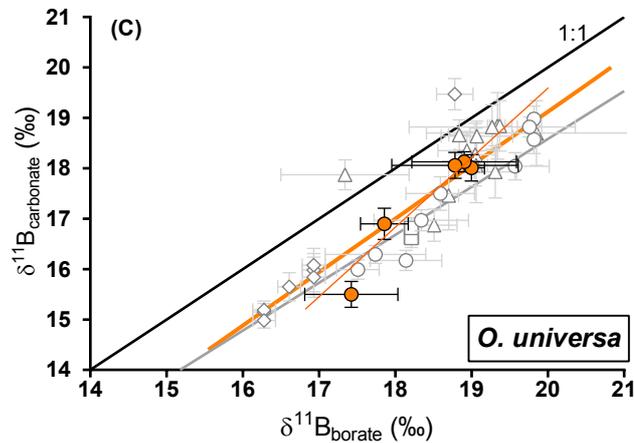
- ● δ¹¹B_{O. universa} (core-top, this study)
- ○ δ¹¹B_{O. universa} (core-top, Henehan et al., 2016)
- □ δ¹¹B_{O. universa} (sediment trap, Henehan et al., 2016)
- ◇ δ¹¹B_{O. universa} (tow, Henehan et al., 2016)
- △ δ¹¹B_{O. universa} (core-top, Raitzsch et al., 2018)
- — *O. universa* calibration line (core-top, this study)
- —— *O. universa* calibration line (this study, Henehan et al., 2016, Raitzsch et al., 2018)
- — *O. universa* calibration line (wild, Henehan et al., 2016)

(A) $\delta^{11}B_{carbonate}$ (‰) vs $\delta^{11}B_{borate}$ (‰)
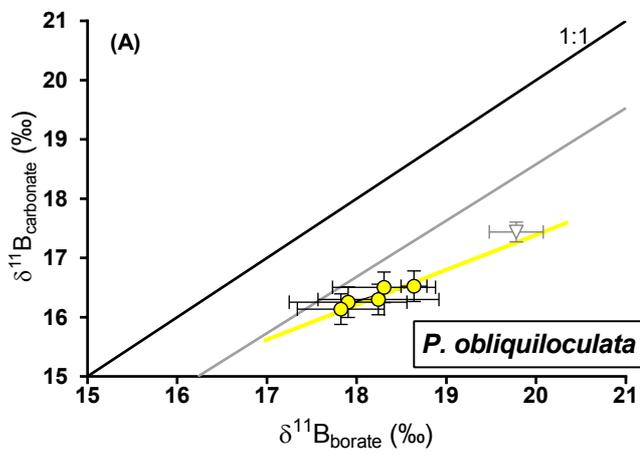
- ● $\delta^{11}B_{P.obliquiloculata}$ (Core-top, this study)
- ▽ $\delta^{11}B_{P.obliquiloculata}$ (Henehan et al., 2016)
- — *P. obliquiloculata* calibration line (this study, Henehan et al., 2016)
- — *O. universa* calibration curve (Henehan et al., 2016)

(B) $\delta^{11}B_{carbonate}$ (‰) vs $\delta^{11}B_{borate}$ (‰)
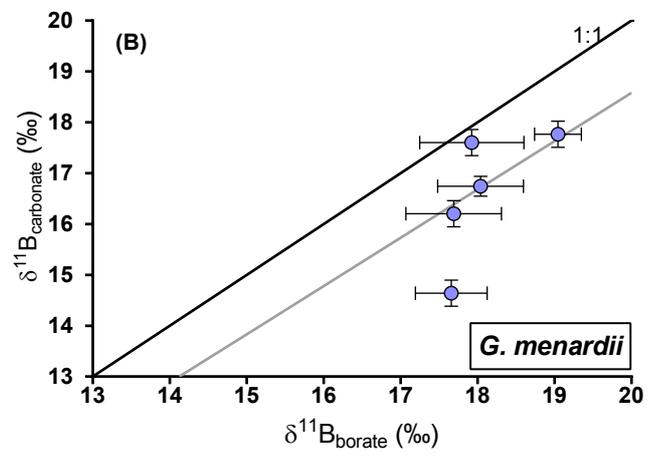
- ● $\delta^{11}B_{G. menardii}$ (this study)
- — *O. universa* calibration curve (Henehan et al., 2016)

(C) $\delta^{11}B_{carbonate}$ (‰) vs $\delta^{11}B_{borate}$ (‰)
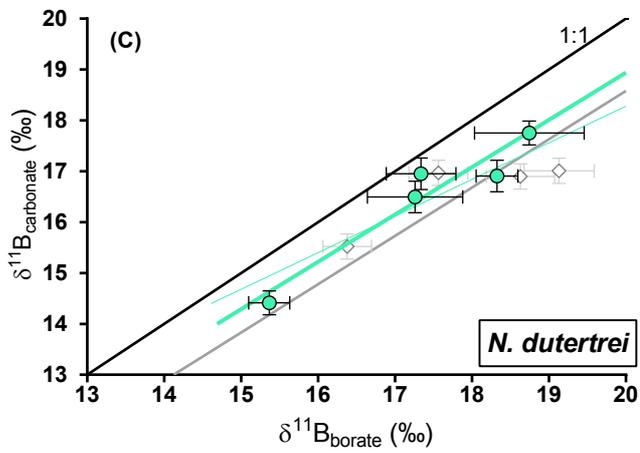
- ● $\delta^{11}B_{N. dutertrei}$ (Core-top, this study)
- ◇ $\delta^{11}B_{N. dutertrei}$ (Core-top, Foster et al., 2008)
- — *O. universa* calibration line (This study)
- — *O. universa* calibration line (This study, Foster et al., 2008)
- — *O. universa* calibration line (Henehan et al., 2016)

(D) $\delta^{11}B_{carbonate}$ (‰) vs $\delta^{11}B_{borate}$ (‰)
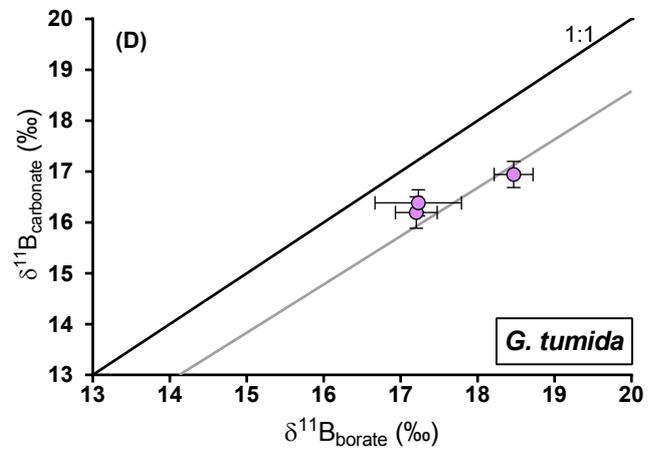
- ● $\delta^{11}B_{G. tumida}$ (this study)
- — *O. universa* calibration curve (Henehan et al., 2016)

(E) $\delta^{11}B_{carbonate}$ (‰) vs $\delta^{11}B_{borate}$
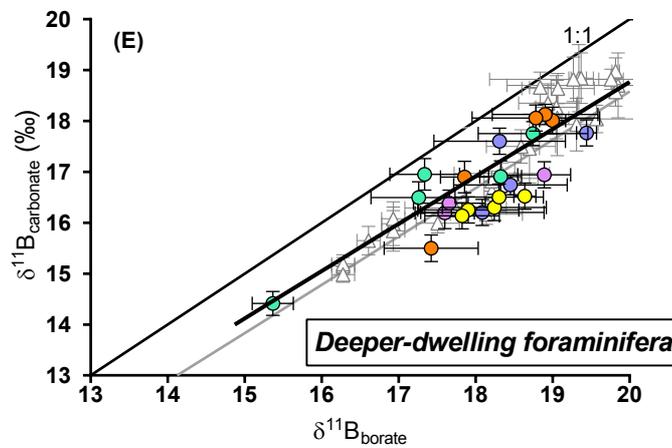
- ● $\delta^{11}B_{O.universa}$
- ● $\delta^{11}B_{P.obliquiloculata}$
- ● $\delta^{11}B_{N. dutertrei}$
- ● $\delta^{11}B_{G. menardii}$
- ● $\delta^{11}B_{G. tumida}$
- △ $\delta^{11}B_{deep-dweller}$ from literature
- — Deep-dweller calibration line
- — *O. universa* calibration line (Henehan et al., 2016)
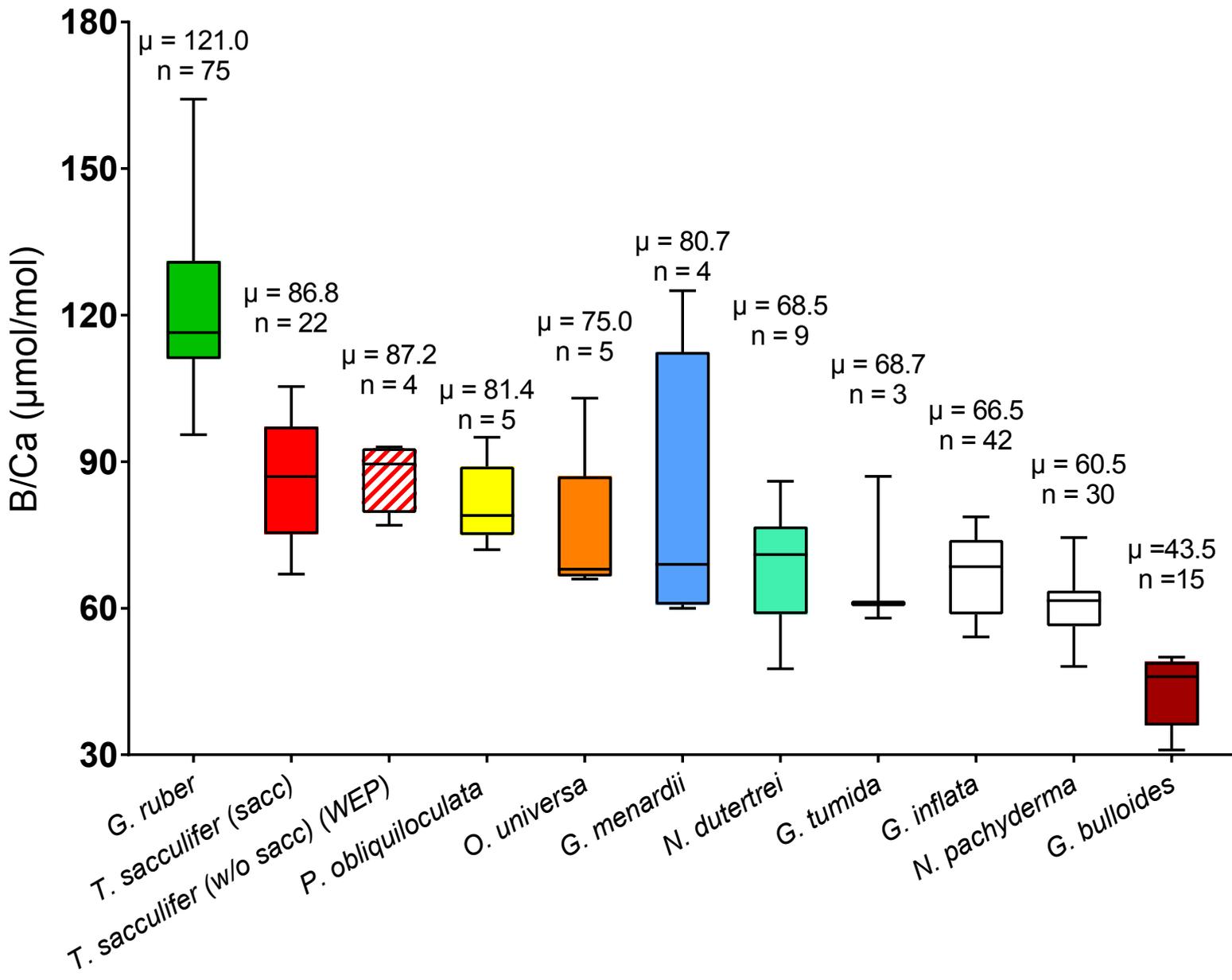
Photosynthesis/respiration-calcification
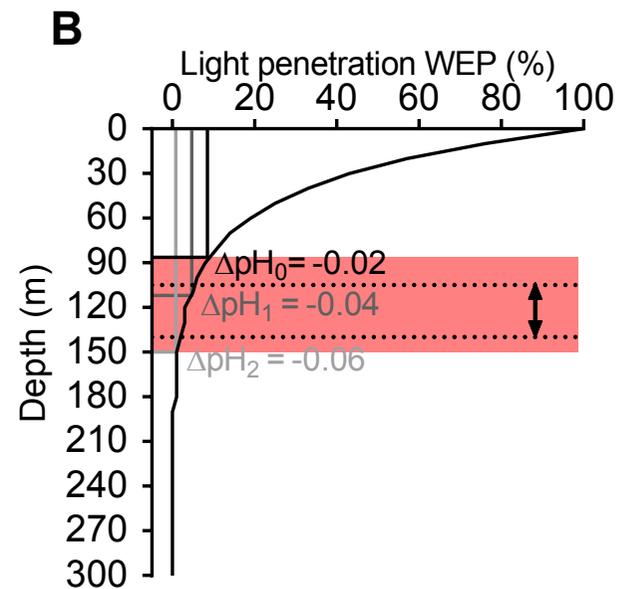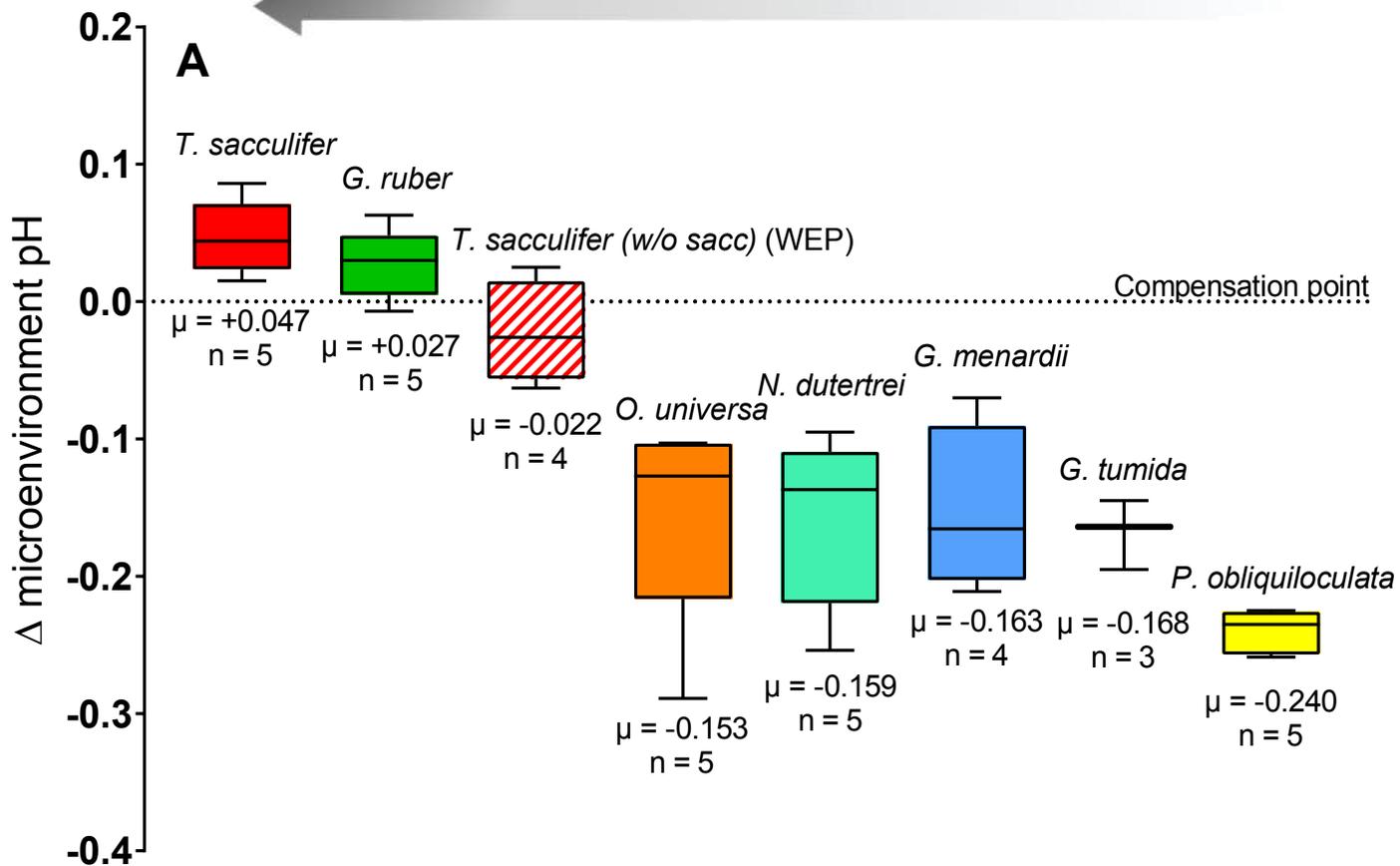
Figure columns (left to right): $\delta^{11}B_{carbonate}$, $\delta^{11}B_{borate}$, pH, pCO_2

Atlantic Ocean

CD107-a
52.9°N, -16.9°E
3569 m

Axis labels: $\delta^{11}B_{calcite}$(‰), $\delta^{11}B_{borate\ calculated}$ (‰), pH $_{calculated}$, pCO_2 $_{calculated}$ (ppm)

Legend: ▽ O. universa

Indian Ocean

FC-01a
-11.2°N, 58.8°E
3520 m

Legend:
▲ T. sacculifer (sacc)   ■ N. dutertrei   ◆ N. dutertrei
● T. sacculifer (w/o sacc) □ G.tumida   ◆ G.tumida
◆ G. ruber (white)   ◆ G. menardii   ◆ G. menardii
△ T. sacculifer (sacc) [4]   ▽ O. universa   ▽ O. universa
○ T. sacculifer (w/o sacc) [4]   ● P. obliquiloculata
◇ G. ruber (white) [2]

FC-02a
-29.1°N, 47.5°E
2871 m

Legend:
▲ T. sacculifer (sacc)   ■ N. dutertrei
● T. sacculifer (w/o sacc) □ G.tumida
◆ G. ruber (white)   ◆ G. menardii
△ T. sacculifer (sacc) [4]   ▽ O. universa
○ T. sacculifer (w/o sacc) [4]   ● P. obliquiloculata
◇ G. ruber (white) [2]

Arabian Sea

FC-12b
23.3°N, 66.7°E
151 m

Legend:
▲ T. sacculifer (sacc)   ■ N. dutertrei
● T. sacculifer (w/o sacc) ◆ G. menardii
◆ G. ruber (white)   ▽ O. universa
△ T. sacculifer (sacc) [4]   ● P. obliquiloculata
○ T. sacculifer (w/o sacc) [4]
◇ G. ruber (white) [2]

FC-13a
20.0°N, 65.6°E
3190 m

Legend:
◆ G. ruber (white)   ■ N. dutertrei
◇ G. ruber (white)[2]   ◆ G. menardii
● P. obliquiloculata

Pacific Ocean

WP07-01
-3.9°N,156.0°E
1800 m

Legend:
▲ T. sacculifer (sacc)   ■ N. dutertrei
● T. sacculifer (w/o sacc) □ G.tumida
◆ G. ruber (white)   ◆ G. menardii
△ T. sacculifer (sacc) [4]   ▽ O. universa
○ T. sacculifer (w/o sacc) [4]   ● P. obliquiloculata
◇ G. ruber (white) [2]

$\delta^{11}B_{borate}$

y-axis: $\delta^{11}B_{borate\ calculated}$ (‰)
x-axis: $\delta^{11}B_{borate\ in\text{-}situ}$ (‰)

1:1

pH

y-axis: $pH_{recalculated}$
x-axis: $pH_{in\text{-}situ}$

1:1

pCO_2

y-axis: $pCO_{2\ recalculated}$ (ppm)
x-axis: $pCO_{2\ in\text{-}situ}$ (ppm)

1:1

Legend:
- *G. ruber* (white) [1]
- *T. sacculifer (sacc)*, [3]
- *T. sacculifer (w/o sacc)* [3]
- *G. ruber* [2]
- *T. sacculifer (sacc)* [4]
- *T. sacculifer (w/o sacc)* [4]
- *N. dutertrei*
- *G. tumida*
- *G. menardii*
- *O. universa*
- *P. obliquiloculata*

Table 1

Label	Box-Core	Site	Latitude (N)	Longitude (E)	Depth (mbsl)	Oceanic Regime	Δ^{14}C age (year)
Atlantic Ocean							
CD107-a	CD107	A	52.92	-16.92	3569	non-upwelling	<3000[a]
Indian Ocean							
FC-01a	WIND-33B	I	-11.21	58.77	3520	non-upwelling	
FC-02a	WIND-10B	K	-29.12	47.55	2871	non-upwelling	7252 ± 27[b]
Arabian Sea							
FC-12b	CD145	A150	23.30	66.70	151	seasonal upwelling	
FC-13a	CD145	A3200	20.00	65.58	3190	seasonal upwelling	
Pacific Ocean							
WP07-01			-3.93	156.00	1800	non-upwelling	7.3-8.6[c]
A14			8.02	113.39	1911	non-upwelling	7.3-8.6[c]
806		A	0.32	159.36	2521	equatorial divergence	7.3-8.6[c]
807		A	3.61	156.62	2804	equatorial divergence	7.3-8.6[c]

[a] Thomson et al., 2000

[b] Wilson et al., 2012

[c] Age for core-top of site 806B from Lea et al., 2000

Table 2

Core	Species	Fraction size (µm)	Cleaning	$\delta^{13}C$* (‰)	$\delta^{18}O$* (‰)	$\delta^{11}Bc_1$ (‰)	$\delta^{11}Bc_2$ (‰)	$\delta^{11}B_{average}$** (‰)	Li/Ca*** (µmol/mol)	B/Ca*** (µmol/mol)	Mg/Ca*** (mmol/mol)	Mn/Ca*** (µmol/mol)	Fe/Ca*** (mmol/mol)
Atlantic Ocean													
CD107a	*O. universa*	>500	Ox-Red	1.99 ± 0.03	1.25 ± 0.11	16.85 ± 0.31 (2SD, nAE121=11)	16.95 ± 0.31 (2SD, nAE121=11)	16.90 ± 0.22	13.9 ± 0.4	68 ± 7	3.60 ± 0.01	13 ± 7	0.16 ± 0.01
Indian Ocean													
FC-01a	*G. ruber (white ss)*	250-300	Ox-Red	1.37 ± 0.03	-1.32 ± 0.11	19.33 ± 0.31 (2SD, nAE121=11)	19.41 ± 0.31 (2SD, nAE121=11)	19.37 ± 0.22	15.4 ± 0.4	109 ± 7	3.98 ± 0.01	10 ± 7	0.07 ± 0.01
FC-01a	*T. sacculifer (sacc)*	300-400	Ox-Red	1.88 ± 0.03	-2.20 ± 0.11	18.71 ± 0.24 (2SD, nAE121=10)	18.73 ± 0.24 (2SD, nAE121=10)	18.72 ± 0.17	12.1 ± 0.4	87 ± 7	3.45 ± 0.01	9 ± 7	0.03 ± 0.01
FC-01a	*T. sacculifer (w/o sacc)*	300-400	Ox-Red	2.02 ± 0.03	-1.05 ± 0.11	19.13 ± 0.24 (2SD, nAE121=10)	19.32 ± 0.24 (2SD, nAE121=10)	19.23 ± 0.17	12.1 ± 0.4	82 ± 7	3.42 ± 0.01	14 ± 7	0.03 ± 0.01
FC-01a	*O. universa*	>500	Ox-Red			15.50 ± 0.26 (2SD, nAE121=14)		15.50 ± 0.26	15.4 ± 0.4	78 ± 7	2.06 ± 0.01	14 ± 7	0.05 ± 0.01
FC-01a	*P. obliquiloculata*	300-400	Ox-Red	1 .00± 0.03	-0.55 ± 0.11	16.40 ± 0.26 (2SD, nAE121=14)	16.10 ± 0.26 (2SD, nAE121=14)	16.25 ± 0.18	15.4 ± 0.4	78 ± 7	2.06 ± 0.01	14 ± 7	0.05 ± 0.01
FC-01a	*G. menardii*	300-400	Ox-Red	1.64 ± 0.03	0.43 ± 0.11	17.52 ± 0.26 (2SD, nAE121=14)	17.69 ± 0.26 (2SD, nAE121=14)	17.60 ± 0.18	12.7 ± 0.4	63 ± 7	2.26 ± 0.01	8 ± 7	0.07 ± 0.01
FC-01a	*N. dutertrei*	300-400	Ox-Red	1.28 ± 0.03	-0.43 ± 0.11	16.40 ± 0.31 (2SD, nAE121=11)	16.59 ± 0.31 (2SD, nAE121=11)	16.50 ± 0.22	18.6 ± 0.4	73 ± 7	1.81 ± 0.01	11 ± 7	0.03 ± 0.01
FC-01a	*G. tumida*	300-400	Ox-Red	1.29 ± 0.03	-0.53 ± 0.11	16.21 ± 0.31 (2SD, nAE121=11)	16.18 ± 0.31 (2SD, nAE121=11)	16.20 ± 0.22	10.0 ± 0.4	61 ± 7	1.79 ± 0.01	11 ± 7	0.02 ± 0.01
FC-02a	*G. ruber (white ss)*	250-300	Ox-Red	0.30 ± 0.03	-1.40 ± 0.11	20.02 ± 0.24 (2SD, nAE121=10)	19.90 ± 0.24 (2SD, nAE121=10)	19.96 ± 0.17	18.2 ± 0.4	125 ± 7	3.47 ± 0.01	10 ± 7	0.07 ± 0.01
FC-02a	*T. sacculifer (sacc)*	300-400	Ox-Red	1.43 ± 0.03	-1.60 ± 0.11	20.07 ± 0.24 (2SD, nAE121=10)	19.93 ± 0.24 (2SD, nAE121=10)	20.00 ± 0.17	14.2 ± 0.4	106 ± 7	3.30 ± 0.01	10 ± 7	0.03 ± 0.01
FC-02a	*T. sacculifer (w/o sacc)*	300-400	Ox-Red	1.52 ± 0.03	-1.40 ± 0.11	23.23 ± 0.24 (2SD, nAE121=10)	23.22 ± 0.24 (2SD, nAE121=10)	23.22 ± 0.17	13.7 ± 0.4	106 ± 7	3.34 ± 0.01	10 ± 7	0.04 ± 0.01
FC-02a	*O. universa*	>500	Ox-Red	1.79 ± 0.03	0.02 ± 0.11	18.05 ± 0.26 (2SD, nAE121=14)	17.97 ± 0.26 (2SD, nAE121=14)	18.01 ± 0.18	14.8 ± 0.4	67 ± 7	4.40 ± 0.01	11 ± 7	0.05 ± 0.01
FC-02a	*P. obliquiloculata*	300-400	Ox-Red	0.34 ± 0.03	0.56 ± 0.11	16.35 ± 0.26 (2SD, nAE121=14)	16.69 ± 0.26 (2SD, nAE121=14)	16.52 ± 0.18	16.6 ± 0.4	83 ± 7	2.33 ± 0.01	7 ± 7	0.03 ± 0.01
FC-02a	*G. menardii*	300-400	Ox-Red	1.73 ± 0.03	-0.51 ± 0.11	17.77 ± 0.26 (2SD, nAE121=14)		17.77 ± 0.26	15.8 ± 0.4	125 ± 7	2.21 ± 0.01	17 ± 7	0.03 ± 0.01
FC-02a	*N. dutertrei*	300-400	Ox-Red	1.03 ± 0.03	-0.55 ± 0.11	16.78 ± 0.31 (2SD, nAE121=11)	17.03 ± 0.31 (2SD, nAE121=11)	16.91 ± 0.22	18.6 ± 0.4	82 ± 7	2.13 ± 0.01	13 ± 7	0.07 ± 0.01
FC-02a	*G. tumida*	300-400	Ox-Red	1.64 ± 0.03	-0.28 ± 0.11	16.93 ± 0.26 (2SD, nAE121=14)	16.95 ± 0.26 (2SD, nAE121=14)	16.94 ± 0.18	15.6 ± 0.4	87 ± 7	1.90 ± 0.01	17 ± 7	0.04 ± 0.01
Arabian Sea													
FC-12b	*G. ruber (white ss)*	250-300	Ox-Red	0.58 ± 0.03	-2.82 ± 0.11	21.30 ± 0.31 (2SD, nAE121=11)	21.23 ± 0.31 (2SD, nAE121=11)	21.26 ± 0.22	19.5 ± 0.4	164 ± 7	5.76 ± 0.01	14 ± 7	0.16 ± 0.01
FC-12b	*G. sacculifer (s)*	300-400	Ox-Red	1.76 ± 0.03	-2.15 ± 0.11	19.65 ± 0.31 (2SD, nAE121=11)	19.57 ± 0.31 (2SD, nAE121=11)	19.61 ± 0.22	14.6 ± 0.4	101 ± 7	4.28 ± 0.01	17 ± 7	0.14 ± 0.01
FC-12b	*T. sacculifer (w/o sacc)*	300-400	Ox-Red	1.97 ± 0.03	-2.19 ± 0.11	20.32 ± 0.31 (2SD, nAE121=11)	20.37 ± 0.31 (2SD, nAE121=11)	20.34 ± 0.22	16.7 ± 0.4	116 ± 7	4.90 ± 0.01	20 ± 7	0.26 ± 0.01
FC-12b	*O. universa*	>500	Ox-Red	1.89 ± 0.03	-1.59 ± 0.11	18.13 ± 0.20 (2SD, nAE121=6)		18.13 ± 0.20	13.6 ± 0.4	103 ± 7	6.91 ± 0.01	10 ± 7	0.06 ± 0.01
FC-12b	*P. obliquiloculata*	300-400	Ox-Red	0.5 ± 0.03	-1.58 ± 0.11	16.45 ± 0.26 (2SD, nAE121=14)	16.15 ± 0.26 (2SD, nAE121=14)	16.30 ± 0.18	16.7 ± 0.4	95 ± 7	3.61 ± 0.01	69 ± 7	0.38 ± 0.01
FC-12b	*G. menardii*	300-400	Ox-Red	1.05 ± 0.03	-0.97 ± 0.11	16.2 ± 0.26 (2SD, nAE121=14)		16.20 ± 0.26	14.8 ± 0.4	75 ± 7	3.44 ± 0.01	52 ± 7	0.17 ± 0.01
FC-12b	*N. dutertrei*	300-400	Ox-Red	1.35 ± 0.03	-1.57 ± 0.11	17.77 ± 0.24 (2SD, nAE121=10)	17.73 ± 0.24 (2SD, nAE121=10)	17.75 ± 0.17	17.1 ± 0.4	75 ± 7	3.25 ± 0.01	46 ± 7	0.25 ± 0.01
FC-13a	*G. ruber (white ss)*	250-300	Ox-Red	0.08 ± 0.03	-3.71 ± 0.11	20.27 ± 0.24 (2SD, nAE121=10)	20.15 ± 0.24 (2SD, nAE121=10)	20.21 ± 0.17	16.4 ± 0.4	147 ± 7	4.52 ± 0.01	13 ± 7	0.08 ± 0.01
FC-13a	*T. sacculifer (w/o sacc)*	300-400	Ox-Red	1.59 ± 0.03	-2.46 ± 0.11	17.85 ± 0.29 (2SD, nAE121=12)		17.85 ± 0.29	15.7 ± 0.4	121 ± 7	5.49 ± 0.01	21 ± 7	0.49 ± 0.01
FC-13a	*P. obliquiloculata*	300-400	Ox-Red	0.00 ± 0.03	-0.97 ± 0.11	16.51 ± 0.26 (2SD, nAE121=14)	16.50 ± 0.26 (2SD, nAE121=14)	16.51 ± 0.18	16.7 ± 0.4	79 ± 7	4.43 ± 0.01	30 ± 7	0.43 ± 0.01
FC-13a	*G. menardii*	300-400	Ox-Red	0.75 ± 0.03	-1.07 ± 0.11	16.74 ± 0.20 (2SD, nAE121=6)		16.74 ± 0.20	9.2 ± 0.4	60 ± 7	1.99 ± 0.01	19 ± 7	0.07 ± 0.01
FC-13a	*N. dutertrei*	300-400	Ox-Red	0.71 ± 0.03	-1.41 ± 0.11	14.43 ± 0.24 (2SD, nAE121=10)	14.40 ± 0.24 (2SD, nAE121=10)	14.41 ± 0.17	15.7 ± 0.4	69 ± 7	1.98 ± 0.01	15 ± 7	0.06 ± 0.01
Pacific Ocean													
WP07-a	*G. ruber (white ss)*	250-400	Ox-Red			19.12 ± 0.29 (2SD, nAE121=12)		19.12 ± 0.29	14.5 ± 0.4	144 ± 7	4.32 ± 0.01	15 ± 7	0.16 ± 0.01
WP07-a	*T. sacculifer (sacc)*	250-400	Ox-Red			20.13 ± 0.21 (2SD, nAE121=11)		20.13 ± 0.21	12.7 ± 0.4	92 ± 7	4.44 ± 0.01	22 ± 7	0.05 ± 0.01
WP07-a	*T. sacculifer (w/o sacc)*	250-400	Ox-Red			18.10 ± 0.31 (2SD, nAE121=11)	18.04 ± 0.31 (2SD, nAE121=11)	18.07 ± 0.22	12.3 ± 0.4	192 ± 7	4.51 ± 0.01	21 ± 7	0.08 ± 0.01
WP07-a	*O.universa*	500-630	Ox-Red			18.13 ± 0.26 (2SD, nAE121=14)	17.99 ± 0.26 (2SD, nAE121=14)	18.06 ± 0.18	11.9 ± 0.4	71 ± 7	7.52 ± 0.01	11 ± 7	0.02 ± 0.01
WP07-a	*P. obliquiloculata*	250-400	Ox-Red			16.08 ± 0.26 (2SD, nAE121=14)	16.19 ± 0.26 (2SD, nAE121=14)	16.14 ± 0.18	13.4 ± 0.4	72 ± 7	3.02 ± 0.01	7 ± 7	0.03 ± 0.01
WP07-a	*G. menardii*	250-400	Ox-Red			14.74 ± 0.26 (2SD, nAE121=14)	14.53 ± 0.26 (2SD, nAE121=14)	14.64 ± 0.18	13.5 ± 0.4	85 ± 7	2.68 ± 0.01	26 ± 7	0.08 ± 0.01
WP07-a	*N. dutertrei*	250-400	Ox-Red			16.91 ± 0.31 (2SD, nAE121=11)	16.99 ± 0.31 (2SD, nAE121=11)	16.95 ± 0.22	21.7 ± 0.4	86 ± 7	3.66 ± 0.01	42 ± 7	0.63 ± 0.01
WP07-a	*G. tumida*	250-400	Ox-Red			16.45 ± 0.26 (2SD, nAE121=14)	16.32 ± 0.26 (2SD, nAE121=14)	16.39 ± 0.18	10.6 ± 0.4	58 ± 7	2.55 ± 0.01	16 ± 7	0.10 ± 0.01
806A	*T. sacculifer (w/o sacc)*	250-400	Ox-Red			17.53 ± 0.36 (2SD, nAE121=11)		17.53 ± 0.36	14.40 ± 0.4	77 ± 7	3.89 ± 0.01	7 ± 7	0.15 ± 0.01
807A	*T. sacculifer (w/o sacc)*	250-400	Ox-Red			18.38 ± 0.21 (2SD, nAE121=11)	18.17 ± 0.21 (2SD, nAE121=11)	18.28 ± 0.15	12.54 ± 0.4	87 ± 7	4.24 ± 0.01	17 ± 7	0.09 ± 0.01
A14	*G. ruber (white ss)*	250-400	Ox-Red			18.91 ± 0.24 (2SD, nAE121=10)	19.17 ± 0.24 (2SD, nAE121=10)	19.04 ± 0.17					
A14	*T. sacculifer (sacc)*	250-400	Ox-Red			19.53 ± 0.24 (2SD, nAE121=10)	19.32 ± 0.24 (2SD, nAE121=10)	19.42 ± 0.17	12.0 ± 0.4	102 ± 7	3.91 ± 0.01	22 ± 7	0.02 ± 0.01
A14	*T. sacculifer (w/o sacc)*	250-400	Ox-Red			18.93 ± 0.24 (2SD, nAE121=10)	18.84 ± 0.24 (2SD, nAE121=10)	18.88 ± 0.17	12.3 ± 0.4	93 ± 7	3.76 ± 0.01	25 ± 7	0.06 ± 0.01
A14	*O. universa*	500-560	Ox-Red			17.33 ± 0.26 (2SD, nAE121=14)	17.08 ± 0.26 (2SD, nAE121=14)	17.20 ± 0.18	11.3 ± 0.4	66 ± 7	6.59 ± 0.01	10 ± 7	0.02 ± 0.01
A14	*N. dutertrei*	250-400	Ox-Red			14.39 ± 0.31 (2SD, nAE121=11)		14.39 ± 0.31	16.9 ± 0.4	75 ± 7	1.99 ± 0.01	35 ± 7	0.04 ± 0.01

* uncertainties given in 1SD (see text)

** When two measurements were carried out uncertaity was calculated with $\Delta a = \sqrt{(1/\sum_i (1/\Delta_{ai})^2)}$; with only one measurement the error was determined on reproducibility of the AE121 standard

***Uncertainty given in 2SD , calculated on the reproducibility of CamWuellestorfi (see text and table S3, ref in Misra et al., 2014)

Table 3

Species	Size fraction (µm)	Material	Instrument (original)	Regression method	$\delta^{11}B_{borate}= f(\delta^{11}B_{calcite})$	n	Calibration number	Reference
G. ruber	~380	Culture/core tops/plankton tows	MC-ICP-MS		$\delta^{11}B_{borate}=[\delta^{11}B_{calcite} - 9.52\ (\pm2.02)]/0.6\ (\pm0.11)$			Henehan et al., 2013
G. ruber	315-355	Core-tops	MC-ICP-MS		$\delta^{11}B_{borate}=[\delta^{11}B_{calcite} - 11.78\ (\pm3.20)]/0.45\ (\pm0.16)$			Raitzsch et al., 2018
T. sacculifer	n.d.	Culture/artificial seawater enriched in B	N-TIMS		$\delta^{11}B_{borate}=[\delta^{11}B_{calcite} - 3.94\ (\pm4.02)]/0.82\ (\pm0.22)$			Sanyal et al., 2001 refitted Martinez-Boti et al., 2015
T. sacculifer	315-355	Core-tops	MC-ICP-MS		$\delta^{11}B_{borate}=[\delta^{11}B_{calcite} - 8.86\ (\pm5.27)]/0.59\ (\pm0.21)$			Raitzsch et al., 2018
O. universa	no effect	Core-tops/plankton tows/sediment traps	MC-ICP-MS		$\delta^{11}B_{borate}=[\delta^{11}B_{calcite} + 0.42\ (\pm2.85)]/0.95\ (\pm0.17)$			Henehan et al., 2016
O. universa	>425	Core-tops	MC-ICP-MS		$\delta^{11}B_{borate}=[\delta^{11}B_{calcite} + 5.69\ (\pm7.51)]/1.26\ (\pm0.39)$			Raitzsch et al., 2018
G. bulloides	300-355	Core-top/sediment trap	MC-ICP-MS		$\delta^{11}B_{borate}=[\delta^{11}B_{calcite} + 3.440\ (\pm4.584)]/1.074\ (\pm0.252)$			Martinez-Boti et al., 2015
G. bulloides	315-355	Core-tops	MC-ICP-MS		$\delta^{11}B_{borate}=[\delta^{11}B_{calcite} + 3.81\ (\pm13.17)]/1.13\ (\pm0.72)$			Raitzsch et al., 2018
N. pachyderma	150-200	Core-tops	MC-ICP-MS		$\delta^{11}B_{borate}= \delta^{11}B_{calcite} + 3.38$			Yu et al., 2013
G. ruber	250-400	Core-tops	MC-ICP-MS	Bootstrap	$\delta^{11}B_{borate}=[\delta^{11}B_{calcite} + 1.23\ (\pm0.59)]/1.12\ (\pm1.67)$	5	**1**	This study
G. ruber	250-400	Core-tops	MC-ICP-MS	Bootstrap	$\delta^{11}B_{borate}=[\delta^{11}B_{calcite} - 11.73\ (\pm0.83)]/0.46\ (\pm0.34)$	40	**2**	This study; Foster et al., 2008; Henehan et al., 2016; Raitzsch et al., 2018
T. sacculifer (sacc and w/o sacc)	250-400	Core-tops	MC-ICP-MS	Bootstrap	$\delta^{11}B_{borate}=[\delta^{11}B_{calcite} + 6.06\ (\pm 0.25)/1.38\ (\pm 1.33)$	11	**3**	This study
T. sacculifer (sacc and w/o sacc)	250-400	Core-tops	MC-ICP-MS	Bootstrap	$\delta^{11}B_{borate}=[\delta^{11}B_{calcite} - 4.09\ (\pm0.86)]/0.83\ (\pm0.48)$	27	**4**	This study; Foster et al., 2008; Raitzsch et al., 2018
N. dutertrei	300-400	Core-tops	MC-ICP-MS	Bootstrap	$\delta^{11}B_{borate}=[\delta^{11}B_{calcite} - 0.34\ (\pm1.83)]/0.93\ (\pm0.55)$	5	**5**	This study
N. dutertrei	300-400	Core-tops	MC-ICP-MS	Bootstrap	$\delta^{11}B_{borate}=[\delta^{11}B_{calcite} - 3.88\ (\pm0.65)]/0.72\ (\pm0.74)$	9	**6**	This study; Foster et al., 2008
O. universa	400-600	Core-tops	MC-ICP-MS	Bootstrap	$\delta^{11}B_{borate}=[\delta^{11}B_{calcite} + 8.01\ (\pm23)]/1.38\ (\pm2.67)$	5	**7**	This study
O. universa	400-600	Core-tops	MC-ICP-MS	Bootstrap	$\delta^{11}B_{borate}=[\delta^{11}B_{calcite} + 2.08\ (\pm0.59)]/1.06\ (\pm0.13)$	36	**8**	This study; Henehan et al., 2016; Raitzsch et al., 2018
G. menardii	400-600	Core-tops	MC-ICP-MS	Bootstrap	$\delta^{11}B_{borate}=[\delta^{11}B_{calcite} - 5.36\ (\pm1.36)]/0.65\ (\pm0.76)$	5	**9**	This study
G. tumida	400-600	Core-tops	MC-ICP-MS	Bootstrap	$\delta^{11}B_{borate}=[\delta^{11}B_{calcite} - 6.33\ (\pm2.52)]/0.57\ (\pm1.2)$	3	**10**	This study
P. obliquiloculata	300-400	Core-tops	MC-ICP-MS	Bootstrap	$\delta^{11}B_{borate}=[\delta^{11}B_{calcite} - 5.59\ (\pm4.16)]/0.59(\pm0.65)$	6	**11**	This study; Henehan et al., 2016
Deep-dweller	300-600	Core-tops	MC-ICP-MS	Bootstrap	$\delta^{11}B_{borate}=[\delta^{11}B_{calcite} -1.99\ (\pm0.13)]/0.82\ (\pm0.27)$	22	**12**	This study
Deep-dweller	300-600	Core-tops	MC-ICP-MS	Bootstrap	$\delta^{11}B_{borate}=[\delta^{11}B_{calcite} - 0.18\ (\pm0.6)]/0.95\ (\pm0.13)$	54	**13**	This study; Foster et al., 2008; Henehan et al., 2016; Raitzsch et al., 2018

Supplemental information

Seawater pH reconstruction using boron isotopes in multiple planktonic foraminifera species with different depth habitats and their potential to constrain pH and pCO₂ gradients

Maxence Guillermic[1,2], Sambuddha Misra[3,4], Robert Eagle[2,5], Alexandra Villa[2,6], Fengming Chang[7], Aradhna Tripati [1,2,5]

[1] Department of Earth, Planetary, and Space Sciences, UCLA, University of California – Los Angeles, Los Angeles, CA 90095 USA
[2] Laboratoire Géosciences Océan UMR6538, UBO, Institut Universitaire Européen de la Mer, Rue Dumont d'Urville, 29280, Plouzané, France
[3] Indian Institute of Science, Centre for Earth Sciences, Bengaluru, Karnataka 560012, India
[4] The Godwin Laboratory for Palaeoclimate Research, Department of Earth Sciences, University of Cambridge, UK
[5] Institute of the Environment and Sustainability, Department of Atmospheric and Oceanic Sciences, University of California – Los Angeles, CA 90095, USA
[6] Department of Geology, University of Wisconsin-Madison, Madison, WI 53706 USA
[7] Key Laboratory of Marine Geology and Environment, Institute of Oceanology, Chinese Academy of Sciences, Qingdao 266071, China

Supplemental Figures

Figure S1: An example of the impact of seasonality on results. Based on data from GLODAP used for site FC13-a. Seasonality has less of an impact that a change in the depth habitats.

Figure S2: Figure showing the offset $\Delta^{11}B=\delta^{11}B_{carbonate}-\delta^{11}B_{borate}$ versus calcification depth, red symbols are from Arabian Sea, green from Indian Ocean and Blue from the WEP, blue with black line symbols are data from site A14. This figure highlights a decrease of $\delta^{11}B_{carbonate}$ for *T. sacculifer* and *G. ruber* with a deeper depth habitat.

Figure S3: Multi-panels figure showing the correlation between B/Ca and boron geochemistry and different variables. A to C show comparison of B/Ca and A) $[B(OH)_4^-]/[HCO_3^-]$, B) $\delta^{11}B_{carbonate}$ and C) temperature. Panel D) shows the correlation between $\delta^{11}B_{carbonate}$ and temperature. Symbol in brackets is high B/Ca; this point is included in the linear regressions. Linea regression (LR - black line) is when compiling *G. ruber* and *T. sacculifer*, LR of *G. ruber* (dotted line green), *T. sacculifer* (red line – $p<0.05$), *T. sacculifer* (w/o sacc – red dotted line).

Figure S4: Boron geochemistry against water depth. A) $\delta^{11}B_{carbonate}$ versus water depth, B) B/Ca against water depth and C) $\delta^{11}B_{carbonate}$ versus calcification depth and linear regressions for *G. ruber*, *T. sacculifer* (w/o sacc), *T. sacculifer* (sacc) and *O. universa*.

Figure S5: Figure evaluating the circularity of our reconstructions. It is showing in the y-axis the difference between reconstruction utilizing calibrations derive from the entire dataset and compare to *in-situ* values and in the x-axis the difference between the reconstruction utilizing the species-specific calibrations derived excluding the site of interest (no circularity) compared to *in-situ* values. Results show that difference is not significant between the two reconstruction methods (e.g. following the 1:1 line), validating the method and the calibrations.

Supplemental Tables

Table S1: Elemental ratios of multi-elemental standards utilized in this study.

Table S2: Reproducibility of boron isotope standards.

Table S3: Reproducibility of elemental ratios for CamWuellestorfi standard.

Table S4: Seasonality of foraminifera utilized in this study.

Table S5: Mg/Ca-T calibrations used for reconstructions and $\delta^{18}O_w$-T calibrations used for calcification depth reconstructions.

Table S6: Calcification depth (CD) calculations from $\delta^{18}O$ (CD1), Mg/Ca (CD2) and literature (CD3).

Table S7: Pre-industrial in-situ parameters estimated using calcification depths for each species and calculated parameters based on analytical results.

Trace element standards

A series of multi-element standards (Table S1) with fixed Ca concentration and variable B, Mg, Sr, Mn, Ba, Zn, Cd, U, Li, Al and Fe concentrations were prepared for elemental ratios analysis in Brest following the method developed by Yu et al., (2005). Multi-element stock standard mixtures were prepared gravimetrically by spiking a 10,000 ppm Ca standard with appropriate amounts of Li, B, Al, Mn, Zn, Sr, Cd and U mono-elemental 1,000 ppm (SCP Science). They were diluted with OPTIMA grade HNO_3 acid and 18.2 MΩ.cm-1water to reach a 0.28M HNO_3 final solution. The stock standards (1500 ppm Ca) were prepared in 500mL cleaned PFA bottles. Working standards were made by diluting the stock solutions to a final concentration of 100 ppm Ca. The multi-element standards were calibrated at the University of Cambridge, elemental ratios are presented in Table S1. An external standard CamWuellestorfi (Misra et al., 2014a) was used in Brest for cross-calibration and reproducibility (Table S3).

Potential contaminations

Possible contamination of samples due to presence of silicate minerals was monitored with the Fe/Mg ratio. Samples with Fe/Mg > 0.1 mol/mol would be rejected due to potential contamination by silicate minerals (Barker et al., 2003). Samples (site E035 excluded) have an average Fe/Mg of 0.03 ± 0.05 mol/mol (2SD, n=42), meaning that silicate minerals have been efficiently removed during our cleaning.

Contribution of Mn-Fe-oxide coatings to Mg/Ca ratio has been calculated to be 0.5 μmol/mol Mg/Ca (change for 5 μmol/mol Mn/Ca ratio Barker et al., 2003). The maximum Mn/Ca ratio in our samples is 89 μmol/mol which can lead to a potential contribution of ~9 μmol/mol Mg/Ca or in other words a decrease of 0.1°C in our reconstructed temperatures. However, the calibration error is much larger and is estimated to be ~1.4°C (Dekens et al., 2002). The range in Mn/Ca values in our samples is 0.021 ± 0.033 mmol/mol (2SD, n=42) which allows us to not be ignore *Mn-Fe-oxide* coating related complications. Additionally, no correlations were found between Mg/Ca and Fe/Ca (R^2=0.006) or with Mn/Ca (R^2=0.008), and between B/Ca ratio and Mn/Ca (R^2=0.003) or Fe/Ca (R^2=0.062) ratios.

Contamination by clays was monitored with Ti/Ca calculated from blank corrected intensities. Al/Ca ratios were not reliable as we are using an alumina injector for HF matrix in our lab. A minor correlation was found between Ti/Ca and Mg/Ca (R^2=0.1388) but none with B/Ca (R^2=0.0887).

Calcification depth determination

The first approach involves comparing measured $\delta^{18}O_c$ with theoretical predictions of $\delta^{18}O_c$ based on vertical profiles of temperature and the $\delta^{18}O$ of seawater ($\delta^{18}O_w$). We assume $\delta^{18}O_c$ is in equilibrium with seawater. First, $\delta^{18}O_w$ was calculated using location-specific $\delta^{18}O_w$-salinity relationships and salinity profiles. We used salinity values from the World Ocean Atlas database (Boyer et al., 2013). Oxygen isotopes may be affected by both temperature and salinity. As our sites present different hydrographic settings and freshwater inputs, location-specific $\delta^{18}O_w$-salinity relationship relationships are utilized for accurate $\delta^{18}O_w$ reconstructions. For Site CD107-a, we used a $\delta^{18}O_w$-salinity relationship of 0.56*S-19.3 (Duplessy et al., 1991). For FC01-a and FC02-a, we used a $\delta^{18}O_w$-salinity relationship of 0.24*S-7.8 (Sime et al., 2005), and for FC13-a and FC12-b, we used a $\delta^{18}O_w$-salinity relationship of 0.28*S-9.24-0.27 (Rosteket al., 1993). Then, we used the calculated ambient $\delta^{18}O_w$ in concert with: (1) temperature profiles from the World Ocean Atlas database (Boyer et al., 2013), and (2) published calcite-water oxygen isotope fractionation factors, to calculate theoretical values for $\delta^{18}O_c$. Species-

specific relationships were used when available, including for *T. sacculifer* (Mulitza et al., 2003), *G. ruber* (Mulitza et al., 2003), and *O. universa* (Bemis et al., 2002, medium light). For all other, species we used the calcite equation from Kim and O'Niel (1997), adapted to a quadratic form by Bemis et al., (1998) following the approach of Sime et al., (2005). To take into account the ecology of each species, theoretical $\delta^{18}O_c$ profiles were made for the season of maximum abundance (Table S4). Therefore spring and summer profiles were used for *T. sacculifer*, summer profiles used for *G. ruber*, and winter and annual average profiles was used for *N. dutertrei*. Annual average profiles were used for the other species.

For the two sites WP07-1 and A14, a different approach was necessary because $\delta^{18}O_c$ data is sparse. At these sites, and for our other sites, we utilized Mg/Ca-derived temperatures to estimate calcification depths (Table S6). $T_{Mg/Ca}$ was derived using species-specific Mg/Ca-temperature calibrations (Table S6) along with the Mg/Ca ratios determined in this study. Calcification depth was estimated by comparing $T_{Mg/Ca}$ to modern temperature profiles from the World Ocean atlas database 2013 (Boyer et al., 2013) in light of the ecology (seasonality of growth) of the species of interest. A caveat is that in certain cases $T_{Mg/Ca}$ may be partially biased by a carbonate ion effect or salinity effect (Russell et al., 2004; Elderfield et al., 2006; Ferguson et al., 2008; Arbuszewski et al., 2010; Martinez-Boti et al., 2011). These artifacts on $T_{Mg/Ca}$ may be significant at high-latitude sites such as CD107-a which is located in the North Atlantic Ocean.

Depth habitat

Planktonic foraminifera live in the upper 500 m of the water column. Their preferred depth habitat depends on their ecology, which in turn relies on the hydrographic conditions. For example, *G. ruber* is commonly found in the mixed layer (Fairbanks and Wiebe, 1980; Dekens et al., 2002; Farmer et al., 2007) during summer (Deuser et al., 1981) whereas *T. sacculifer* (n or ns) is present in the mixed layer until the mid-thermocline depth (Farmer et al., 2007) during spring and summer (Deuser et al., 1981, 1989). Specimens of *P. obliquiloculata* and *N. dutertrei* are found during winter (Deuser et al., 1989), in the mixed layer (~60m) for *P. obliquiloculata*, and at mid-thermocline depth for *N. dutertrei* (Farmer et al., 2007). Whereas, *O. universa* tends to record annual average conditions and is living within the mixed layer. Specimens of *G .menardii* calcify within the seasonal thermocline (Fairbanks et al., 1982, Farmer et al., 2007, Regenberg et al., 2009) even upper thermocline (Farmer et al., 2007) and records annual temperatures. And specimens of *G. tumida* are found at the lower thermocline or below the thermocline and record annual average conditions (Fairbanks and Wiebe, 1980; Farmer et al., 2007, Birch et al., 2013). Our calcification depth reconstructions are summarized in Table 3, also see Table S6 for comparison.

Atlantic Ocean

Farmer et al., (2007) determined the depth habitat for *O. universa* to be ranging from 0 to 60m (LL, Bemis et al., 1998). Our calculation, through $\delta^{18}O$ measurement, suggests a deeper habitat of around 70m (LL, Bemis et al., 1998), 80m (ML, Bemis et al., 2002). Whereas, the Mg/Ca method derived depth habitat calculation yields a depth habitat of 50 m. The lower habitat depth can also come from the different size fractions, as our size fraction is lower than Farmer's. *O.universa* is thought to migrate to shallower depth along its ontogeny (Emiliani et al., 1954) younger individuals are thus living deeper but smaller individuals might also have a

deeper habitat as already suggested by Hönisch and Heming, (2004). Since most of the published studies have used the δ^{18}O-based depth calcification, we will preferentially adopt this method.

Indian Ocean

Calcification depths for the Indian Ocean cores have already been determined for majority of the species by Sime et al., (2005). Additionally, Birch et al., (2013) have reconstructed the depth habitat of multiple species from a core collected in the offshore region of Tanzania (Glow 3). In Indian Ocean specimens of *G. ruber* is found in the top 50m (Birch et al., 2013) and until 60 m (Sime et al., 2005), *T. sacculifer* is found in the surface mixed layer (SML) but also in the upper thermocline between 50-70 m for Birch et al., (2013) and between 60 to 80 m for Sime et al., (2005). Our results are consistent with these reported depth habitats. We calculate that specimens of *G. ruber*, *T. sacculifer* with and without sac are living in the top 80m; *O. universa* lives between 50 to 90 m (Sime et al., 2005, Birch et al., 2013). For *N. dutertrei* we calculate a depth habitat of 90m at site FC01a, calcification depths derived from both δ^{18}O and Mg/Ca methods agree with the 93 m estimate by Sime et al., (2005). At site FC02a the calculated calcification depth based on δ^{18}O method is 65 m, and, the Mg/Ca derived depth is 100m; however, Sime et al., (2005) proposed a calcification depth of 146 m. A deeper depth habitat than site FC01a seems to be in line with the weaker stratification of the water column at site FCO2a. The depth habitat for *P. obliquiloculata*'s was determined to be 106–120m by Sime et al., (2005); however, our calculations predict a lower and narrower depth habitat of 60 – 70m. Calcification depth for *G.menardii* has been calculated to be 60 – 70m, which is consistent with an upper thermocline depth habitat. Specimens of *G.tumida* is commonly found at the bottom of the thermocline which is around 200-250m at our Indian Ocean sites, Birch et al., (2013) found this species ranging from 100 to 200 m but our δ^{18}O based habitat reconstruction suggests a shallower depth of 70m at both sites. It seems that the calcification derived Mg/Ca for *G. tumida* is more realistic than with our δ^{18}O$_c$ reconstructions, the Mg/Ca based calculation predicts a depth habitat of 100 – 130 m.

Arabian Sea

In the Arabian Sea foraminifera are affected by changes in local hydrology caused by the Indian summer and winter monsoons. The specimens of different species collectively record a shallower habitat during SW monsoon (e.g., upwelling) and a deeper habitat during NE monsoon (Peeters and Brummer, 2002). Except for *N. dutertrei,* our two methods of calcification depth reconstruction closely agree with each other within their respective uncertainties. The depth habitat reconstructions for *G. ruber* and for *T. sacculifer* are consistent with species living in the shallow mixed layer (SML) at a depth of 30m for *G. ruber* and 40 m for *T. sacculifer*. Specimens of *O. universa* are calculated to live at 30m depth; *N. dutertrei* at site FC12-b (water depth 151m) is living around 40m and at 150m at site FC13-b (water depth 3200m), which is consistent with the hydrography at this site (Fig. 4). The depth habitat of *P. obliquiloculata* is calculated to be 50m at both sites. Specimens of *G. menardii* is found at depths of 60m, consistent with Peeters and Brummer, (2002) estimate of 50 – 130m.

Pacific Ocean

For Pacific Ocean samples the Mg/Ca derived calcification depths were used in absence of δ^{18}O$_c$ values. The Sites WP07-01 and A14 are located in the Western Equatorial Pacific with Site WP07-01

characterized by a deep thermocline. At these sites *G. ruber* and *T. sacculifer* have deep depth habitat of around 100m for *G. ruber* (Elderfield and Ganssen, 2000) and around 125m for *T. sacculifer* (Rickaby et al., 2005). The depth habitat for specimens of *O. universa* was determined to be 75m depth at site WP07-01 and at 55m depth at site A14. We calculate that *P. obliquiloculata* is living at 125m deep. Rickaby et al., (2005) estimated the living depth of *N. dutertrei* at 165m in agreement with our calculated depths (~125m). Specimens of *G. menardii* were determined to live at 180m like *G. tumida* (Rickaby et al., 2005).

The data are not consistent with a dissolution effect to explain the low $\delta^{11}B$ *T. sacculifer* in the WEP

Documented dissolution effects have been attributed to the preferential dissolution of ontogenic calcite relative to the light $\delta^{11}B$ of gametogenic calcite (Ni et al., 2007; Seki et al., 2010; Henehan et al., 2016). *T. sacculifer* (w/o sacc) should be less impacted compared to the *T. sacculifer* (sacc). Hönisch and Hemming, (2004) and Ni et al., (2007) reported a dissolution effect at site 806 (close to our WP07-01 site) for *T. sacculifer* (sacc), however, in our data the $\delta^{11}B_{carbonate}$ for *T. sacculifer* (sacc) is not decreasing with water depth when *T. sacculifer* (w/o sacc) is which suggests that at these sites and at the same size-fraction no dissolution is observed (eg. different water depth). $\Delta^{11}B$ for *T. sacculifer* (w/o sacc) and for *G. ruber* shift to lighter with higher calcification depth, a trend that does not support a dissolution effect. The lethal temperature for *T. sacculifer* is 14°C, which at site WP07-01 corresponds to a $\delta^{11}B_{borate}$ of 17.5 ‰ which makes our low $\delta^{11}B_{carbonate}$ realistic. If no dissolution is observed, a deep depth habitat inducing a respiration-driven microenvironment might explain the low $\delta^{11}B$ of the measured carbonate.

Microenvironment calculations

We observe a trend between $\Delta^{11}B$ (eg. $\Delta^{11}B = \delta^{11}B_{carbonate} - \delta^{11}B_{borate}$) with derived calcification depth (Fig. S2). In order to verify why the WEP $\delta^{11}B_{carbonate}$ of *T. sacculifer* (w/o sacc) is low and to test the hypothesis of the depth habitat we try to recalculate independently the theoretical water depth habitat based on culture results from Jorgensen et al., (1985) and our microenvironment pH results. A change of microenvironment pH for *T. sacculifer* will change the theoretical light intensity needed to reach this microenvironment pH. The compensation light intensity (E_c) for *T. sacculifer* has been calculated by Jorgensen et al., (1985) to be ~30 $\mu Eistn.m^{-2}.s^{-1}$, E_c corresponds to the energy where photosynthesis compensates respiration or where $\delta^{11}B_{carbonate}$ reaches the 1:1 theoretical line. We tested two microenvironment pH, $\Delta pH_1 = -0.04$ and $\Delta pH_2 = -0.06$ (Fig S3). We've recalculated the light energy needed to decrease the pH of ΔpH_1 and ΔpH_2 and apply these changes to the light penetration profile determined with an insolation E_0 in the WEP of 220 $J.s^{-1}.m^{-2}$ (Weare et al., 1981) and a light attenuation coefficient of 0.028 (Wang et al., 2008). A decrease of ΔpH_1 would lead to a decrease of 15 $\mu Eistn.m^{-2}.s^{-1}$ and a decrease of ΔpH_2 would lead to a decrease of 24 $\mu Eistn.m^{-2}.s^{-1}$ (Jorgensen et al., 1985). These results correspond in our case of a light penetration of 12% to reach E_c, 5% for a decrease of ΔpH_1 and 1% for a decrease of ΔpH_2. This means that in the WEP if *T. sacculifer* calcifies below 75m where E_c is reached the $\delta^{11}B_{carbonate}$ is below the theoretical 1:1 line. *T. sacculifer* (w/o sacc) in the WEP is decreasing its pH of ~ΔpH_1 which would imply a calcification depth of 110m consistent with the reconstruction of Rickaby et al., (2005).

$$\Delta \text{microenvironment pH} = -\log(\frac{(\delta 11Bseawater - \delta 11Bcarbonate) \times Kb*}{\varepsilon - \delta 11Bseawater + \delta 11Bcarbonate}) - pHseawater$$

References

Arbuszewski, J., DeMenocal, P., Kaplan, A. and Farmer, E. C.: On the fidelity of shell-derived δ18Oseawater estimates, Earth Planet. Sci. Lett., 300, 185–196, 2010.

Barker, S., Greaves, M. and Elderfield, H: A study of cleaning procedures used for foraminiferal Mg/Ca paleothermometry, Geochemistry, Geophys. Geosystems 4, 1–20, 2003.

Bemis, B. E., Spero, H. J. and Thunell, R. C.: Using species-specific paleotemperature equations with foraminifera: a case study in the Southern California Bight, Mar. Micropaleontol., 46, 405–430, 2002.

Bemis, B. E., Spero, H. J., Bijma, J. and Lea, D. W.: Reevaluation of the oxygen isotopic composition of planktonic foraminifera: Experimental results and revised paleotemperature equations, Paleoceanography, 13, 150–160, 1998.

Birch, H., Coxall, H. K., Pearson, P. N., Kroon, D. and O'Regan, M.: Planktonic foraminifera stable isotopes and water column structure: Disentangling ecological signals, Mar. Micropaleontol., 101, 127–145, 2013.

Boyer, T.P., J. I. Antonov, O. K. Baranova, C. Coleman, H. E. Garcia, A. Grodsky, D. R. Johnson, R. A. Locarnini, A. V. Mishonov, T.D. O'Brien, C.R. Paver, J.R. Reagan, D. Seidov, I. V. Smolyar, and M. M. Zweng: World Ocean Database 2013, NOAA Atlas NESDIS 72, S. Levitus, Ed., A. Mishonov, Technical Ed.; Silver Spring, 2013

Dekens, P. S., Lea, D. W., Pak, D. K. and Spero, H. J.: Core top calibration of Mg/Ca in tropical foraminifera: Refining paleotemperature estimation, Geochemistry, Geophys. Geosystems, 3, 1–29, 2002.

Deuser, W.G., Ross, E.H., Hemleben, Ch., Spindler, M.: Seasonal changes in species composition, numbers, mass, size, and isotopic composition of planktonic foraminifera settling into the deep Sargasso Sea, Palaeogeogr., Palaeoclimat., Palaeoecol., 33:103-127, 1981.

Deuser, W. G. and Ross, E. H., Seasonally abundant planktonic foraminifera of the Sargasso Sea; succession, deep-water fluxes, isotopic compositions, and paleoceanographic implications, J. Foraminifer. Res., 19, 268–293, 1989.

Duplessy, J., Labeyrie, L., Juilletleclerc, A., Maitre, F., Duprat, J. and Sarnthein, M., Surface salinity reconstruction of the north-atlantic ocean during the last glacial maximum, Oceanol. Acta, 14, 311–324, 1991.

Elderfield, H., Yu, J., Anand, P., Kiefer, T. and Nyland, B.: Calibrations for benthic foraminiferal Mg/Ca paleothermometry and the carbonate ion hypothesis, Earth Planet. Sci. Lett., 250, 633–649, 2006.

Farmer, E. C., Kaplan, A., de Menocal, P. B. and Lynch-Stieglitz, J.: Corroborating ecological depth preferences of planktonic foraminifera in the tropical Atlantic with the stable oxygen isotope ratios of core top specimens, Paleoceanography, 22, 1–14, 2007.

Fairbanks, R. G., Sverdlove, M., Free, R., Wiebe, P. H. and Bé, A. W. H.: Vertical distribution and isotopic fractionation of living planktonic foraminifera from the Panama Basin, Nature, 298, 841–844, 1982.

Fairbanks, R. G. and Wiebe, P. H., Foraminifera and Chlorophyll Maximum: Vertical Distribution, Seasonal Succession, and Paleoceanographic Significance, Science, 209, 1524–1526, 1980.

Ferguson, J. E., Henderson, G. M., Kucera, M. and Rickaby, R. E. M.: Systematic change of foraminiferal Mg/Ca ratios across a strong salinity gradient, Earth Planet. Sci. Lett., 265, 153–166, 2008.

Henehan, M. J., Foster, G. L., Bostock, H. C., Greenop, R., Marshall, B. J. and Wilson, P. A.: A new boron isotope-pH calibration for Orbulina universa, with implications for understanding and accounting for 'vital effects.', Earth Planet. Sci. Lett., 454, 282–292, 2016.

Hönisch, B. and Hemming, N. G.: Ground-truthing the boron isotope-paleo-pH proxy in planktonic foraminifera shells: Partial dissolution and shell size effects, Paleoceanography, 19, 1–13, 2004.

Jørgensen, B. B., Erez, J., Revsbech, P. and Cohen, Y.: Symbiotic photosynthesis in a planktonic foraminiferan, Globigerinoides sacculifer (Brady), studied with microelectrodes, Limnol. Oceanogr. 30, 1253–1267, 1985.

Kim, S.-T. and O'Neil, J. R.: Equilibrium and nonequilibrium oxygen isotope effects in synthetic carbonates, Geochim. Cosmochim. Acta, 61, 3461–3475, 1997.

Martínez-Botí, M. A., Mortyn, P. G., Schmidt, D. N., Vance, D. and Field, D. B.: Mg/Ca in foraminifera from plankton tows: Evaluation of proxy controls and comparison with core tops, Earth Planet. Sci. Lett., 307, 113–125, 2011.

Misra, S., Greaves, M., Owen, R., Kerr, J., Elmore, A. C. and Elderfield, H.: Determination of B/Ca of natural carbonates by HR-ICP-MS, Geochemistry, Geophys. Geosystems, 15, 1617–1628 ,2014.

Mulitza, S., Boltovskoy, D., Donner, B., Meggers, H., Paul, A. and Wefer, G.: Temperature:δ18O relationships of planktonic foraminifera collected from surface waters, Palaeogeogr. Palaeoclimatol. Palaeoecol, 202, 143–152, 2003.

Ni, Y., Foster, G. L., Bailey, T., Elliott, T., Schmidt, D. N., Pearson, P., Haley, B. and Coath, C.: A core top assessment of proxies for the ocean carbonate system in surface-dwelling foraminifers, Paleoceanography, 22, 2007.

Peeters, F. J. C. and Brummer, G.-J. a.: The seasonal and vertical distribution of living planktic foraminifera in the NW Arabian Sea, Geol. Soc. London, Spec. Publ., 195, 463–497, 2002.

Rostek, F., Ruhland, G., Bassinot, F. C., Muller, P. J., Labeyrie, L. D., Lancelot, Y. and Bard, E.: Reconstructing Sea-Surface Temperature and Salinity Using δ18O and Alkenone Records, Nature, 364, 319–321, 1993.

Russell, A. D., Hönisch, B., Spero, H. J. and Lea, D. W.: Effects of seawater carbonate ion concentration and temperature on shell U, Mg, and Sr in cultured planktonic foraminifera, Geochim. Cosmochim. Acta, 68, 4347–4361, 2004.

Seki, O., Foster, G. L., Schmidt, D. N., Mackensen, A., Kawamura, K. and Pancost, R. D.: Alkenone and boron-based Pliocene pCO2records, Earth Planet. Sci. Lett., 292, 201–211, 2010.

Sime, N. G., De La Rocha, C. L. and Galy, A.: Negligible temperature dependence of calcium isotope fractionation in 12 species of planktonic foraminifera, Earth Planet. Sci. Lett., 232, 51–66, 2005.

Yu, J., Day, J., Greaves, M. and Elderfield, H.: Determination of multiple element/calcium ratios in foraminiferal calcite by quadrupole ICP-MS, Geochemistry, Geophys. Geosystems 6, 2005

Rickaby, R. E. M. and Halloran, P.: Cool La Nina During the Warmth of the Pliocene?, Science, 307, 1948–1952, 2005.

Wang, G., Cao, W., Yang, D. and Xu, D. Variation in downwelling diffuse attenuation coefficient in the northern South China Sea, Chinese J. Oceanol. Limnol., 26, 323–333, 2008.

Weare, B. C., Strub, P. T. and Samuel, M. D.: Annual Mean Surface Heat Fluxes in the Tropical Pacific Ocean, J. Phys. Oceanogr., 11, 705–717, 1981.

$\Delta^{11}B$ ((‰)) vs Calcification depth (m)

Arabian Sea

Indian Ocean

Western equatorial Pacific

$R^2= 0.44, p=0.005$
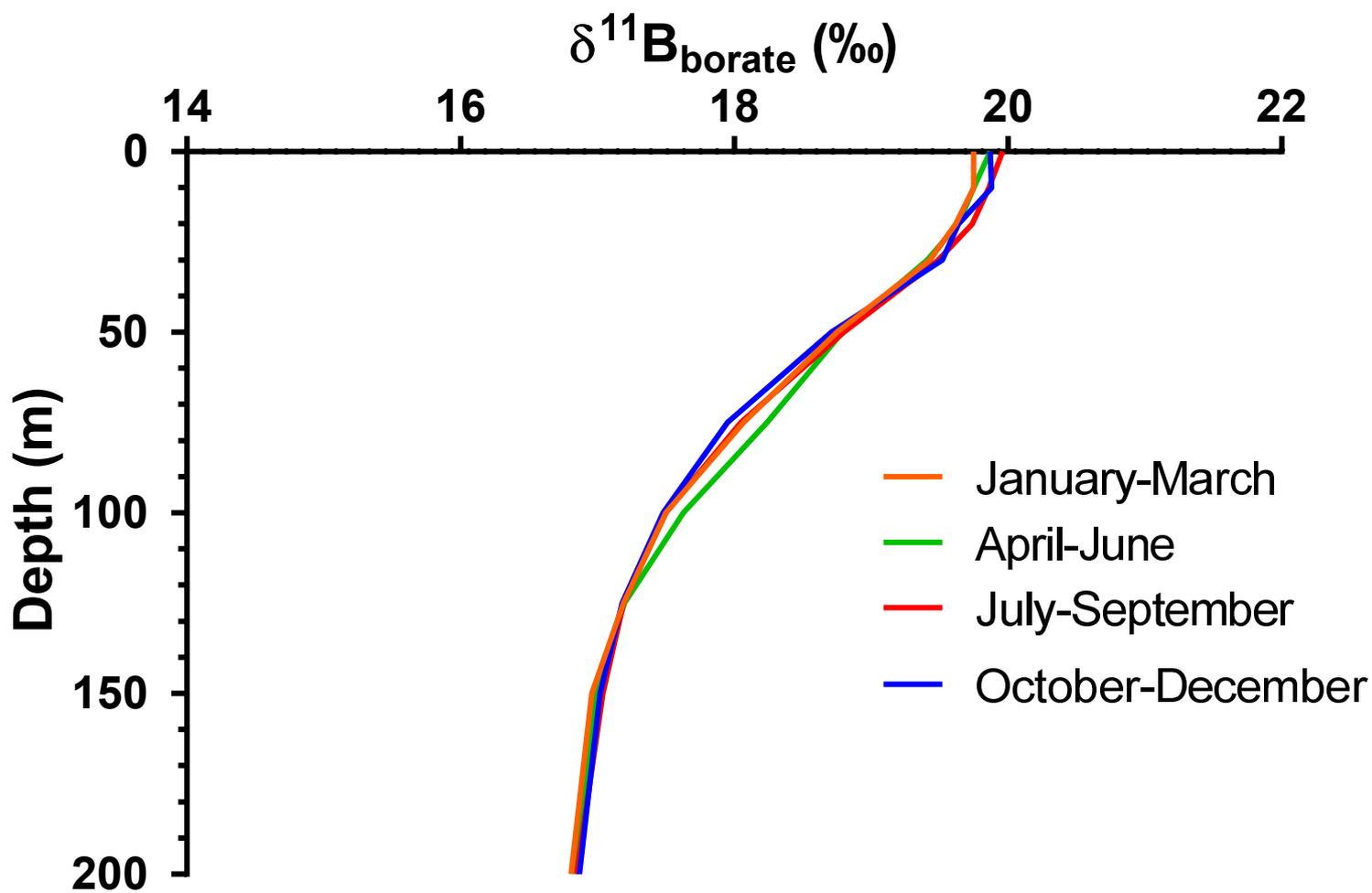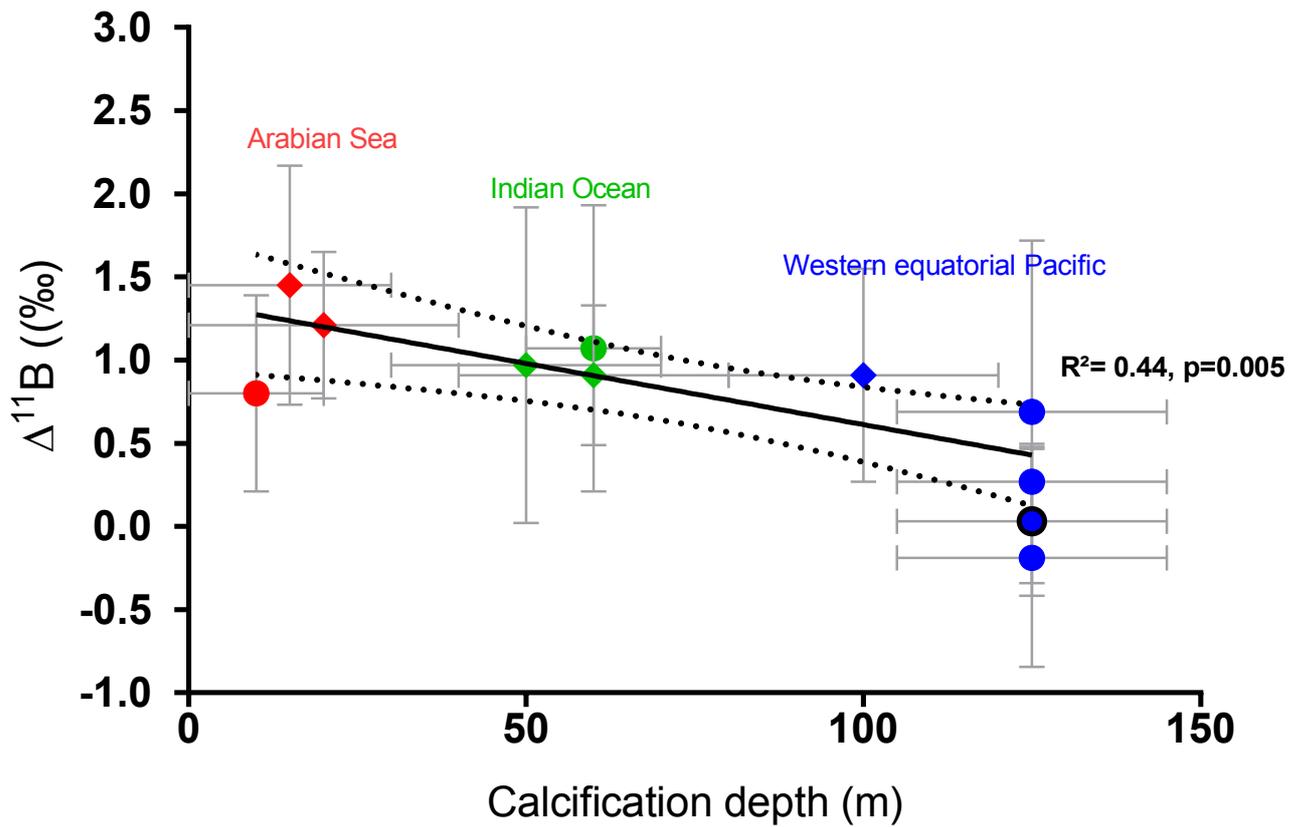
♦ *G. ruber* (Arabian Sea)

● *T. sacculifer (w/sacc)* (Arabian Sea)

♦ *G. ruber* (Indian Ocean)

● *T. sacculifer (w/o sacc)* (Indian Ocean)

♦ *G. ruber* (WEP)

● *T. sacculifer (w/o sacc)* (WEP)

— Linear reg. All

A

R²=0.4496 ,p=0.0045

R²=0.2234 ,p=0.0197

B/Ca (μmol/mol)

$[B(OH)_4^-]/[HCO_3^-]$

- ▲ *T. sacculifer* (sacc)
- ● *T. sacculifer* (w/o sacc)
- ● *G. ruber* (white)
- ● *O. universa*
- ● *P. obliquiloculata*
- ● *N. dutertrei*
- ● *G. menardii*
- ● *G. tumida*

B

B/Ca (μmol/mol)

$\delta^{11}B_{carbonate}$ (‰)

R²=0.3026, p=0.005

C

B/Ca (μmol/mol)

Temperature$_{derived\ Mg/Ca}$ (°C)

R²=0.4542 ,p<0.0001

D

$\delta^{11}B_{carbonate}$ (‰)

Temperature$_{derived\ Mg/Ca}$ (°C)

R²=0.2327 ,p=0.014

A — δ¹¹B_carbonate (‰) vs Water depth (m):
R²= 0.0003, p=0.98 (green)
R²= 0.15, p=0.52 (red)
R²= 0.38, p=0.27 (blue)
R²= 0.45, p=0.15 (orange)

B — B/Ca (μmol/mol) vs Water depth (m):
R²= 0.65, p=0.10 (green)
R²= 0.13, p=0.55 (blue)
R²= 0.13, p=0.55 (red)
R²= 0.70, p=0.08 (orange)

Legend:
- *G. ruber* (green)
- *T. sacculifer* (w/o sacc) (blue)
- *T. sacculifer* (sacc) (red)
- *O. universa* (orange)
- *P. obliquiloculata* (yellow)
- *N. dutertrei* (teal)
- *G. menardii* (purple)
- *G. tumida* (pink)

C — δ¹¹B_carbonate (‰) vs Calcification depth (m):
R²= 0.15, p=0.84 (red)
R²= 0.75, p=0.03 (green)
R²= 0.27, p=0.37 (blue)
R²= 0.45, p=0.14 (orange)

D — B/Ca (μmol/mol) vs Calcification depth (m):
R²= 0.11, p=0.04 (black)

$\delta^{11}B_{borate}$

pH

Table S1

Elemental ratios	Li/Ca μmol/mol	B/Ca μmol/mol	Mg/Ca mmol/mol	Al/Ca mmol/mol	Sr/Ca mmol/mol	Cd/Ca μmol/mol	Ba/Ca μmol/mol	U/Ca nmol/mol	Mn/Ca μmol/mol	Fe/Ca mmol/mol
Standard solution 0	0.8	9	0.10	0.131	0.00	0.03	0.6	31	1	0.01
Standard solution 1	2.3	38	0.31	0.112	0.49	0.05	1.9	38	12	0.02
Standard solution 3	6.8	108	1.31	0.177	1.06	0.13	3.0	53	39	0.04
Standard solution 5	14.6	216	3.17	0.223	1.57	0.23	5.1	62	129	0.08
Standard solution 6	19.0	278	5.23	0.352	1.97	0.28	5.5	74	196	0.11
Standard solution 8	25.0	281	6.07	0.602	2.99	0.50	20.1	390	501	0.50
Standard solution 9		408			4.89					
Standard solution 10		519			8.01					
Standard solution 11		607			9.93					

Table S2

Standard	$\delta^{11}B_1$ (‰)	$2SD_{AE121}$	n_{AE121}	$\delta^{11}B_2$ (‰)	$2SD_{AE121}$	n_{AE121}	Reference
NEP1	25.21	0.25	11	25.22	0.25	11	This study
NEP2	25.00	0.30	12				This study
NEP3	24.70	0.30	12				This study
NEP4	25.40	0.21	11				This study
NEP5	25.32	0.21	11	25.33	0.21	11	This study
NEP6	25.22	0.21	11				This study
NEP7	25.26	0.26	15				This study
NEP8	25.39	0.26	15				This study
NEP9	26.15	0.26	15				This study
NEP10	25.97	0.26	15				This study
NEP11	26.09	0.26	15	26.09	0.26	15	This study
NEP12	26.22	0.26	15	26.29	0.26	15	This study
NEP13	26.19	0.26	15	26.21	0.26	15	This study
NEP14	26.12	0.26	15	26.13	0.26	15	This study
NEP15	26.00	0.26	15				This study
NEP16	26.04	0.26	15				This study
NEP17	26.02	0.29	12				This study
NEP18	25.86	0.29	12	25.86	0.26	14	This study
NEP19	25.78	0.26	14				This study
NEP20	25.42	0.15	3	25.32	0.15	3	This study
NEP21	25.54	0.22	6	26.16	0.22	6	This study
NEP22	26.42	0.22	6				This study
JCP-1-1	24.07	0.10					This study
JCP-1-2	24.17	0.11		24.17	0.10		This study
JCP-1-3	24.01	0.11					This study
JCP-1-4	23.92	0.26					This study
JCP-1-5	24.03	0.26		24.05	0.39		This study
JCP-1-6	24.18	0.36		24.16	0.36		This study

Standard	Average $\delta^{11}B$	*2SD*	n				Reference
NEP	25.70	*0.93*	22				This study
NEP	26.20	0.88	27				Holcomb et al., 2015
NEP	25.80	0.89	6				Sutton et al., 2018
JCP-1	24.06	0.20	6				This study
JCP-1	24.37	*0.32*	57				Holcomb et al., 2015
JCP-1	24.42	*0.28*	7				Sutton et al., 2018

Table S3

Date of analysis	Standard	Li/Ca μmol/mol	B/Ca μmol/mol	Mg/Ca mmol/mol	Sr/Ca mmol/mol	Cd/Ca μmol/mol	Ba/Ca μmol/mol	U/Ca nmol/mol	Mn/Ca μmol/mol	Fe/Ca mmol/mol	Reference
10/7/17	CamWuel 1	16.0	204	1.22	1.31	0.26	4.6	43	67	0.04	This study
10/7/17	CamWuel 2	16.3	209	1.24	1.32	0.28	4.6	45	69	0.04	This study
10/7/17	CamWuel 3	16.3	209	1.23	1.31	0.26	4.6	44	77	0.04	This study
10/7/17	CamWuel 4	16.0	207	1.23	1.32	0.28	4.6	44	74	0.04	This study
10/7/17	CamWuel 5	16.4	210	1.23	1.32	0.27	4.6	42	74	0.04	This study
10/7/17	CamWuel 6	16.0	208	1.24	1.31	0.26	4.6	42	74	0.04	This study
10/7/17	CamWuel 7	16.6	213	1.23	1.32	0.28	4.6	44	74	0.04	This study
11/7/17	CamWuel 1	16.0	203	1.22	1.32	0.26	4.6	41	72	0.04	This study
11/7/17	CamWuel 2	16.1	205	1.22	1.32	0.27	4.6	42	76	0.04	This study
11/7/17	CamWuel 3	16.2	204	1.22	1.32	0.27	4.6	41	72	0.04	This study
11/7/17	CamWuel 4	16.1	205	1.22	1.32	0.27	4.5	41	71	0.04	This study
11/7/17	CamWuel 5	15.8	204	1.21	1.32	0.27	4.6	42	73	0.04	This study
11/7/17	CamWuel 6	16.1	206	1.22	1.32	0.27	4.6	42	68	0.04	This study
11/7/17	CamWuel 7	16.0	207	1.22	1.32	0.26	4.6	43	66	0.04	This study
11/7/17	CamWuel 8	15.9	203	1.21	1.32	0.27	4.6	42	68	0.04	This study
12/7/17	CamWuel 1	16.3	201	1.22	1.31	0.22	4.6	41	66	0.03	This study
12/7/17	CamWuel 2	16.1	203	1.22	1.32	0.23	4.6	42	67	0.03	This study
12/7/17	CamWuel 3	16.4	202	1.22	1.32	0.23	4.6	42	69	0.04	This study
12/7/17	CamWuel 4	16.3	202	1.22	1.31	0.22	4.6	41	68	0.04	This study
12/7/17	CamWuel 5	16.6	202	1.22	1.31	0.23	4.6	44	67	0.03	This study
12/7/17	CamWuel 6	16.6	205	1.22	1.31	0.24	4.5	42	66	0.03	This study
12/7/17	CamWuel 7	16.1	204	1.22	1.31	0.22	4.6	40	67	0.03	This study
12/7/17	CamWuel 8	16.4	204	1.22	1.31	0.23	4.6	43	67	0.03	This study
12/7/17	CamWuel 9	16.4	202	1.22	1.32	0.23	4.6	43	64	0.03	This study
13/7/2017	CamWuel 1	16.2	198	1.22	1.31	0.31	4.6	42	74	0.04	This study
13/7/2017	CamWuel 2	16.4	200	1.22	1.30	0.30	4.6	43	73	0.04	This study
13/7/2017	CamWuel 3	16.2	201	1.23	1.31	0.31	4.7	43	74	0.04	This study
13/7/2017	CamWuel 4	16.3	198	1.22	1.31	0.30	4.6	42	73	0.04	This study
13/7/2017	CamWuel 5	16.6	200	1.23	1.30	0.30	4.6	42	73	0.04	This study
13/7/2017	CamWuel 6	16.5	198	1.22	1.31	0.31	4.6	44	74	0.04	This study
13/7/2017	CamWuel 7	16.1	201	1.22	1.30	0.32	4.7	43	74	0.04	This study
	Average CamWuel	**16.2**	**204**	**1.22**	**1.31**	**0.27**	**4.6**	**42**	**71**	**0.04**	**This study**
	2SD	*0.4*	*7*	*0.01*	*0.01*	*0.06*	*0.1*	*2*	*7*	*0.01*	
	n	31	31	31	31	31	31	31	31	31	
	Published CamWuel	**16.4**	**202**	**1.23**	**1.30**	**0.29**	**4.8**	**44**	**71**		**Misra et al., 2014**
	2SD	*0.8*	*7*	*0.06*	*0.02*	*0.02*	*0.2*	*2*	*2*		
	n	180	180	180	180	180	180	180	180		

Table S4

Specie	Seasonality
T. sacculifer (sacc)	Spring
T. sacculifer (w/o sacc)	Spring
G. ruber (white)	Summer
N. dutertrei	Winter
G. tumida	Annual average
G. menardii	Annual average
O. universa	Annual average
P. obliquiloculata	Winter

Table S5

Species	B	A	Reference
T. sacculifer (sacc)	0.377	0.090	Anand et al., 2003
T. sacculifer (w/o sacc)	0.347	0.090	Anand et al., 2003
G. ruber (white)	0.300	0.089	Dekens et al., 2002
N. dutertrei	0.600	0.008	Dekens et al., 2002
G. tumida	0.380	0.090	Anand et al., 2003
G. menardii	0.360	0.091	Regenberg et al., 2009
O. universa	0.595	0.090	Anand et al., 2003
P. obliquiloculata	0.328	0.090	Anand et al., 2003

Species	A	B	C	dw correction	Condition	Reference	Equation
O. universa	16.500	4.800		-0.27	LL	Bemis et al., 1998	T=A-B* (δ18Oc-δ18Ow)
O. universa	15.700	4.460	0.35	-0.27	ML	Bemis et al., 2002	T=A-B* (δ18Oc-δ18Ow)+C*(δ18Oc-δ18Ow)^2
O. universa	14.900	4.800		-0.27	HL	Bemis et al., 1998	T=A-B* (δ18Oc-δ18Ow)
T. sacculifer	14.910	4.350		-0.27		Mulitza et al., 2003	T=A-B* (δ18Oc-δ18Ow)
G. ruber	14.200	4.440		-0.27		Mulitza et al., 2003	T=A-B* (δ18Oc-δ18Ow)
All	16.900	4.380	0.1	-0.2		Shackleton et al., 1974	T=A-B* (δ18Oc-δ18Ow)+C*(δ18Oc-δ18Ow)^2
All	17.000	4.520	0.03	-0.22		Erez and Luz, 1983	T=A-B* (δ18Oc-δ18Ow)+C*(δ18Oc-δ18Ow)^2
All^3	16.100	4.640	0.09	-0.27		Kim and O'Neil 1997	T=A-B* (δ18Oc-δ18Ow)+C*(δ18Oc-δ18Ow)^3

Table S6

Core	Species	CD$_1$	CD$_2$	CD$_3$	Reference
FC-01a	*G. ruber (white ss)*	83 ± 20	30 ± 10	50 ± 20	Sime thesis 2006
FC-02a	*G. ruber (white ss)*	56 ± 10	15 ± 10	60 ± 20	Sime thesis 2006
FC-12b	*G. ruber (white ss)*	Surface ± 10	0-30	60 ± 10	Peeters and Brumer, 2012 (non upwelling station Arabian sea)
FC-13a	*G. ruber (white ss)*	Surface ± 10	20 ± 20	60 ± 10	Peeters and Brumer, 2012 (non upwelling station Arabian sea)
WP7-01	*G. ruber (white ss)*			100±20	Elderfield and Ganssen, 2000
A14	*G. ruber (white ss)*		60 ± 10	100±20	Elderfield and Ganssen, 2000
FC-01a	*T. sacculifer (sacc)*	48 ± 10	50 ± 10	60 ± 10	Sime et al., 2005
FC-02a	*T. sacculifer (sacc)*	7 ± 10	30 ± 10	80 ± 20	Sime et al., 2006
FC-12b	*T. sacculifer (sacc)*	15 ± 10	40 ± 10		
WP7-01	*T. sacculifer (sacc)*		80 ± 20	125 ± 15	Rickaby et al., 2005
A14	*T. sacculifer (sacc)*		60 ± 10	125 ± 15	
FC-01a	*T. sacculifer (w/o sacc)*	88 ± 20	50 ± 10	60 ± 10	Sime thesis 2006 (Wind22-b)
FC-02a	*T. sacculifer (w/o sacc)*	32 ± 10	10 ± 10	80 ± 20	Sime thesis 2006
FC-12b	*T. sacculifer (w/o sacc)*	0-15 ± 10	30 ± 10	45 ± 20	Peeters and Brumer, 2012 (non upwelling station Arabian sea)
WP7-01	*T. sacculifer (w/o sacc)*		80 ± 20	125 ± 15	Rickaby et al., 2005
A14	*T. sacculifer (w/o sacc)*		60 ± 10	125 ± 15	Rickaby et al., 2005
CD107a	*O. universa*	80 ± 20	50 ± 20	0-50	Farmer et al., 2007
FC-01a	*O. universa*	45 ± 10	60 ± 10	90 ± 20	Sime et al., 2005
FC-02a	*O. universa*	127 ± 20	45 ± 15	65 ± 10	Birshe et al., 2013
FC-12b	*O. universa*	35 ± 10	30 ± 20		
WP7-01	*O. universa*		75 ± 25		
A14	*O. universa*		55 ± 15		
FC-01a	*P. obliquiloculata*	70 ± 20	75 ± 15	106 ± 20	Sime et al., 2005
FC-02a	*P. obliquiloculata*	226 ± 20	60 ± 10		
FC-12b	*P. obliquiloculata*	40 ± 10	50 ± 10		
FC-13a	*P. obliquiloculata*	65 ± 10	50 ± 10		
WP7-01	*P. obliquiloculata*		125 ± 25		
FC-01a	*N. dutertrei*	95 ± 20	90 ± 20	93 ± 20	Sime et al., 2005
FC-02a	*N. dutertrei*	65 ± 10	100 ± 20	146 ± 20	Sime et al., 2005
FC-12b	*N. dutertrei*	40 ± 10	50 ± 10		
FC-13a	*N. dutertrei*	45 ± 10	150 ± 20		
WP7-01	*N. dutertrei*		125 ± 25	165	Rickaby et al., 2005
A14	*N. dutertrei*		110 ± 20	165	Rickaby et al., 2005
FC-01a	*G. menardii*	135 ± 20	70 ± 20		
FC-02a	*G. menardii*	60 ± 10	60 ± 10		
FC-12b	*G. menardii*	65 ± 10	55 ± 15	60 ± 10	Peeters and Brumer, 2012 (non upwelling station Arabian sea)
FC-13a	*G. menardii*	55 ± 10	70 ± 10	60 ± 10	Peeters and Brumer, 2012 (non upwelling station Arabian sea)
WP7-01	*G. menardii*		180 ± 20		
FC-01a	*G. tumida*	70 ± 20	100 ± 10	160 ± 20	Birshe et al., 2013
FC-02a	*G. tumida*	70 ± 20	130 ± 20	160 ± 20	Birshe et al., 2013
WP7-01	*G. tumida*		180 ± 20	210 - 240	Rickaby et al., 2005

CD$_1$: Depth habitat estimated from $\delta^{18}O_c$

CD$_2$: Depth habitat estimated from Mg/Ca derived temperature

CD$_3$: Depth habitat from literature

Table S7

		PRE INDUSTRIAL IN-SITU PARAMETERS																				CALCULATED PARAMETERS										
Core	Species	Depth habitat (m)	Temperature	2sd*	Salinity	2sd*	pH (pre-ind)	2sd*	pCO_2	2sd*	HCO_3^-	2sd*	CO_3^{2-}	2sd*	DIC	2sd*	ALK	2sd*	$\delta^{11}B_{borate}$	2sd*	$T_{Mg/Ca}$	2sd	$pH_{\delta11B}$	2sd**	pCO_2	2sd***	Calibration	$pH_{\delta11B}$	2sd**	pCO_2	2sd***	Calibration
			(°C)																													
Atlantic Ocean																																
CD107a	*O. universa*	80 ± 20	12.0	0.3	35.6	0.01	8.19	0.03	274	21	1856	29	192	12	2059	18	2333	1	17.86	0.31	20.0	1.4	8.19	0.06	285	*39*	[8]					
Indian Ocean																																
FC-01a	*G. ruber (white ss)*	50 ± 20	23.4	5.9	35.0	0.4	8.10	0.04	338	41	1743	138	226	48	1979	93	2299	22	18.40	0.90	26.1	1.4	8.07	0.05	387	29	[1]	7.88	0.16	630	42	[2]
FC-01a	*T. sacculifer (sacc)*	60 ± 10	21.9	5.7	35.1	0.3	8.09	0.03	346	38	1773	126	215	45	1998	84	2303	18	18.15	0.81	24.5	1.4	8.06	0.04	400	79	[3]	8.04	0.06	417	82	[4]
FC-01a	*T. sacculifer (w/o sacc)*	60 ± 10	21.9	5.7	35.1	0.3	8.09	0.03	346	38	1773	126	215	45	1998	84	2303	18	18.16	0.82	25.3	1.4	8.10	0.04	357	49	[3]	8.10	0.05	356	49	[4]
FC-01a	*O. universa*	90 ± 20	18.2	4.0	35.2	0.0	8.07	0.04	374	43	1856	94	184	35	2053	62	2311	9	17.42	0.61			7.98	0.06	499	63	[8]					
FC-01a	*P. obliquiloculata*	106 ± 20	20.5	4.6	35.2	0.1	8.09	0.03	353	32	1802	99	204	36	2018	65	2306	11	17.91	0.66	20.3	1.4	8.10	0.08	356	48	[11]					
FC-01a	*G. menardii*	70 ± 20	20.5	4.6	35.2	0.1	8.09	0.03	353	32	1802	99	204	36	2018	65	2306	11	17.93	0.68	20.2	1.4	8.16	0.05	304	43	[13]					
FC-01a	*N. dutertrei*	95 ± 20	17.7	4.0	35.1	0.0	8.06	0.04	380	43	1868	94	180	35	2061	62	2313	9	17.26	0.62	18.5	1.4	8.09	0.06	373	49	[13]					
FC-01a	*G. tumida*	100 ± 20	17.1	1.6	35.1	0.0	8.06	0.02	386	22	1881	41	175	15	2070	27	2314	3	17.21	0.27	17.2	1.4	8.06	0.07	400	52	[13]					
FC-02a	*G. ruber (white ss)*	60 ± 20	20.4	2.4	35.5	0.0	8.19	0.01	268	10	1724	26	246	10	1979	17	2332	2	19.06	0.34	24.6	1.4	8.13	0.04	332	26	[1]	8.03	0.10	428	31	[2]
FC-02a	*T. sacculifer (sacc)*	80 ± 20	19.3	1.9	35.6	0.1	8.19	0.01	268	7	1741	38	240	15	1989	24	2333	3	18.89	0.30	24.0	1.4	8.18	0.03	286	57	[3]	8.21	0.05	267	54	[4]
FC-02a	*T. sacculifer (w/o sacc)*	80 ± 20	19.3	1.9	35.6	0.1	8.19	0.01	268	7	1741	38	240	15	1989	24	2333	3	18.90	0.30	25.1	1.4										
FC-02a	*O. universa*	65 ± 10	20.1	1.1	35.5	0.0	8.19	0.00	268	2	1728	15	245	6	1981	9	2332	1	19.00	0.17	22.2	1.4	8.18	0.04	287	42	[8]					
FC-02a	*P. obliquiloculata*	60 ± 10	18.3	0.5	35.6	0.0	8.18	0.01	277	8	1769	17	228	7	2007	10	2334	1	18.64	0.14	21.7	1.4	8.16	0.08	302	43	[11]					
FC-02a	*G. menardii*	60 ± 10	20.4	1.9	35.5	0.0	8.19	0.01	268	10	1724	19	246	7	1979	12	2332	2	19.05	0.30	19.9	1.4	8.17	0.05	293	42	[13]					
FC-02a	*N. dutertrei*	146 ± 20	17.5	1.0	35.6	0.1	8.16	0.02	292	14	1798	31	216	13	2024	18	2333	2	18.33	0.27	20.3	1.4	8.12	0.06	339	46	[13]					
FC-02a	*G. tumida*	130 ± 20	17.8	0.8	35.6	0.0	8.17	0.02	284	17	1784	32	222	14	2015	19	2334	1	18.47	0.25	17.9	1.4	8.12	0.05	339	46	[13]					
Arabian Sea																																
FC-12b	*G. ruber (white ss)*	0-30	25.9	0.3	36.6	0.1	8.18	0.05	271	39	1655	53	292	23	1954	31	2374	8	19.81	0.65	30.2	1.4	8.15	0.04	305	28	[1]	8.20	0.10	265	26	[2]
FC-12b	*T. sacculifer (sacc)*	40 ± 10	25.3	0.6	36.5	0.0	8.10	0.06	350	64	1756	75	249	31	2015	46	2369	2	18.71	0.77	26.9	1.4	8.09	0.04	374	54	[3]	8.10	0.06	366	53	[4]
FC-12b	*T. sacculifer (w/o sacc)*	15 ± 10	25.9	0.0	36.5	0.1	8.16	0.04	290	34	1681	45	281	19	1970	28	2374	8	19.54	0.50	29.3	1.4	8.13	0.04	332	50	[3]	8.16	0.06	302	47	[4]
FC-12b	*O. universa*	35 ± 10	25.5	0.6	36.5	0.0	8.11	0.06	334	56	1738	68	257	28	2004	41	2369	1	18.90	0.69	27.2	1.4	8.13	0.03	336	50	[8]					
FC-12b	*P. obliquiloculata*	50 ± 10	25.0	0.9	36.5	0.1	8.06	0.06	382	69	1794	75	233	32	2038	45	2368	3	18.24	0.67	26.6	1.4	8.05	0.08	415	58	[11]					
FC-12b	*G. menardii*	65 ± 10	24.1	1.1	36.4	0.1	8.02	0.06	438	72	1850	75	209	32	2072	45	2365	4	17.69	0.62	24.8	1.4	7.97	0.06	514	68	[13]					
FC-12b	*N. dutertrei*	40 ± 10	25.3	0.6	36.5	0.0	8.10	0.06	350	64	1756	75	249	31	2015	46	2369	2	18.75	0.71	25.0	1.4	8.11	0.04	350	52	[13]					
FC-13a	*G. ruber (white ss)*	20 ± 20	27.1	1.1	36.7	0.1	8.10	0.03	343	27	1724	43	263	17	1996	26	2371	2	19.00	0.37	27.5	1.4	8.11	0.04	351	29	[1]	8.05	0.09	417	32	[2]
FC-13a	*T. sacculifer (w/o sacc)*	45 ± 20	25.7	0.7	36.6	0.0	8.07	0.03	380	34	1782	38	239	16	2032	23	2371	2	18.86	0.45	30.6	1.4										
FC-13a	*P. obliquiloculata*	50 ± 10	25.4	1.2	36.6	0.1	8.06	0.05	391	59	1797	66	233	29	2041	40	2370	4	18.31	0.57	28.9	1.4	8.08	0.08	385	55	[11]					
FC-13a	*G. menardii*	55 ± 10	25.1	1.3	36.6	0.1	8.04	0.05	409	65	1815	69	225	30	2052	41	2369	5	18.04	0.56	18.8	1.4	7.98	0.04	503	68	[13]					
FC-13a	*N. dutertrei*	150 ± 20	19.4	2.3	36.0	0.1	7.80	0.03	766	45	2056	37	118	15	2199	25	2348	1	15.37	0.27	19.5	1.4	7.79	0.08	811	101	[13]					
Pacific Ocean																																
WP07-a	*G. ruber (white ss)*	100±20	26.1	2.4	35.2	0.4	8.05	0.05	387	51	1753	81	224	31	1988	52	2305	7	18.21	0.64	27.0	1.4	8.03	0.05	426	32	[1]	7.80	0.16	778	52	[2]
WP07-a	*T. sacculifer (sacc)*	80 ± 20	27.4	2.2	35.0	0.5	8.08	0.05	357	56	1708	89	242	33	1960	58	2303	10	18.68	0.65	27.3	1.4	7.99	0.04	478	63	[3]	8.13	0.04	324	49	[4]
WP07-a	*T.sacculifer (w/o sacc)*	125 ± 20	24.7	1.8	35.4	0.2	8.03	0.00	413	30	1797	31	209	9	2017	23	2311	10	17.80	0.23	28.4	1.4	8.03	0.05	427	58	[3]	7.92	0.08	573	73	[4]
WP07-a	*O. universa*	75 ± 25	27.7	2.6	34.9	0.6	8.09	0.07	349	68	1696	110	247	39	1953	73	2303	15	18.78	0.83	28.2	1.4	8.10	0.04	352	52	[8]					
WP07-a	*P. obliquiloculata*	125 ± 25	24.7	3.6	35.4	0.4	8.03	0.02	413	30	1797	80	209	26	2017	56	2311	18	17.82	0.48	24.6	1.4	8.03	0.08	430	58	[11]					
WP07-a	*N. dutertrei*	165 ± 20	20.6	3.8	35.5	0.2	8.03	0.01	408	10	1855	44	189	18	2057	26	2322	0	17.34	0.45	26.4	1.4	8.09	0.06	369	50	[13]					
WP07-a	*G. tumida*	180 ± 20	18.7	5.0	35.4	0.2	8.04	0.01	403	13	1877	58	180	24	2070	35	2322	0	17.23	0.56	21.2	1.4	8.05	0.06	406	53	[13]					

* uncertainties calculated using Henehan's 2016 R code
** propagated uncertainty on pH including d11B, temperature, salinity uncertainties
*** propagated uncertainty on pCO2 including d11B, temperature, salinity, Alk uncertainties